学位論文

Dynamics and bacterial control of organic aggregates in marine environments

（海洋環境における有機凝集体の動態と
細菌による制御）

平成２６年１２月博士（理学）申請

東京大学大学院理学系研究科
生物科学専攻
山田 洋輔

Dynamics and bacterial control of organic aggregates in marine environments

（海洋環境における有機凝集体の動態と細菌による制御）

A dissertation submitted to the graduate school of science, the University of Tokyo, as a partial fulfillment of the requirements for the Degree of Doctor of Philosophy

March 2015

By

Yosuke Yamada

Abstract

Organic aggregates play an important role in the transport and sequestration of carbon and other elements in the oceans. Transparent exopolymer particles (TEP) represent a major class of organic aggregates in marine environments, being primarily composed of bio-polymers (e.g. polysaccharide, protein, lipid) released from marine organisms. Since the discovery of the presence of large quantities of TEP in seawater in 1990s, extensive studies have been conducted to elucidate the formation mechanisms, chemical compositions and settling fluxes of TEP in the oceans. However, there still remain large gaps in our understanding of the regulation of TEP and other particle dynamics in oceanic environments. The present study focused on, 1) distribution patterns in TEP and other suspended particles in the Arctic Ocean and 2) mechanisms by which TEP settling velocities are controlled by bacteria.

In Chapter 2, I examined horizontal and vertical distribution patterns in suspended particles [TEP, particulate organic carbon (POC), and particles as determined by laser in situ scattering and transmissometry (LISST)] in the Chukchi Sea and the Canada Basin in the western Arctic Ocean, during the late summer of 2012. Suspended particle concentrations were high in the shelf region and gradient patterns were identified from the shelf to basin. A hotspot (extremely high concentration) of suspended particles,

accompanied by high prokaryote abundance and production, was observed at near the seafloor (depth, 50 m) of the shelf region. In general, the ratios of TEP to POC were high (0.3–3.6) in the investigated region, relative to the corresponding ratios previously reported for other oceanic regions, suggesting that TEP play an important role in the regulation of particle dynamics. LISST determination revealed high concentrations of particles near the pycnocline (depth of 10–30 m). An analysis of particle size distribution (range, 5.2–119 μm) indicated that relatively small particles were dominant in the shelf region compared to the slope-basin region, which implied that smaller precursor aggregation was occurring in the shelf region. These results suggest that aggregates, including TEP, are produced in the shelf region and are transferred to the slope-basin region along the pycnocline. The lateral transport of these aggregates could support productivity and material cycles in the nutrient-depleted basin region of the western Arctic Ocean.

In Chapter 3, I investigated whether attached bacteria affect the settling velocity of TEP via modifications of the physical properties of aggregates, including density, porosity, and morphology. Model aggregates, prepared by mixing 2 different polysaccharides (fucoidan and chitosan), were incubated in coastal seawater passed through either 0.8 μm ($AGG_{0.8}$) or 0.2 μm ($AGG_{0.2}$) filters. After incubation for 48 h,

$AGG_{0.8}$ were much more densely (3.2- to 10.1-fold) colonized by bacteria than $AGG_{0.2}$. Based on median settling velocities (W_{50}), as determined by LISST, the W_{50} of $AGG_{0.8}$ was lower (1.6- to 4.5-fold) than that of $AGG_{0.2}$ for a size class of 62 to 119 μm. Stokes model analyses indicated that this reduction in W_{50} could be largely attributed to the higher porosities of $AGG_{0.8}$ (0.932−0.981) than those of $AGG_{0.2}$ (0.719−0.929). My results support the notion that the modification of aggregate structure by attached bacteria (porosity enhancement) can be an important factor controlling the settling velocity of marine particles.

In Chapter 4, I investigated whether marine bacteria enhance the coagulation of TEP, to enhance organic aggregate settling velocity. Model aggregates [equivalent spherical diameter (ESD), ca. 0.01 cm] were suspended in seawater contained in rotating tubes to examine time-course changes in particle ESD and abundance. Results indicated that marine bacterial assemblages strongly enhanced the coagulation of aggregates into large aggregates (ESD, 0.1–1 cm) over a period of 24–96 hours. Catalyzed reporter deposition-fluorescence in situ hybridization results indicated that one group of bacteria that grew rapidly on the aggregates was affiliated with the genus *Pseudoalteromonas*. Experiments using *Pseudoalteromonas* isolates indicated that four of 11 isolates enhanced the coagulation of aggregates and specific types of the group was one of key species of

aggregate coagulation in seawater. High settling velocities (up to 270 m d^{-1}) were determined for larger aggregates (ESD, >0.4 cm), which agreed with theoretical predictions derived from a hydrodynamic model. My results demonstrate that specific types of bacteria readily colonize aggregates to impose a strong biotic force that enhances small organic aggregate coagulation and the formation of fast-settling large aggregates in seawater.

In Chapter 5, I summarize the above findings to conclude that, 1) TEP and TEP-induced aggregation process could contribute to particle transport along the shelf to basin transit of the western Arctic and 2) bacteria can control TEP settling velocity by their enhancement of aggregate porosity and coagulation efficiency. These findings added several important aspects to the previous knowledge regarding organic aggregate distributions in the Arctic Ocean and the regulation of organic aggregate settling velocity in marine environments.

Contents

Chapter 1 General introduction

1.1 Background

1.1.1 Contribution of particulate organic carbon (POC) to carbon cycles in the ocean

The rate of global photosynthetic fixation of dissolved inorganic carbon (DIC) in seawater by phytoplankton (primary production) is estimated to be 37–50 pg C per year (Antoine et al., 1996; Balkanski et al., 1999; Falkowski, 1998; Field et al., 1998), which is comparable to the level of terrestrial primary production (48–60 pg C per year) (Field et al., 1998; Fung et al., 1987; Melillo et al., 1993; Ruimy et al., 1994). Phytoplankton production is important not only as a basis for marine food webs but also as a regulatory element of carbon cycles in the ocean. Of particular importance is the vertical delivery of photosynthetically produced organic carbon from the sunlit layer (euphotic zone, extending from the surface to a depth of 50–200 m, depending on the oceanic region) to deeper layers (depth >1000 m) or the abyssal seafloor, which can contribute to the sequestration (or storage) of carbon in the ocean over a time scale of 100–1000 years (Passow and Carlson, 2012). This mechanism of ocean carbon sequestration is called the “biological carbon pump” (De La Rocha and Passow, 2007; Falkowski, 1998; Sabine et al., 2004). Modeling studies have suggested that the biological carbon pump influences atmospheric carbon dioxide concentrations and, hence, the Earth’s climate (Henson et al., 2011; Passow and Carlson, 2012; Riebesell et al., 2007). Thus, elucidation of the variability and control of vertical carbon delivery by the biological carbon pump is important for a better understanding of the role of marine ecosystems in the regulation

of global carbon cycles.

There are two forms of organic carbon fixed by phytoplankton in seawater: particulate (POC) and dissolved organic carbon (DOC). POC is defined operationally as organic carbon retained on filters with a pore size of 0.4–1.0 μm, while the organic carbon passing through the filters is defined as DOC (Koike and Fukuda, 2007; Sheldon, 1972; Wangersky, 1994). DOC is the largest pool of organic carbon in seawater, accounting for >95% (Eglinton and Repeta, 2004; Hansell and Carlson, 1998) of total organic carbon, and is delivered to deeper layers mainly by diffusion and convective mixing (advection) (Hansell, 2002). Globally, the vertical delivery of DOC to the deeper layer of the ocean is estimated to be in the order of 1.4 pg C per year (Hansell, 2002). POC is also transported by diffusion and mixing, but the main process that mediates the vertical delivery of POC is gravitational settling (Alldredge and Silver, 1988; Wotton, 1994). Vertical settling fluxes of POC in the ocean have been extensively studied during the past three decades using sediment traps (Eppley, 1989; Tréguer et al., 2003). According to estimates produced by those studies, the settling of POC accounts for approximately 20% of primary production, although this value varies greatly depending on the oceanic region (range: 2–50%) (Buesseler, 1998; Ducklow et al., 2001; Karl et al., 1996). The global estimate of the POC settling flux is in the order of 10 pg C per year, which largely exceeds the corresponding flux mediated by DOC (Hansell, 2002). Thus, the settling of POC is a key process that regulates the magnitude and variability of the biological carbon pump in the oceans (Honjo et al., 2014;

Sanders et al., 2014).

1.1.2 Organic aggregates play an important role in the vertical delivery of POC

POC is a complex mixture of diverse particles with various chemical compositions and physical features. These particles include both living and non-living forms, the latter consisting of polymeric substances excreted by organisms, fecal pellets, abandoned organismal structures (e.g., larvacean houses and exuviae), and detritus from decaying organisms (Stemmann and Boss, 2012; Verdugo et al., 2004; Yamasaki et al., 1998). These particles readily stick together in seawater, owing to hydrophobic interactions, ionic bonds, and entanglement (Johnson et al., 1994), forming "organic aggregates" that are composed of smaller particles. The process of aggregate formation is important since larger particles usually settle faster than smaller particles and enhance the vertical settling flux of POC. In fact, analyses of the materials collected by sediment traps deployed in the oceans have often revealed the abundance of aggregates (Herndl and Reinthaler, 2013; Honjo et al., 2008), indicating that they play a major role in mediating vertical carbon delivery (Grossart et al., 2006; McDonnell and Buesseler, 2012; Simon et al., 2002).

1.1.3 Transparent exopolymer particles (TEP): a major component of marine organic aggregates

In the 1990s, investigators found that many polymeric aggregates in seawater were within the size range of <2 to >100 μm (Alldredge et al., 1993; Mari and Kiorboe, 1996; Passow, 2002). These aggregates were invisible (transparent) under conventional light microscopy, but could be stained with Alcian blue, which binds acidic polysaccharides (Mopper et al., 1995; Passow, 2002). As a new class of marine organic aggregates, these so-called "transparent exopolymer particles" (TEP) (Alldredge et al., 1993; Passow and Alldredge, 1995) attracted the interest of oceanographers and marine ecologists, who recognized their potential importance in the promotion of large aggregate formation and as a food resource for marine detritivores. Later studies were indeed able to show that TEP are abundantly produced by various marine organisms, including algae and prokaryotes (Cowen, 1992; Engel and Passow, 2001; Passow, 2002; Stoderegger and Herndl, 1998; Sugimoto et al., 2007), are an important contributor to total POC concentrations in seawater (Martín and Miquel, 2010; Passow et al., 2001), serve as a food source for zooplankton (Decho and Moriaty, 1990; Kepkay, 2000; Passow, 2002), and are a major component of sinking POC in the oceans (Alldredge et al., 1993; Azam and Malfatti, 2007). Moreover, TEP are sticky and act as a glue that enhances the coagulation of other, non-adherent particles in seawater. Some studies have reported that the large organic aggregates (ranging in size from millimeters to a few tens of centimeters) observed during the later period of phytoplankton blooms can be explained by the promotion of particle coagulation mediated by the TEP (Alldredge and Gotschalk, 1989; Riemann et al., 2000; Teeling et al., 2012)

produced by phytoplankton and bacteria (Engel, 2000; Passow, 2002). Thus, TEP are now recognized as a key component of marine particles (Burd and Jackson, 2009; Passow, 2002; Verdugo, 2012). However, the abundance, composition and physicochemical features of TEP are highly variable and dependent on environmental conditions and microbial community composition (Engel and Passow, 2001; Passow, 2002). There are many unknown aspects in the regulation of TEP dynamics in marine environments especially with regard to the control of TEP settling velocity, as discussed in the following sections.

1.1.4 Physicochemical properties of TEP

Although the constituents of TEP are chemically diverse and heterogeneous, their polysaccharide component is thought to strongly affect their integrity. Indeed, previous studies showed that the addition of glucosidase resulted in the disintegration of TEP (Passow, 2002; Smith et al., 1995). Analyses of the monomeric sugar compositions of TEP after acid hydrolysis showed that TEP are rich in fucose and rhamnose and, to a lesser extent, in arabinose, but are relatively depleted in glucose and galactose (Mopper et al., 1995; Passow, 2002; Zhou et al., 1998). The acidity of TEP is explained by the presence of carboxyl groups ($R\text{-}COO^-$) and halfester-sulfate groups ($R\text{-}OSO_3^-$) (Mopper et al., 1995; Passow, 2002; Passow and Alldredge, 1995; Zhou et al., 1998). As mentioned above, Alcian blue forms ionic bonds with acidic polysaccharides, but the actual mechanism of the reaction between the dye and the substrate is

not entirely clear (Horobin, 1988; Passow and Alldredge, 1995). The chemical compositions and structure of TEP largely determine their stickiness and other physicochemical properties (Burd and Jackson, 2009; Engel, 2000).

1.1.5 Geographic and vertical distributions of TEP in marine environments

Alcian blue has been widely used in colorimetric assays to determine the concentration of TEP in seawater. In these assays, xanthan gum (a polysaccharide excreted by bacteria) is generally used as a calibration standard (Passow and Alldredge, 1995) and the TEP concentration is often reported as "xanthan gum-equivalents". These values can be converted to carbon quantities using an appropriate conversion factor (Engel and Passow, 2001). In the following, published data on the distribution of TEP concentrations in marine environments are summarized (Table 1). Note that although TEP have been studied since the 1990s, data on their distribution are still limited in terms of geographic coverage. The data compiled in Table 1 are mostly from studies that focused on the coastal marine environments of temperate oceans (Bar-Zeev et al., 2011; Corzo et al., 2005; Garcia et al., 2002; Hong et al., 1997; Malpezzi et al., 2013; Ortega-Retuerta et al., 2009; Passow and Alldredge, 1995; Ramaiah et al., 2001; Riebesell et al., 1995). Relatively few studies have examined TEP distributions in high-latitude oceans and open oceans, except the Antarctic Ocean (Corzo et al., 2005; Hong et al., 1997; Ortega-Retuerta et al., 2009).

The available data indicate that TEP concentrations typically vary within the range of 50–300 μg xanthan gum equivalents L^{-1} (μg Xeq. L^{-1}), although values > 1000 μg Xeq. L^{-1} have been also measured during phytoplankton blooms (Passow, 2002; Passow et al., 2001; Ramaiah et al., 2001). TEP concentrations tend to increase with increasing chlorophyll a concentrations (an indicator of phytoplankton biomass), consistent with the notion that phytoplankton are an important source of TEP (Corzo et al., 2005; Hong et al., 1997; Passow, 2002). Some phytoplankton taxonomic groups, such as diatoms (Bacillariophyceae) and haptophytes (Prymnesiophyceae) (Passow, 2002), may excrete larger quantities of TEP than other groups. In a given region, TEP often display prominent patterns in vertical distributions, with higher TEP concentrations in the upper layer (euphotic zone) and lower concentrations with depth, following the vertical gradient of chlorophyll a distribution (Engel, 2004; Ortega-Retuerta et al., 2009; Passow and Alldredge, 1995). This pattern is consistent with the notion that TEP are abundant in the water layers where they are produced by phytoplankton (Corzo et al., 2005; Wurl et al., 2011). However, in some studies, TEP concentrations were apparently unrelated to the vertical distribution of chlorophyll a; instead, they were concentrated high in the pycnocline, which is the depth horizon where the vertical water density gradient is steep [the density gradient in the ocean is established by the vertical gradient of salinity (halocline), temperature (thermocline), or both] (Malpezzi et al., 2013; Mari et al., 2012; Wurl and Holmes, 2008). The presence of TEP concentration peaks in the pycnocline is important because it implies that the

bulk density of TEP is much lower than expected from the density of their polysaccharide components (1.6 g cm^{-3}; Harding, 1995; Rickwood, 1984) but close to the density of subsurface seawater (1.03 g cm^{-3}), indicating that TEP are highly porous. In a recent study, Kindler et al. (2010) showed that porous polysaccharide aggregates were indeed retained on the surface of the pycnocline because of the transient storage of surface water (low density) in the interstitial spaces of the aggregates, which slows the organic aggregate settling velocity. However, the factors that determine TEP porosity and settling velocity are still not entirely clear.

1.1.6 Size distribution of TEP

Aggregate size distribution is an important feature that may reflect the balance of aggregate production (coagulation) and decay (disintegration) in seawater, as described by the polymer assembly theory (Burd and Jackson, 2009; Chin et al., 1998; Verdugo, 2012). According to this theory, smaller aggregates stick together to form larger ones, while larger aggregates disintegrate to become smaller ones. Under equilibrium conditions, and at a given concentration of source polymers, aggregate size distribution is determined by the stickiness of the aggregates and other physicochemical factors, including pH, temperature, hydrostatic pressure, shear, and ion density (Fig. 1). Biological factors may also affect aggregate size distribution in seawater. For example, zooplankton can break up large aggregates during feeding, resulting in a shift in particle size distribution toward smaller particles (Jhonson et al., 1994).

Bacterial enzymatic hydrolysis of polymers may also be an important mechanism by which large aggregates disintegrate to produce smaller ones (Smith et al., 1995). Conversely, the excretion of sticky polymers (e.g., TEP) by bacteria and diatoms can result in the formation of large organic aggregates (flocs) that may contain intact cells as one of their constituents (Biddanda, 1985; Gardes et al., 2011; Grossart et al., 2006; Pomeroy, 1974). Thus, bacteria play a dual role in both the enlargement and the fragmentation of marine particles by serving as "coagulators" and "disintegrators" of organic aggregates in seawater. It also possible that different groups of bacteria play different roles in aggregate formation and disintegration. In support of this hypothesis, in a laboratory experiment, Gardes et al. (2011) found that a bacterium belonging to the genus *Marinobacter* was responsible for the enhancement of aggregate formation by a diatom, *Thalassiosira rotula*. These results imply that bacterial community composition is important in determining the role of bacteria in controlling aggregate size distribution. However, data are still scarce regarding the general applicability of these findings to natural marine environments.

1.1.7 Settling velocity of TEP

The settling velocity of aggregates is a key parameter that can greatly affect the vertical delivery of POC in the ocean via the biological carbon pump (see Section 1.1.1). Variations in the settling velocity of aggregates in aquatic systems have been described in theoretical models,

which differ depending on the Reynolds number (*Re*), a dimensionless quantity defined as the ratio of inertial to viscous resistances (White, 1974):

$$R_e = \frac{UD\rho_f}{\mu} \qquad \text{[Equation 1–1]}$$

where U is the settling velocity (cm s^{-1}), D is the equivalent spherical diameter of aggregate (cm), ρ_f is the density of seawater (g cm^{-3}), and μ is the viscosity of seawater (cm^2 s^{-1}). For smaller aggregates (Re <0.5), the settling velocity (U) is largely affected by the viscous resistance (White, 1974) and described as a function of the properties [D, density (ρ', g cm^{-3}) and morphology (φ, a dimensionless coefficient of form resistance)] of the aggregates, according to the Stokes equation (Oliver et al., 1981):

$$U = \frac{gD^2(\rho' - \rho_f)}{18\mu\varphi} \qquad \text{[Equation 1–2]}$$

where g is the gravitational acceleration (cm s^{-2}).

For larger aggregates ($Re \geqq 0.5$), U is predominantly affected by the inertial resistance (White, 1974) and described by the following model (Alldredge and Gotschalk, 1988b; Ploug et al., 2008):

$$U = \left[\frac{2g(\rho' - \rho_f)V}{\rho_f C_D A} \right]^{0.5} \quad \text{[Equation 1–3]}$$

where V is the volume of the aggregate (cm^3), A is the cross-sectional area of the aggregate (cm^2), and C_D is the drag coefficient (dimensionless). Equations 1–2 and 1–3 indicate that, regardless of the sizes of the aggregates, three inherent aggregate properties, i.e., size, density, and morphology, greatly affect the aggregate settling velocity.

Previous studies have emphasized the role of "ballast particles" as a controlling factor in the settling velocity of aggregates in seawater (Iversen and Ploug, 2010; Ploug et al., 2008). There are many kinds of high-density mineral particle constituents in seawater. They include the crystallized silica, or opal cell walls (so-called frustules; density, 2.1 g cm^{-3}) of diatoms, an algal group belonging to the *Bacillariophyta*; the calcium carbonate shells (density, 2.71 g cm^{-3}) of coccolithophores, an algal group belonging to the Haptophyta; and mineral dust particles of terrestrial origin (e.g., quartz, density, 2.65 g cm^{-3}) that are introduced into the ocean via atmospheric deposition. These high-density particles are readily incorporated into organic aggregates by coagulation and contribute to an increase in their bulk density (ρ), thereby serving as ballast particles that increase U (mineral ballasting hypothesis; Fischer et al., 2003; Armstrong et al., 2002; Francois et al., 2002). In support of this scenario, natural aggregates collected by sediment traps were found to contain an abundance of ballasting particles (Klaas

and Archer, 2002), and aggregate settling fluxes were shown to correlate positively with the mass of ballasting particles in aggregates (Honjo, 1997; Honjo et al., 2008; Sanders et al., 2010). However, according to Lam et al. (2011) and Fischer and Karakas (2009), aggregates containing large quantities of opal do not necessarily enhance vertical POC transport. This discripancy suggests that mineral ballasting alone cannot fully explain the regulation of aggregate settling velocity in marine environments.

Bacteria may affect the settling velocity of aggregates in seawater, for example, by altering aggregate size, porosity, and morphology (Azam and Malfatti, 2007; Passow and Alldredge, 1994). However, the relative importance of these bacterial actions in determining aggregate settling velocity in seawater has yet to be clarified fully and there are, as yet, no studies explicitly embedding a role for bacteria in theoretical models that describe the variability in aggregate settling velocity.

1.2 Objectives of the present study

The objectives of the present study were to address the distribution patterns of TEP and other particles in the Arctic Ocean (Chapter 2) and the regulation of aggregate settling velocity in seawater (Chapters 3 and 4). A general discussion of these two aspects is provided in Chapter 5.

Chapter 2: Localized accumulation and a shelf-basin gradient of suspended particles in the Chukchi Sea and the Canada Basin, western Arctic

Chapter 2 examines the distribution patterns of TEP and other particles in the Arctic Ocean. As mentioned in Section 1.1.5, the distribution of TEP in marine environments has been mostly examined in temperate coastal environments. The Arctic Ocean is one of the oceanic regions where data on TEP and other particles are severely limited. In the Arctic, the available data are from sea ice or in seawater around the ice (Juhl et al., 2011; Meiners et al., 2008). Whereas TEP distributions with a broad coverage of environments, including shelf, slope, and basin regions, have been largely ignored. TEP may play an important role in material cycling in the Arctic Ocean. The shallow, adjacent seas of the Arctic Ocean, such as the Chukchi Sea, are highly productive shelf regions (Arrigo and van Dijken, 2011; Dunton et al., 2005; Grebmeier et al., 2006) where phytoplankton are often dominated by diatoms and haptophytes during the annual ice retreat (Fujiwara et al., 2014). Because both phytoplankton groups are known to produce large amounts of TEP (Passow, 2002), these particles should be abundant in the shelf regions of the Arctic. By contrast, in the nutrient-depleted environments of Arctic basins, such as the Canada Basin, productivity is low (Forest et al., 2007; Moran and Smith, 2000). Therefore, the lateral transport of TEP from shelf regions to basins might play an important role in supporting productivity in the latter.

The hydrographic, physicochemical, and biological conditions of the Arctic Ocean are

rapidly changing in response to the dramatic effects of climate change (Hopcroft et al., 2008; Kirchman et al., 2009; Lee et al., 2012; Nishino et al., 2011). By examining TEP dynamics and associated material cycling in the Arctic Ocean, the dynamic features of Arctic ecosystems, and thus their response to climate change, can be better understood.

Chapter 3: Effects of attached bacteria on the settling velocity of organic aggregates in seawater

Chapter 3 addresses the effects of attached bacteria on aggregate settling velocity in seawater. As discussed in Section 1.1.7, attached bacteria can influence aggregate properties (size, density, and morphology), thereby changing the settling velocity. Previous studies have suggested that bacterial hydrolysis and excretion of polymers alter the properties of aggregates (Azam and Malfatti, 2007; Cowen, 1992; Passow and Alldredge, 1994; Stoderegger and Herndl, 1998; Sugimoto et al., 2007), although these complex bacterial effects on aggregate settling velocity have yet to be analyzed quantitatively. Attached bacteria may control aggregate settling velocity by modifying aggregate porosity and morphology. Bacteria actively proliferate on the surface of aggregates and in the interstitial spaces of aggregate matrices, cleaving polymer chains to create pores (Azam and Malfatti, 2007; Passow and Alldredge, 1994). Alternatively, bacteria may excrete sticky polymeric materials to fill interstitial spaces (Cowen 1992, Stoderegger & Herndl 1998, Sugimoto et al. 2007). Furthermore, the replacement of aggregate

matrices by bacterial cells may alter bulk aggregate density.

To understand how bacterial modification of the physical properties of aggregates affects settling velocities, the settling velocities of model aggregates with different degrees of bacterial colonization were examined. Data on the physical parameters of aggregates, including size, porosity, and morphology, were collected to investigate the dominant mechanism by which attached bacteria affect the settling velocities of organic aggregates in marine environments.

Chapter 4: Bacterial control of large organic aggregate formation in seawater

Chapter 4 examines whether attached bacteria affect the particle settling velocity by enlarging aggregate size. As noted in Section 1.1.6, bacteria play a dual role in the regulation of aggregate size. On the one hand, bacterial enzymatic cleavage of the polymer chains of aggregates may result in aggregate disintegration and size reduction (Azam and Malfatti, 2007; Passow and Alldredge, 1994). This process has been extensively investigated (Nagata et al., 2003; Smith et al., 1992; Ziervogel and Arnosti, 2008) and the results have been incorporated into the conceptual model of aggregate dynamics in marine environments (Nagata, 2008; Smith et al., 1995). On the other hand, bacteria may increase aggregate size and thus enhance aggregate settling, although this activity has not been well studied. Bacteria release large amounts of extracellular polymers and possess fibrillar appendages, depending on the bacterial type and growth conditions, which facilitate the formation of large organic aggregates

(Biddanda, 1985; Simon et al., 2002). Other studies found that the bacteria present in a diatom culture substantially enhance large aggregate formation, perhaps as a consequence of bacterial stimulation of extracellular polymer excretion by the diatom (Gardes et al., 2011).

To better understand the role of bacteria in the regulation of large organic aggregate dynamics in seawater, the effects of bacteria on the integration of model aggregates (size: ca. 0.01 cm, Chapter 3) suspended in seawater were investigated. Specifically, changes in aggregate abundance and mean volume were examined in rotating tubes in the presence and absence of live bacterial assemblages.

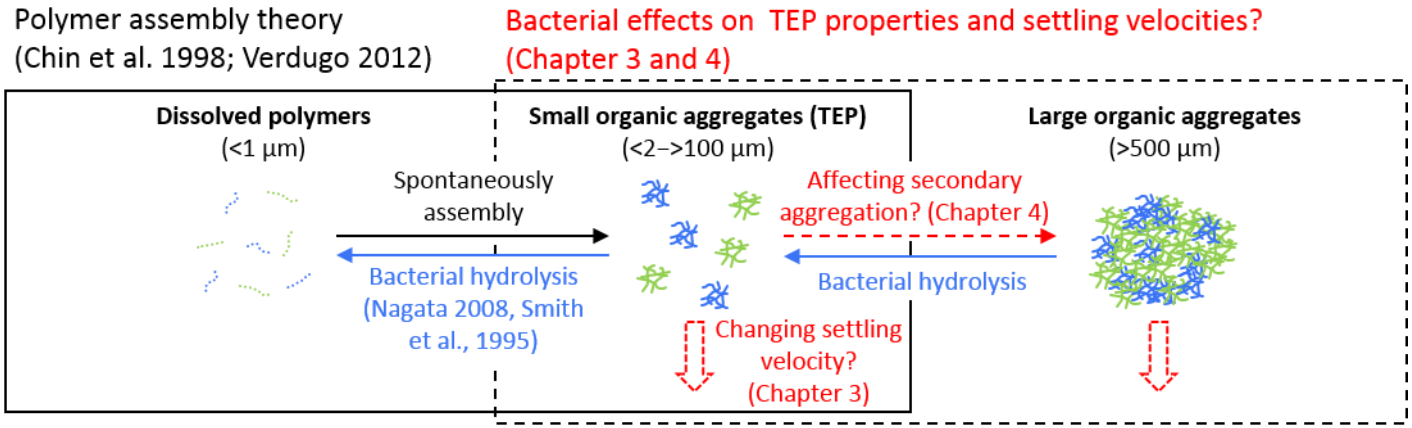

Fig. 1. Polymeric organic aggregation in seawater. This figure schematically depicts the hypothetical processes that I deal with in Chapters 3 and 4. This scheme is framed in the context of the gel assembly theory (Chin et al., 1998; Verdugo, 2012), with an emphasis of multiple roles of bacteria.

Table 1. The ranges of TEP and Chl.a concentration in different geographic locations. Mean values are given in parentheses wherever possible. –: no data

Location	Sampling depth and comments	TEP (μg Xeq. L^{-1})	Chl.a (μg L^{-1})	References
Pacific				
Monterey Bay, USA	0–50 m	46–310	–	Passow and Alldredge 1995
Santa Barbara Channel, USA	0–75 m	29–252	0.1–12	Passow and Alldredge 1995
Otsuchi Bay, Japan	0–15 m, Spring bloom	24–2321 (1344)	<1–12	Ramaiah et al. 2001
Atlantic				
Chespeake Bay, USA	0–24 m, Spring bloom	(1326)	–	Malpezzi et al. 2013
Gulf of Cadiz, Spain	0–100 m	<25–609 (118)	0.05–6.9	Garcia et al. 2002
eastern Mediterranean Sea	0–200 m	120–290	0.12–0.99	Bar-Zeev et al. 2011
Polar				
Norwegian Fjord	0–36 m	(193)	–	Riebesell et al. 1995
Bransfield Strait, Antarctica	0–100 m	0–346 (50)	(0.98)	Corzo et al. 2005
Ross Sea, Antarctica	0–150 m, Phaecystis bloom	0–2800 (308)	(3.61)	Hong et al. 1997
around Antarctic Peninsula	0–200 m	<2.2–48.9 (15.4)	0.01–5.36 (0.38)	Ortega-Retuerta et al. 2009

Chapter 2 Localized accumulation and a shelf-basin gradient of suspended particles in the Chukchi Sea and Canada Basin, western Arctic

2.1 Introduction

Suspended particles in marine environments have various origins, including inputs from rivers, in situ primary production, and polymer coagulation (Chester, 2000; Chin et al., 1998; Falkowski and Davis, 2004), and range from submicron (colloidal) (Koike et al., 1990; Wells and Goldberg, 1992) to macro particles (marine snow: millimeters or centimeters in size) (Alldredge and Silver, 1988). Transparent exopolymer particles (TEP), in a size range of 0.4 to >100 μm, are a category of suspended particles, and are mainly produced by phytoplankton and prokaryotes in pelagic environments (Mari and Kiorboe, 1996; Passow, 2002). Because TEP are abundant in seawater and contain a large amount of carbon, they can affect largely the carbon cycle in marine environments (Engel and Passow, 2001; Kepkay, 2000). Furthermore, TEP are considered to facilitate particle aggregation (the coagulation of living microbes, detritus, and inorganic particles) because of their stickiness (Burd and Jackson, 2009; Verdugo, 2012), and therefore they also have a significant role in enlarging particle size and material cycle in the ocean.

In the Arctic Ocean, rapid and large climate change can affect hydrographic conditions (Morison et al., 2012), sea ice extent (Kwok and Rothrock, 2009; Perovich et al., 2010), and freshwater input (Yamamoto-Kawai et al., 2009). These changes can also have a large influence on primary production, and carbon and other chemical cycles (Kirchman et al., 2009; Lee et al., 2012; Nishino et al., 2011). In general, high primary production is found in the shelf region of

the Arctic Ocean during summer when ice retreats (Arrigo and van Dijken, 2011). Organic materials produced in the shelf region are transferred laterally and make a large contribution to production in the basin (Forest et al., 2007; Moran and Smith, 2000). One of the major shelf regions in the Arctic Ocean is the Chukchi Sea, which is located in the western Arctic Ocean and is known to be a productive ocean (Grebmeier et al., 2006; Hopcroft et al., 2008) because large amounts of nutrient rich water enter from the Bering Strait and surrounding rivers (Aagaard et al., 2006; Springer and McRoy, 1993). However, there have been few studies of suspended particles in the Chukchi Sea [only in the slope area (Bates et al., 2005; Wegner et al., 2003)], which has limited our understanding of particle dynamics in the western Arctic Ocean.

In this study I collected data for suspended particle parameters [TEP, particulate organic carbon (POC), particle volume, and size distribution], prokaryote parameters (abundance and production), and environmental parameters from the shelf to the basin in the Chukchi Sea and Canada Basin during the late summer of 2012, to determine the detailed distribution of suspended particles from the Chukchi Sea to the Canada basin. The obtained data provide a basis for inferring the mode of suspended particle production and transport along the transect crossing the shelf and basin.

2.2 Materials and methods

2.2.1 Collection of seawater samples

Seawater samples were collected during a cruise of the R/V Mirai (MR12-E03, September 3 to October 17, 2012). Seawater was sampled from the Bering Strait to the Chukchi Shelf and the Canada Basin (Fig. 2–1 and Table 2–1) using 12-L Niskin bottles (Model 1010X, General Oceanics, Miami, FL, USA) mounted on a conductivity-temperature-depth (CTD) system (SBE11Plus, Sea-Bird Electronics, Bellevue, WA, USA). Surface water was collected using a clean bucket. Figure 2–1 shows the sampling stations and Fig. 2–2 shows the sections sampled. I divided these stations into two groups, shelf and slope-basin regions, according to their depths (Table 2–1). The large green plots in Fig. 2–1 indicate the stations where the suspended particle parameters [TEP, POC, particle volume, and particle size distribution (PSD)], prokaryote parameters (abundance and production), and other environmental variables were obtained. The black plots in Fig. 2–1 indicate the stations where only environmental variables were obtained. Samples for the measurement of TEP, prokaryote production, and abundance were collected in acid-washed 2- or 1-L polycarbonate bottles (Nalgene), and samples for POC measurement were collected in acid-washed 20- or 10-L polyethylene bottles. They were carefully transferred to an onboard laboratory for further processing, with gloves being worn to minimize contamination.

2.2.2 Particle volume and size distribution

Particle volume and the particle size distribution (PSD) in seawater [from surface to

200 m at stations with water depths greater than 200 m, or to the depth of 10 m above the seabed (hereafter, -10 m) at other stations] were measured by an optical measurement based on laser in situ scattering and transmissometry (LISST) [LISST-100X, Sequoia Scientific, Bellevue, WA, USA; Agrawal and Pottsmith (2000)]. The LISST instrument was mounted on a winch wire and lowered slowly through the water column, at a mean winch speed of 0.15 m s^{-1} and with a 1-s data collection interval. The depths for the particle volume and PSD measurements were calculated from the wire length and the time of transit from the surface to the deepest layer (200 m or -10 m) at each station. For depth calibration, a depth profiler (Alec Eiko2180, ALEC Co. Ltd., Kobe, Japan) was attached to the LISST instrument at five stations (Stas. 27, 29, 82, 89 and 93). By comparison with the depth obtained from a depth profiler, the error of the depth obtained from the above calculation was determined to be 0.26 ± 0.85 m (mean ± SD, n = 5).

Styles (2006) indicated that the LISST instrument might overestimate the particle volume in the upper LISST bins when salinity fluctuations (over 2 ppt) occur in a stratified field. Andrews et al. (2011) indicated that the LISST instrument might produce an underestimation in the lower LISST bins in environments with low particulate concentrations or high ambient light conditions (where the ratio of natural downwelling sunlight to scattered laser light sensed by the photodetectors was high). To minimize these effects, I excluded four of the upper LISST bins and eight of the lower LISST bins and used a range of 5.2–119 μm in the size classes (20 LISST bins). The integrated value across this size range was used as the particle volume (μL L^{-}

^{1}). Size classes in this range (5.2–119 μm) were also used for the PSD to calculate its slope using a power relationship (Gonzalez and Hill, 1998; Jouon et al., 2008); $N = k \times ESD^{m}$, where N is the number of particles per unit volume per size class (particle abundance L^{-1} μm^{-1}), k is a constant, ESD is the equivalent spherical diameter of particles in μm, and m (generally <0) indicates the particle size distribution of the sample. In this study, m was calculated from regressions between log [N] and log [ESD], and was used only where the coefficient of determination for regressions (r^2) was over 0.7.

2.2.3 TEP

Replicate seawater samples for the determination of TEP concentration (n = 3 replicates; 100–1000-mL seawater per replicate) were filtered through 0.4-μm-pore-size polycarbonate filters (47 mm diameter; Whatman, Maidstone, UK) with a vacuum of less than 15 mmHg, and stained with 0.02% w/v cationic dye Alcian Blue (8GX; Sigma-Aldrich Corp., St. Louis, MO, USA) dissolved in 0.06% v/v acetic acid (Passow and Alldredge, 1994). The filters were frozen at -20°C until colorimetric determination.

The filters were soaked in 80% sulfuric acid for 3 h and the absorbance at 787 nm was measured using a spectrophotometer (UV-1800, Shimadzu, Kyoto, Japan). The TEP concentration was expressed in terms of μg Gum Xanthan equivalent per liter (μg Xeq. L^{-1}). The value of TEP-carbon (TEP-C) was calculated using a conversion factor of 0.75 μg C (μg

Xeq.)$^{-1}$ (Engel and Passow, 2001; Passow, 2002).

2.2.4 POC

To determine the concentration of POC in seawater samples they were collected on a pre-combusted (450°C for 4 h) glass fiber filter (GF/F, Whatman). The filter was kept frozen until analysis (-20°C). The filter was fumed overnight with HCl (using the vapor method) to remove carbonates and then dried at 60°C for 24 h. POC was quantified using an elemental analyzer (NA-1500, Fisons Instruments, Beverly, MA, USA).

2.2.5 Prokaryote abundance

For the prokaryote abundance (PA), a 2-mL seawater sample was collected in a sterile cryogenic vial (Nalgene) and fixed by adding 100 μL of 20% glutaraldehyde (final concentration 1%). The fixed sample was frozen in liquid nitrogen and then stored in a deep freezer (-80ºC) until analysis. Following Yang et al. (2010), samples were diluted 10-fold with TE buffer in a 7-mL sterile test tube (Becton Dickinson, Franklin Lakes, NJ, USA) (10 mmol L^{-1} Tris-HCl, 1 mmol L^{-1} EDTA, pH 8.0, Nippon Gene Co., Tokyo, Japan) and stained with SYBR Green I (Invitrogen, Waltham, MA, USA, final concentration of 10^{-4} of commercial stock). After adding reference size beads (diameter 1 mm, Molecular Probes, Eugene, OR, USA), the samples were analyzed using a flow cytometer (FACSCalibur, Becton Dickinson)

equipped with a 15 mW, 488 nm air-cooled laser and standard filter set, with the event rate for each run being <400 events s^{-1}. The data were analyzed using CellQuest (Becton Dickinson). The value of prokaryote-carbon (biomass) (Prok-C) was calculated using a conversion factor of 12 fg C cell $^{-1}$ (Fukuda et al., 1998).

2.2.6 Prokaryote production

Prokaryote production (ProkP) was estimated from the rate of ^{3}H-leucine incorporation (Kirchman, 2001; Uchimiya et al., 2013). A 1.5-mL seawater sample was placed in a 2-mL sterile tube and 10 µL of ^{3}H-leucine (NET1166, PerkinElmer Inc., Waltham, MA, USA; specific activity 5.42 TBq $mmol^{-1}$, final concentration 10 nmol L^{-1}) were added. This mixture was incubated in the dark at in situ temperature (± 0.5ºC) for 2 h. Incubation was stopped by adding 80 µL of 100% w/v trichloroacetic acid (TCA), and then the sample was centrifuged at 14,000 rpm for 10 min using a microcentrifuge (Kubota 1130, Kubota, Osaka, Japan). After the extraction of the precipitate with 1 mL of 5% TCA and 1 mL of 80% ethanol, samples were completely dried and 1 mL of liquid scintillation cocktail (Ultima Gold, PerkinElmer) was added to the sample. The radioactivity was measured using a liquid scintillation counter (TRI-CARB 3110TR, PerkinElmer) and ProkP was calculated using a leucine-to-carbon conversion factor of 1.55 kg C mol^{-1}, assuming no isotopic dilution (Simon and Azam, 1989). For each sample, three replicates and one TCA-killed control were prepared.

The coefficient of variation among the triplicate samples averaged ca. 10%.

2.2.7 Environmental parameters

Environmental data were provided by the Japan Agency for Marine-Earth Science and Technology (JAMSTEC). Salinity, temperature, and potential density (σ_θ) were determined with a CTD system (SBE9Plus, Sea-Bird Electronics). The chlorophyll-a (Chl.a) concentration was determined by the extraction of Chl.a with *N*,*N*-dimethylformamide after the collection of suspended materials on glass fiber filters (GF/F, 25 mm, Whatman) using a fluorometer (model 10-AU; Turner Designs, Sunnyvale, CA, USA) (Welschmeyer, 1994). The value of Chl.a-carbon (Chl.a-C) was calculated using a conversion factor of 40 μg C (μg Chl.a)$^{-1}$ (Banse, 1977).

2.3 Results

2.3.1 Hydrographic and chemical variables

Water temperature ranged from -1.7 to 8.1°C, with higher values in the shallow layers (depth <30 m) of the shelf region (Fig. 2–2a). Salinity ranged from 22.9 to 35.0, with a distribution of low-salinity water in the shallow layers (depth <30 m), except for around Stas. 20 and 81 (Fig. 2–2b). Potential densities (σ_θ) varied from 18.8 to 28.1 g L^{-1} and a conspicuous pycnocline was observed at 10–30 m, except for around Stas. 20 and 81 (Fig. 2–2c).

The concentration of Chl.a varied in the range of <0.1–4.8 μg L^{-1}, with the highest

value observed in the surface layer of Sta. 89. The Chl.a concentration generally decreased from the shelf to slope-basin regions (Fig. 2–2d). The percentage of Chl.a-C to POC in the shallow layers (0–50 m) of the shelf and slope-basin regions was 29.3 ± 15.5 % (mean ± SD, n = 24) and 20.2 ± 15.4 % (mean ± SD, n = 32), respectively (Fig. 2–3).

2.3.2 Suspended particles

The TEP and POC concentrations, and the particle volume (determined by LISST) ranged from 43 to 645 μg Xeq. L^{-1}, from 8 to 622 μg C L^{-1}, and from 0.03 to 110.7 μL L^{-1}, respectively (Figs. 2e, 2f and 2g), with extremely high values of these parameters (a 'hot-spot' of suspended particles) at the bottom of the shelf region (Sta. 89). Fig. 2–4 shows typical vertical profiles of particle volume at four stations (Stas. 24, 29, 68 and 89) with water temperature, salinity, and potential density (σ_θ).

When a strong pycnocline formed (Stas. 29, 68 and 89), particles were distributed in a thin layer (a few to several meters). When a relatively weak pycnocline formed (Sta. 24), particles were distributed in a broad range (from a depth of 10 to 30 m). Compared to the surrounding seawater, a relatively high TEP (ca. 150 μg Xeq. L^{-1}) and particle volume (ca. 1 μL L^{-1}) were observed at a depth of around 100 m in the slope area (Figs. 2e and 2g).

The TEP concentration increased with increasing Chl.a concentration in the shallow layers (0–50 m) of both the shelf and slope-basin regions (Fig. 2–5). An empirical equation that

related the concentration of TEP to that of Chl.a was obtained using a linear regression model after a double logarithmic transformation. The following regression equation was derived: log TEP = 2.27 + 0.24 × log Chl.a (r^2 = 0.35, p <0.001, n = 60).

The concentration of TEP and POC and the particle volume generally decreased with increasing latitude (*NL*) (Fig. 2–6). Table 2–2 lists the mean values of these parameters for suspended particles in the shallow layers (depth 0–50 m). The concentrations in the shelf region were significantly higher than those in the slope-basin region (p <0.001). The slope of the PSD (m) in the shelf region was slightly (-0.39 vs -0.38) but highly significantly (p <0.001) steeper than that in the slope-basin region, reflecting a systematic shift in m toward larger values in the slope-basin region relative to the shelf region (Fig. 2–7). The percentage of TEP-C to POC in the shallow layers (0–50 m) of the shelf and slope-basin regions was 131.2 ± 55.9% (mean ± SD, n = 42) and 179.0 ± 65.0% (mean ± SD, n = 55), respectively (Fig. 2–3).

2.3.3 PA and ProkP

PA and ProkP ranged from 1.2 × 10^7 to 2.5 × 10^9 cells L^{-1}, and from <0.01 to 2.45 μg C L^{-1} d^{-1}, respectively (Figs. 2h and 2i). For these parameters, higher values were observed in the surface and shallow layers of the shelf region than in the slope-basin region. PA and ProkP were high near the bottom of the shelf region around Sta. 89, coinciding with a ‘hot-spot’ of suspended particles (Figs. 2e, 2f and 2g). Compared to the surroundings, a relatively high PA

(ca. 0.5×10^9 cells L^{-1}) and ProkP (ca. 0.5 µg C L^{-1} d^{-1}) were also observed at a depth of around 100 m in the slope area (Figs. 2h and 2i). The percentage of Prok-C to POC in the shallow layers (0–50 m) of the shelf and slope-basin region was 12.4 ± 6.4% (mean ± SD, n = 37) and 15.3 ± 6.1% (mean ± SD, n = 58), respectively (Fig. 2–3).

Table 2–3 lists the correlations between suspended particle parameters and hydrographic or prokaryote parameters. The concentration of suspended particles (TEP, POC and particle volume) tended to increase with increasing Chl.a, prokaryote parameters (PA and ProkP) and temperature (p <0.001). The concentration of TEP and POC increased with decreasing salinity (p <0.05 and p <0.001, respectively), whereas such a trend was not evident for particle volume (p = 0.06). The slope of PSD (m) increased with decreasing salinity (p <0.05), but there were no significant correlation between m and other parameters (p >0.05).

2.4 Discussion

2.4.1 TEP concentration in the western Arctic Ocean

The concentration of TEP in the western Arctic Ocean has been determined only in sea ice (and around the ice) (Juhl et al., 2011; Krembs et al., 2002; Meiners et al., 2008), and has not been determined in the wider area of seawater. This study was the first to measure it in detail in this region, and to compare the values to those reported for other locations in the literature (Table 2–4). The concentrations in the shelf and slope-basin regions were generally

higher than or equal to those reported in the upper layers of the water column in other marine environments, although the maximum values obtained in this study were lower than those reported during a phytoplankton bloom (>1000 μg Xeq. L^{-1}, Passow, 2002).

The percentage of TEP-C to POC (% TEP-C) was much higher than for Chl-a-C and Prok-C (Fig. 2–3). The % TEP-C in shelf and slope-basin regions were relatively high (>100%) compared to other marine environments (Table 2–5), which indicated that the western Arctic Ocean was a TEP dominant ocean. Large values of the %TEP-C ratio (>100 %) are sometimes observed in marine environments (Bar-Zeev et al., 2011; Engel and Passow, 2001). One of the reasons for the high % TEP-C value was likely to be the difference in the filter used for TEP and POC collection from seawater; i.e., a 0.4-μm pore-size filter for TEP and a 0.7-μm pore-size filter for POC. It is possible that the western Arctic Ocean contains a large amount of TEP in the size range of 0.4–0.7 μm. This notion is consistent with my LISST results indicating that the abundance of small particles were high in the investigated region (see below). Another reason for the large %TEP-C ratio was considered to be the conversion factor [0.75 μg C (μg Xeq.) $^{-1}$] used for the calculation of TEP-C. The conversion factor was determined from laboratory experiments using diatoms (Engel and Passow, 2001). The conversion factor could vary depending on species and growth condition, which may introduce an error to the estimation of TEP-C. However, TEP concentrations in the other studies listed in Table 2–5 were calculated using the same conversion factor [0.75 μg C (μg Xeq.) $^{-1}$]. A comparison with my

data indicated that the ratio of TEP to POC was relatively high in the western Arctic Ocean compared to other geographic locations.

It is generally believed that some kinds of phytoplankton species (e.g. diatoms) excrete large amounts of TEP (Passow, 2002). Hong et al. (1997) observed a high concentration of TEP when Haptophytes bloomed in the Ross Sea, Antarctic. Fujiwara et al. (2014) reported that Haptophytes dominated in relatively warm surface water (2–4^{o}C) in the same region of the western Arctic Ocean at the time of sea ice retreat during late summer 2008. Sea ice retreat was also observed during this study [September 2012; the ice melt was the greatest since records began in 1979 (Parkinson and Comiso, 2013)], which suggests that Haptophytes could have dominated during the cruise and excreted TEP to seawater.

TEP concentration increased with increasing Chl.a concentration in the shallow layers (0–50 m) of both the shelf and slope-basin regions (Fig. 2–5). Previous studies have examined the relationship between TEP and Chl.a, and the slope obtained in this study ($\beta = 0.24$) was the lowest among the available published data. Passow (2002) reported that the value of β decreased in situations with either low TEP production rates by phytoplankton or high TEP loss processes, mainly by prokaryotes. In addition, this study identified two other possible reasons for low β values: (1) the Chl.a concentration in the hot-spot (at the bottom of sta. 89) was relatively low compared to the TEP concentration, and (2) the TEP concentration in the slope-basin region was relatively high compared to the Chl.a concentration. The first reason indicated that TEP

was produced by other organisms in addition to phytoplankton. Prokaryotes were possible candidates because they are known to be TEP producers in some marine environments (Cowen, 1992; Stoderegger and Herndl, 1998; Sugimoto et al., 2007), which was supported by the relatively high PA and ProkP at the hotspot (Figs. 2h and 2i). Furthermore the TEP concentration was significantly correlated to PA (r = 0.55, n =144, p <0.001) and ProkP (r = 0.51, n =132, p <0.001) (Table 2–3), which also suggested that prokaryotes were related to TEP production. The second reason indicated that the transport of TEP from the shelf to the slope-basin regions occurred and created an area of low Chl.a and high TEP in the slope-basin region, which corresponded to the hypothesis of lateral transport of suspended particles (see below).

2.4.2 A hotspot of suspended particles at the bottom of the shelf

The concentrations of TEP and POC, and particle volume were extremely high at the bottom of the shelf (Sta. 89). The bottom depth at this station was deeper (by 4–22 m) than at the adjacent stations (Fig. 2–1 and Table 2–1). This hollow is called Hope Basin and is a geographical feature that readily accumulates sediments (Verzhbitsky et al., 2008). At this station the highest concentration of Chl.a (4.8 μg L^{-1}) was observed in the surface layer and relatively high concentrations (2.5 μg L^{-1}) were also detected at the bottom layer (Fig. 2–2d), which suggested that organic substances produced at the surface might settle to the bottom. The fact that high primary production was often observed around this station (Dunton et al., 2005;

Grebmeier et al., 2006) supported the notion of a large supply of organic substances to the bottom. Because it is believed that a large amount of TEP is produced after a phytoplankton bloom (Passow, 2002), it is reasonable to assume that post-bloom phytoplankton settling to the bottom might lead to the formation of a TEP hotspot. At the same station, a relatively high prokaryote abundance and production were observed in the bottom layer (Figs. 2–2h and 2–2i), which implies that organic substances derived from phytoplankton were decomposed by prokaryotes. However, prokaryotes can also produce TEP during decomposition (Cowen, 1992; Stoderegger and Herndl, 1998; Sugimoto et al., 2007) and the prokaryote hydrolysis of polymers from phytoplankton cells can enhance the formation of free TEP (Passow, 2002; Smith et al., 1995). Thus, prokaryotes could have contributed to the formation of a TEP hot spot near the bottom of the shelf.

2.4.3 Possible lateral transport of aggregates and the implications for material cycling in the western Arctic Ocean

A TEP concentration gradient was observed from the shelf to basin in the upper 50 m of the water column (Fig. 2–6a), which suggests that TEP produced in the shelf region might be transferred to the slope-basin region by the water current from the Bering Strait to the Canada Basin (Aagaard et al., 2006; Hopcroft et al., 2008). The distribution of POC and particle volume also had the same gradient (Figs. 2–6b and 2–6c), with values in the shelf region being

significantly higher than those in the slope-basin region. Note that the TEP and POC concentration gradients might not completely describe their distributions. Although a high particle volume was observed in the thin layer (a few to several meters) near the pycnocline, such distribution pattern was not detected for TEP and POC, which is possibly due to the low vertical resolution (the interval of sea water sampling was >10 m). Thus, TEP and POC concentrations were likely underestimated in both the shelf and slope-basin regions.

The slopes (*m*) of the PSD determined in this study are within the corresponding values reported in other marine environments (*m* = 3–5, Jonasz and Fournier, 2007; Reynolds et al., 2008). The higher particle volume and steeper PSD slope in the shelf region indicated that relatively small particles dominated in the shelf region compared to the slope-basin region, suggesting that particle aggregation (size enlargement) occurred (Reynolds et al., 2008) along the lateral transit from the shelf to the basin. Given high TEP concentrations observed in the shelf region, TEP could have contributed to this particle aggregation process as I discuss below.

My data revealed that particle volume was high in a thin layer at the pycnocline, both in the shelf and slope-basin regions. These results suggest that non-settling (or slowly-settling) particles accumulated on the density interface and could have been transported laterally from the shelf to slope-basin regions. Accumulation of particles at the density interfaces has been reported in other marine environments (Malpezzi et al., 2013; Mari et al., 2012; Wurl and Holmes, 2008). Although I did not determine chemical properties of particles accumulated on

the pycnocline, I consider that TEP contributed to the formation of these particles. In support of this notion, TEP-induced aggregation is generally known to result in the formation of less dense, porous aggregates (Azetsu-Scott and Passow, 2004), which can accumulate on density interfaces due to slow solute exchange between inside and outside of the aggregates (Kindler et al., 2010). These aggregates can become even more porous and less easily settlable due to the action of attached bacteria that cleave aggregate polymers (see Chapter 3). The increasing aggregate concentration could further accelerate the aggregation of particles entrained at the shear interfaces (Alldredge and Crocker, 1995; Burd and Jackson, 2009; Gallager et al., 2004). In addition, salinity-induced aggregation (Thill et al., 2001) might also occur in this region because haloclines were observed at almost all stations.

In addition to the thin layer at the pycnocline, I also observed relatively high concentrations of particles and TEP in the deeper layer (around 100 m) of the slope area, suggesting that suspended particles were also transported in deeper layers. In the investigated region, it has been suggested that the residue of shelf-derived primary production (Ashjian et al., 2005) and iron (Hioki et al., 2014) can be transported from the slope to the basin in the same layer. These materials might contain or be adsorbed to TEP and TEP-induced aggregates.

Previous studies conducted in the western Arctic Ocean have reported a high concentration of particles around the halocline in the Chukchi and Beaufort seas (Bates et al., 2005), and in the slope area of the Laptev Sea (Wegner et al., 2003). However, this study is the

first to show the distribution of suspended particles in detail and over a wider area. My results have improved the understanding of particle dynamics in this region and imply the lateral transport of TEP-induced aggregates from the shelf to the basin at the pycnocline (depth of 10–30 m) and in the deeper layer (around 100 m). These processes might have a significant role in supporting reproduction and food webs in the nutrient-depleted basin area of the western Arctic Ocean (Forest et al., 2007; Moran and Smith, 2000). It is important for further research to quantify the transport of aggregates and clarify their contribution in the basin area in this region.

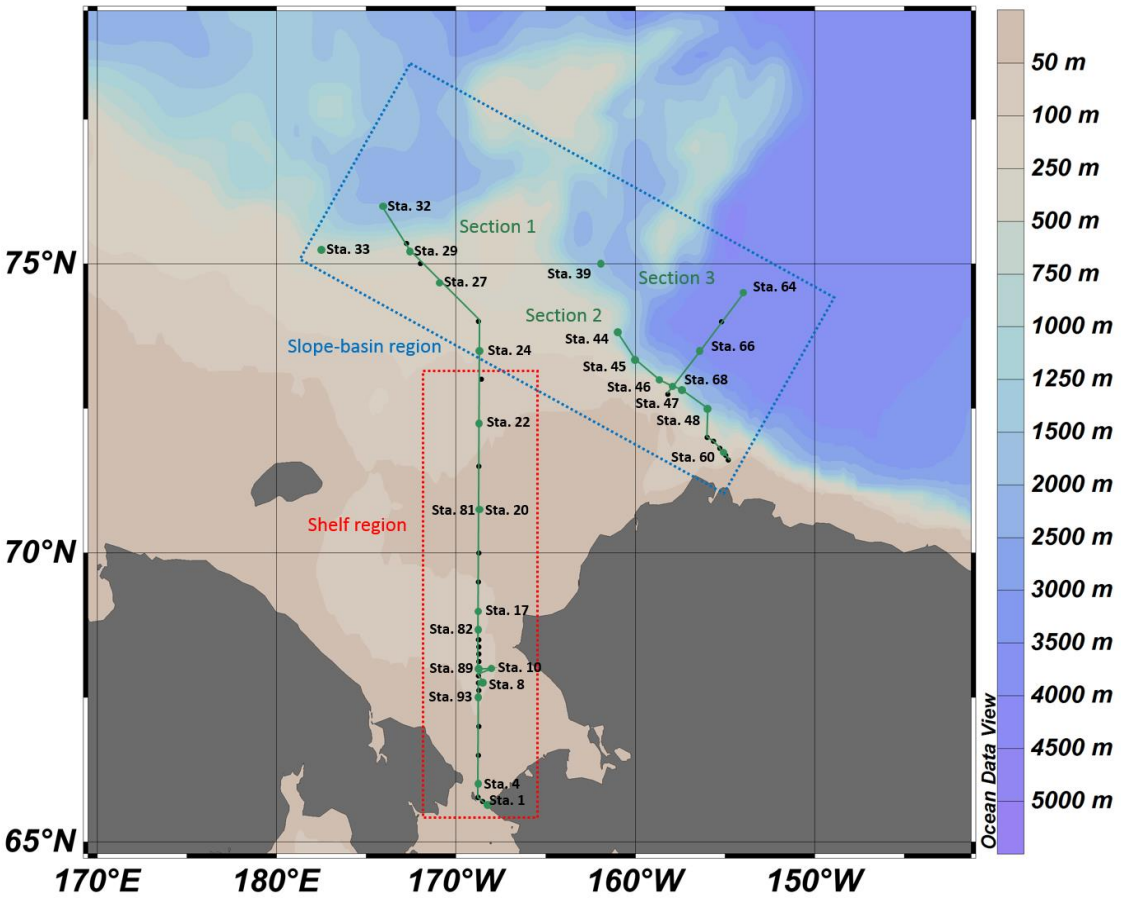

Fig. 2–1. Locations of the sampling stations during the MR12-E03 cruise. The map was created using Ocean Data View (http://odv.awi.de/). Dotted squares separate stations into shelf and slope-basin regions (see text). Stations along 3 sections were used to create contour graphs (Fig. 2–2).

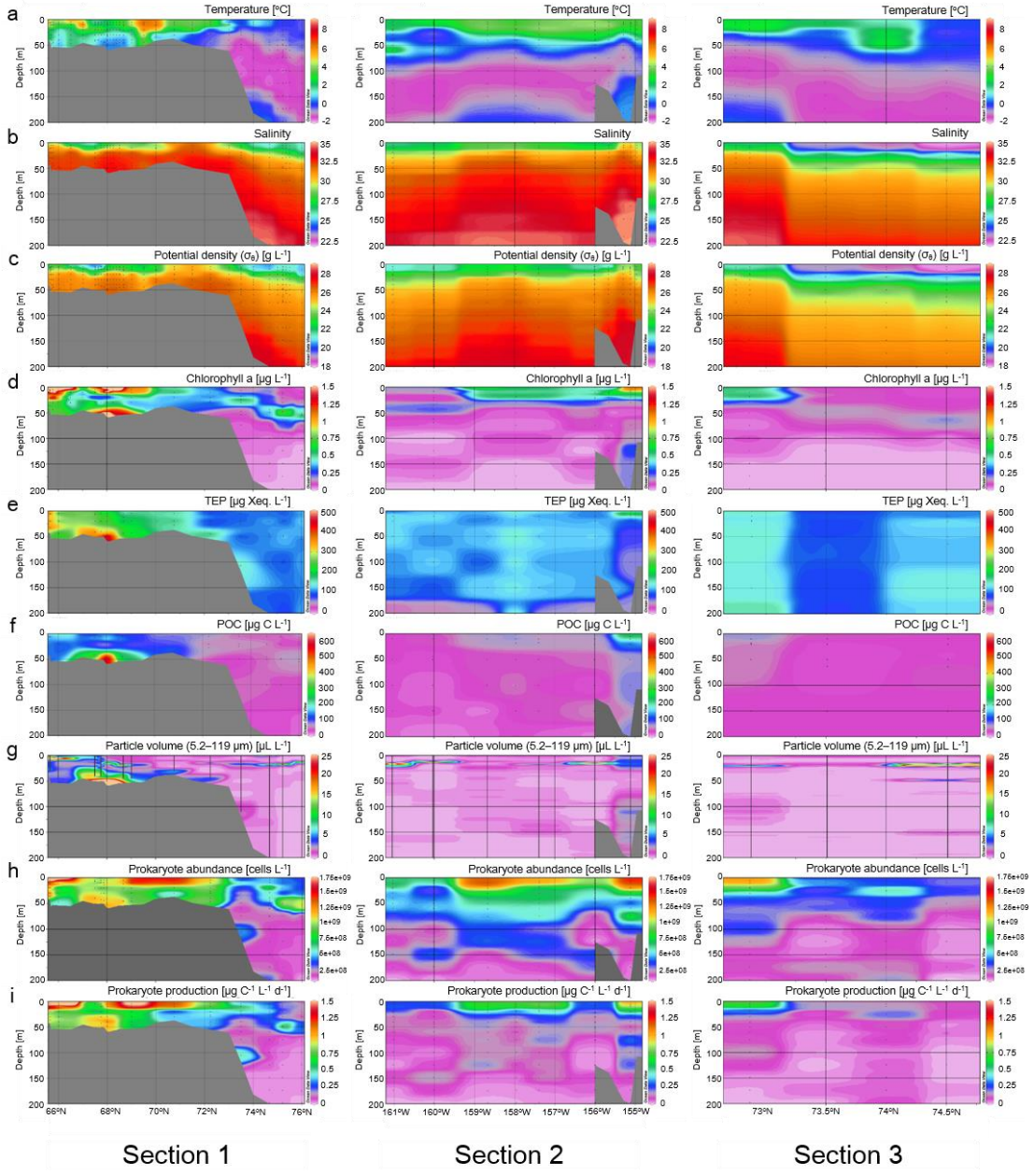

Fig. 2–2. Spatial istribution of environmental, suspended particles and prokaryote parameters in Chukchi shelf, slope and Canada basin. Figures indicate the spatial distribution of (a) Temperature, (b) Salinity, (c) Potential density (σ_θ), (d) Chlorophyll a, (e) TEP, (f) POC, (g) Particle volume (5.2–119 µm), (h) Prokaryote abundance, (i) Prokaryote production. 3 sections are arranged in Section 1 (left), section 2 (middle) and section 3 (right).

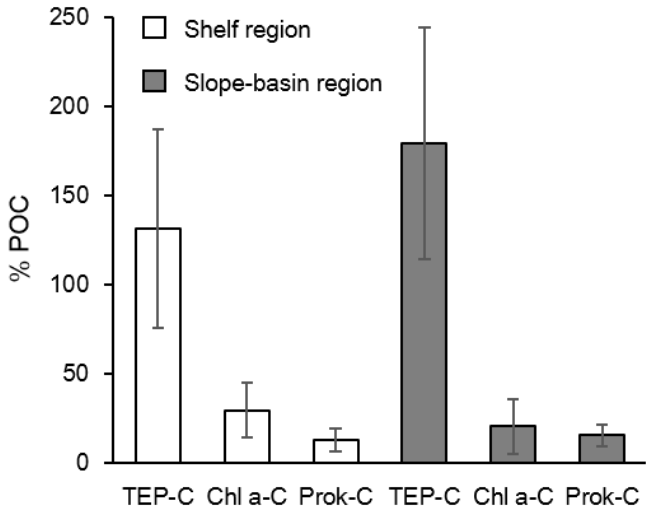

Fig. 2–3. The percentage of TEP-C, Chl.a-C and Prok-C to POC in both shelf and slope-basin regions in the upper 50 m. *n* = 42 and 55; TEP-C, *n* = 24 and 32; Chl.a-C, *n* = 37 and 58; Prok-C, for shelf and slope-basin regions, respectively.

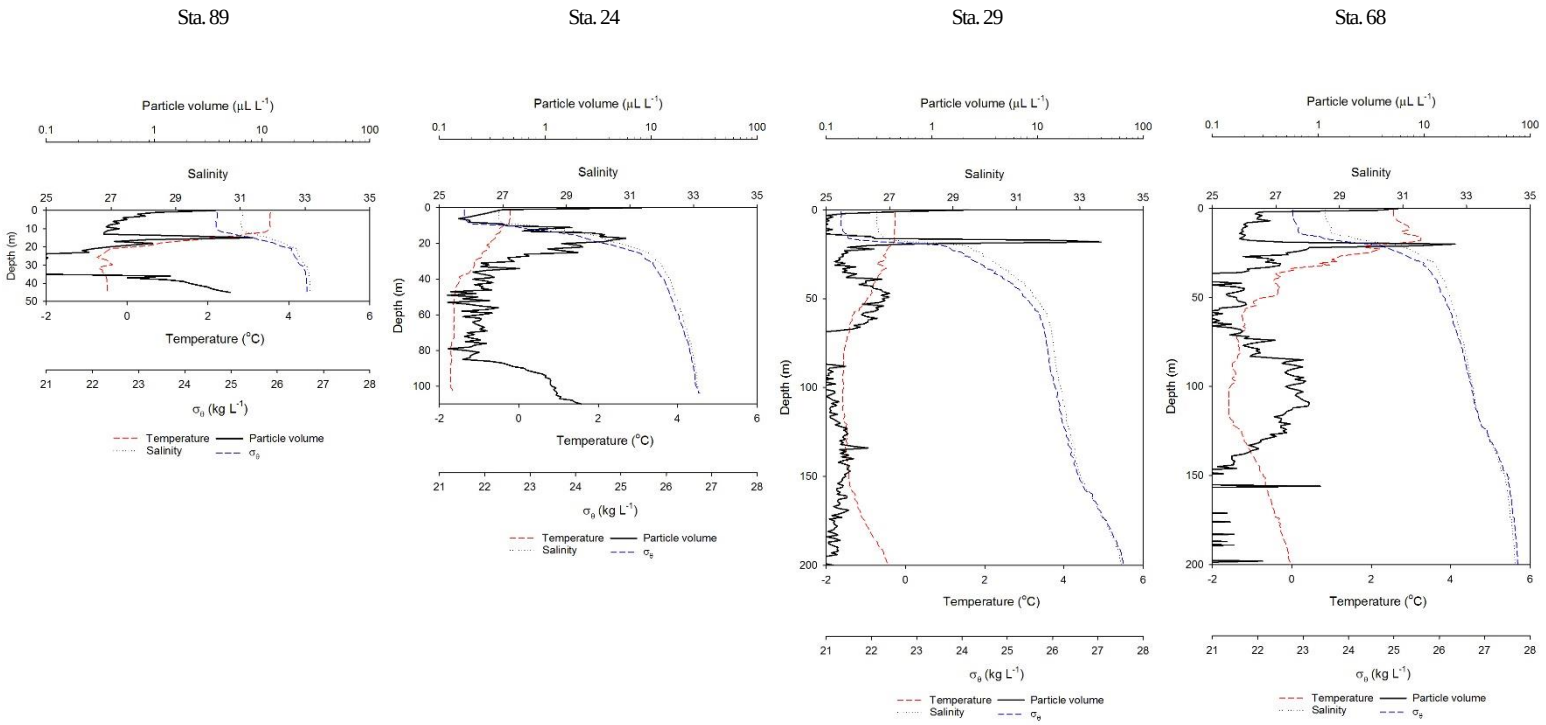

Fig. 2–4. Vertical profiles of particle volume and environmental parameters [water temperature, salinity and potential density (σ_θ)] at six stations (Stas. 89, 24, 29, and 68). The intervals of depth are 1 m for particle volume and environmental parameters.

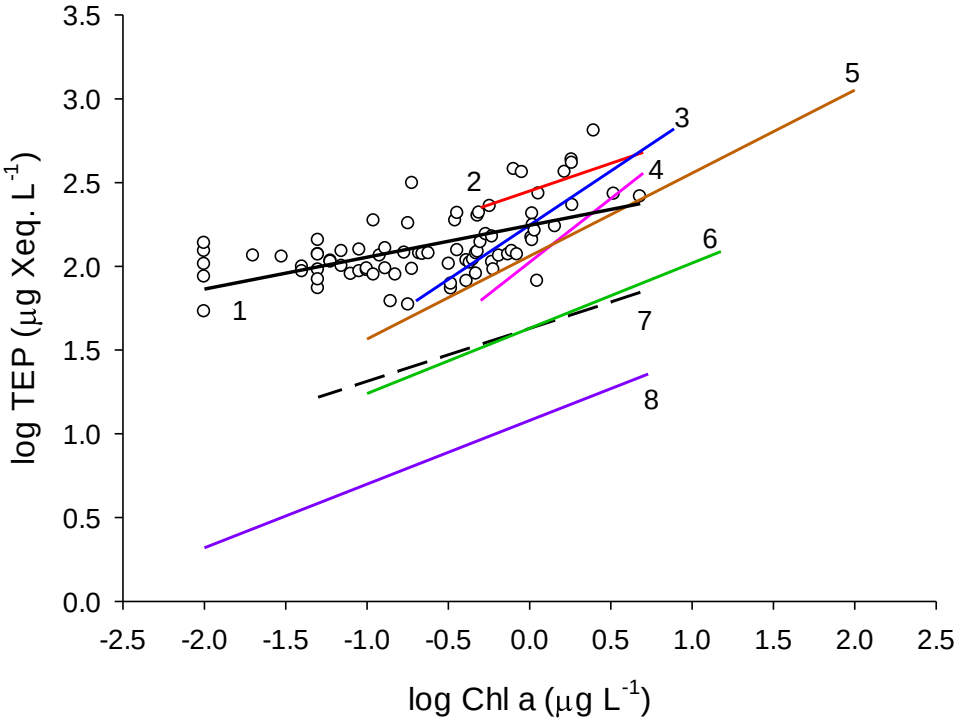

Fig. 2–5. Relationship between TEP and the Chl.a concentration in the upper 50 m of the shelf and slope-basin regions with a linear regression line (line 1, see text for the regression equation). For comparison, regression lines reported in the literature are also shown. α and β indicate the *y*-intercept and slope, respectively, for a linear regression model after a double logarithmic transformation; log TEP (µg Xeq. L^{-1}) = α + β × log Chl.a (µg L^{-1}); line 2, α = 2.45, β = 0.33, (Engel, 1998 in Passow, 2002); line 3, α = 2.25, β = 0.65, (Hong et al., 1997); line 4, α = 2.03, β = 0.76, (Passow, 2002); line 5, α = 2.06 and *β* = 0.50, (Ramaiah and Furuya, 2002); line 6, α = 1.63, β = 0.39, (Passow and Alldredge, 1995); line 7, α = 1.63, β = 0.32, (Corzo et al., 2005); line 8, α = 1.08 and β = 0.38, (Ortega-Retuerta et al., 2009).

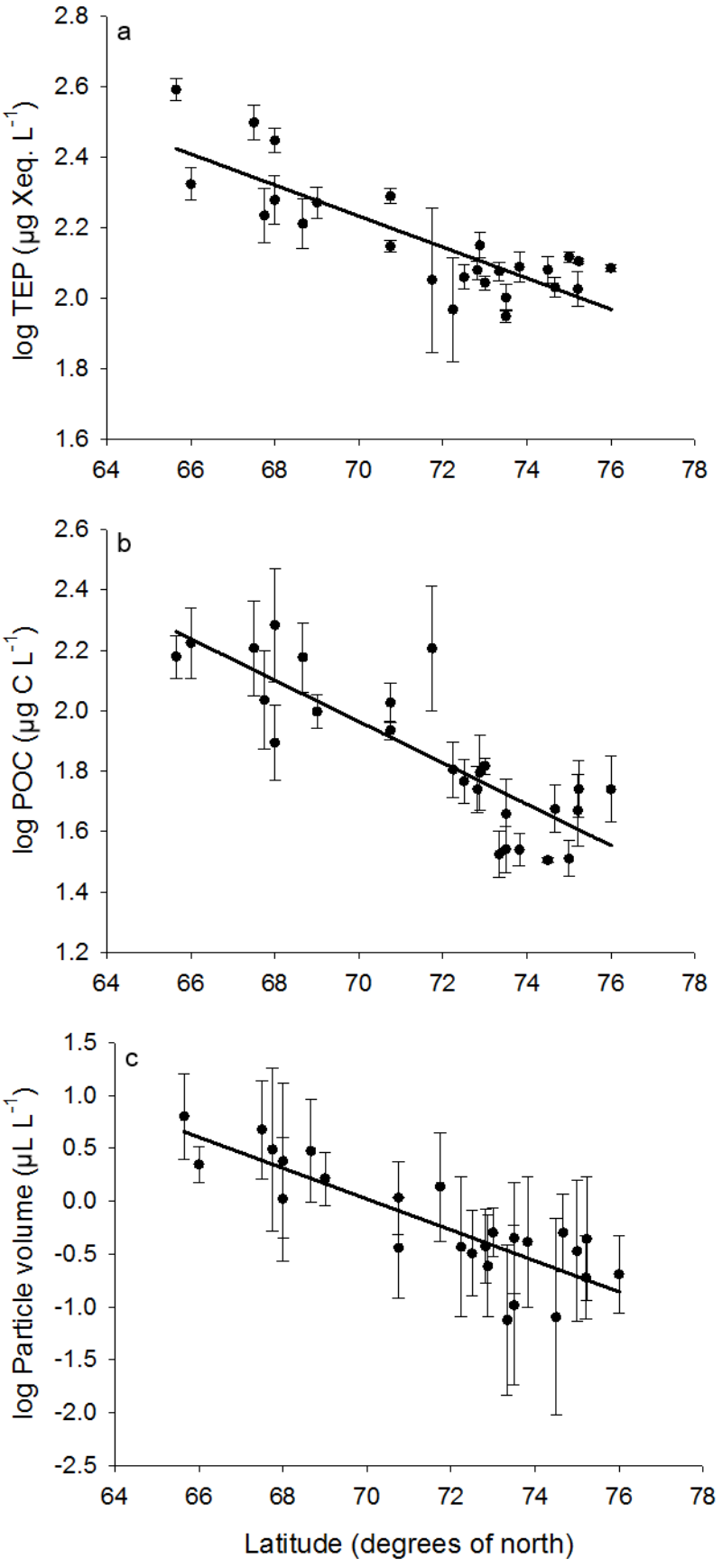
a
log TEP (µg Xeq. L-1)
2.8
2.6
2.4
2.2
2.0
1.8
1.6
64
66
68
70
72
74
76
78
b
log POC (µg C L-1)
2.6
2.4
2.2
2.0
1.8
1.6
1.4
1.2
c
log Particle volume (µL L-1)
1.5
1.0
0.5
0.0
-0.5
-1.0
-1.5
-2.0
-2.5
Latitude (degrees of north)

Fig. 2–6. Relationships between latitude and suspended particles (a) TEP, (b) POC and (c) particle volume in the upper 50 m. Plots are mean ± SD of each station (n = 3–5 for TEP and POC, n = 184–365 for PV) Solid lines are linear regressions after a logarithmic transformation of Y variables. log TEP = – 0.044 × NL + 5.31 (r^2 = 0.67, p <0.001, n = 26), log POC = – 0.068 × NL + 6.75 (r^2 = 0.69, p <0.001, n = 26), and log PV = – 0.146 × NL + 10.25 (r^2 = 0.70, p <0.001, n = 26)

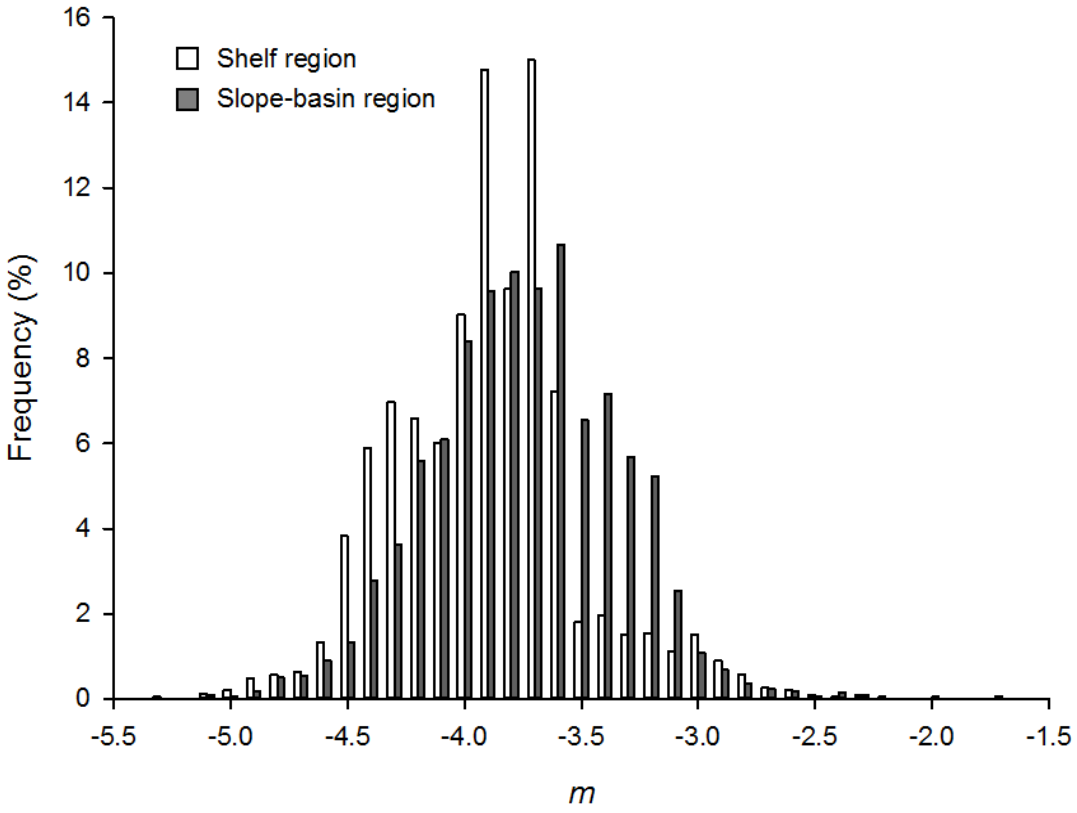

Fig. 2–7. Frequency distribution of *m* for particle size distributions in shelf and slope-basin regions. *n* = 2327 and 2202 for shelf and slope-basin regions, respectively.

Table 2–1. Locations of the sampling stations during the MR12-E03 cruise.

Region	Sta. #	Latitude_ North (Degree)	Longitude_ West (Degree)	Bottom depth (m)	Sampling date
Shelf	1	65.6	168.3	43	09/13/2012
	4	66.0	168.8	54	09/14/2012
	8	67.8	168.5	50	09/14/2012
	8	67.8	168.5	50	09/14/2012
	10	68.0	168.0	55	09/14/2012
	17	69.0	168.8	53	09/15/2012
	20	70.8	168.7	37	09/15/2012
	22	72.2	168.7	55	09/16/2012
Slope-basin	24	73.5	168.7	118	09/16/2012
	27	74.7	170.9	233	09/17/2012
	29	75.2	172.6	453	09/17/2012
	29	75.2	172.6	460	09/17/2012
	32	76.0	174.0	2137	09/18/2012
	33	75.2	177.5	721	09/19/2012
	39	75.0	161.9	1987	09/20/2012
	44	73.8	161.0	1552	09/23/2012
	45	73.3	160.0	1390	09/23/2012
	46	73.0	158.7	1249	09/24/2012
	47	72.8	157.4	1008	09/24/2012
	48	72.5	156.0	1896	09/24/2012
	60	71.7	155.1	257	09/27/2012
	64	74.5	154.0	3851	09/29/2012
	66	73.5	156.4	3684	09/29/2012
	68	72.9	158.0	1573	09/30/2012
Shelf	81	70.8	168.7	37	10/02/2012
	82	68.7	168.8	54	10/03/2012
	89	68.0	168.7	59	10/03/2012
	93	67.5	168.8	51	10/04/2012

Table 2–2. The comparison of TEP, POC, particle concentrations and the slope of PSD (*m*) between shelf and slope-basin region.

Parameters	Region		Mann-Whitney Rank Sum Test
	Shelf	Slope-basin	
TEP (μg Xeq. L^{-1})	213.6 ± 87.7 (49)	116.9 ± 26.4 (60)	***
POC (μg C L^{-1})	144.3 ± 93.4 (44)	59.0 ± 43.8 (59)	***
Particle volume (μL L^{-1})	5.9 ± 32.2 (2991)	2.1 ± 21.1 (4575)	***
m	-3.9 ± 0.4 (2366)	-3.8 ± 0.0 (2241)	***

Values are means ± SD and *n* is given in parentheses. *** p <0.001

Table 2–3. Summary of the statistical parameters of Pearson correlations that relate suspended particle parameters to environmental or prokaryote parameters. PV: particle volume, *m* : the slope of particle size distribution

X variable	Y variable	*n*	*r*	*p*
Chl.a	TEP	81	0.54	***
	POC	79	0.72	***
	PV	105	0.33	***
	m	105	-0.04	0.70
PA	TEP	144	0.55	***
	POC	136	0.74	***
	PV	138	0.49	***
	m	138	-0.01	0.90
ProkP	TEP	132	0.51	***
	POC	123	0.80	***
	PV	127	0.51	***
	m	127	0.07	0.42
Temperature	TEP	152	0.49	***
	POC	143	0.60	***
	PV	227	0.31	***
	m	227	0.08	0.25
Salinity	TEP	150	-0.21	*
	POC	141	-0.32	***
	PV	230	-0.12	0.06
	m	230	-0.14	*

Note the concentration of TEP, POC, PV, Chl.a, and PA and ProkP were log transformed. *** $p < 0.001$, * $p < 0.05$

Table 2–4. The comparison of TEP and Chl.a concentration and prokaryote abundance reported from different geographic locations. Mean values are given in parentheses wherever possible. –: no data

Location	Sampling depth and comments	TEP (μg Xeq. L^{-1})	Chl.a (μg L^{-1})	PA (× 10^5 cells mL^{-1})	References
Santa Barbara Channel, USA	0–75 m	29–252	0.1–12	–	Passow and Alldredge, 1995
Gulf of Cadiz, Spain	0–100 m	<25–609 (118)	0.05–6.9	–	Garcia et al., 2002
eastern Mediterranean Sea	0–200 m	120–290	0.12–0.99	–	Bar-Zeev et al., 2011
Otsuchi Bay, Japan	0–15 m, Spring bloom	24–2321 (1344)	<1–12	3.1–9.9*	Ramaiah et al., 2001
Bransfield Strait, Antarctica	0–100 m	0–346 (50)	(0.98)	(3.61)*	Corzo et al., 2005
Ross Sea, Antarctica	0–150 m, Phaecystis bloom	0–2800 (308)	(3.61)	–	Hong et al., 1997
around Antarctic Peninsula	0–200 m	<2.2–48.9 (15.4)	0.01–5.36 (0.38)	0.6–17.6*	Ortega-Retuerta et al., 2009
Chukchi Sea, Camada basin, Arctic	0–50 m, Shelf	74–645 (222)	0.11–4.80 (0.9)	4.7–24.6 (11.5)	This study
	0–200 m, Slope–basin	43–272 (112)	0.01–1.22 (0.2)	1.0–15.0 (4.4)	

* Bacterial abundance (× 10^5 cells mL^{-1})

Table 2–5. The comparison of % TEP-C, % Chl.a-C and % Prok-C to POC reported from different geographic locations. Mean values are given in parentheses wherever possible. –: no data

Location	Sampling depth and comments	% TEP-C	% Chl.a-C	% Prok-C	References
Indian estuary	1 m below the surface, Coastal	2–23 (6)	8–84 (35)	1–18 (5)	Bhaskar and Bhosle, 2006
around Antarctic Peninsula	0–200 m	<2–37 (12)	(62)	(18)	Ortega-Retuerta et al., 2009
eastern Mediterranean Sea	near-surface depths	(93*)	–	–	Bar-Zeev et al., 2011
	deep, 300–1000 m	(>>100)	–	–	
South China	Estuary	(10)	–	–	Sun et al., 2012
Santa Barbara Channel, USA	0–75 m	(27)	–	–	Passow and Alldredge, 1995
Chukchi Sea, Camada basin, Arctic	0–50 m, Shelf	64–270 (131)	8–68 (29)	2–27 (12)	This study
	0–200 m, Slope–basin	25–362 (179)	3–68 (20)	4–27 (15)	

* Recalculation using the conversion factor of 0.75 μg C (μg Xeq.) $^{-1}$ (Engel and Passow 2001)

Chapter 3 Effects of attached bacteria on organic aggregate settling velocity in seawater

3.1 Introduction

Organic aggregates, including transparent exopolymer particles (TEP) and hydrogels, play an important role in the regulation of material cycling and food webs in marine ecosystems (Alldredge, 1979; Simon et al., 2002; Verdugo, 2012). Organic aggregate settling from the sunlit layer to the deeper layers of the oceans mediates the vertical delivery of organic carbon and other bioelements, representing an important regulatory element of carbon sequestration (De La Rocha and Passow, 2007; Fisher et al., 1991; Passow and De La Rocha, 2006) and a means of energy and nutrient supply to heterotrophic organisms in aphotic layers and on the seafloor (Alldredge, 1979; Grossart et al., 1998; Passow et al., 2001). Because the settling velocity of aggregates is a key variable that influences the length-scale of vertical carbon delivery and remineralization depth (Passow and Carlson, 2012), it is important to clarify the variability and control of aggregate settling velocities in marine environments.

Aggregate settling velocity is affected by the physical properties of aggregates including size, porosity, morphology, and association with ballast particles such as diatom frustules and coccolith shells (Iversen and Ploug, 2010; Ploug et al., 2008). These aggregate properties may reflect not only the composition of, and physicochemical interactions among, polymeric materials and other constituents (Chin et al., 1998; Verdugo, 2012) but also the modification of aggregate structures by attached microbes. Bacteria can actively proliferate on the surface and in the interstitial spaces of aggregate matrices, cleaving polymer chains to create

pores and reduce aggregate size (Azam and Malfatti, 2007; Passow and Alldredge, 1994). Alternatively, bacteria may excrete sticky polymeric materials to fill interstitial spaces and promote aggregate production (Cowen, 1992; Stoderegger and Herndl, 1998; Sugimoto et al., 2007). Furthermore, the replacement of aggregate matrices by bacterial cells may alter bulk aggregate density. However, the prevailing mode and net outcome of these complex bacterial actions in controlling organic aggregate settling velocities in seawater are not entirely clear.

To understand how bacterial modification of the physical properties of aggregates affects aggregate settling velocities, I examined the settling velocities of model aggregates with different degrees of bacterial colonization. Data on the physical parameters of aggregates, including size, porosity, and morphology, were collected to investigate the dominant mechanism by which attached bacteria affect the settling velocities of organic aggregates in marine environments.

3.2 Materials and methods

3.2.1 Preparation of model aggregate

I used compositionally defined, spontaneously assembled gels (Verdugo, 2012) as model aggregates to investigate bacterial effects on aggregate settling velocity with minimal effects of compositional variability of organic aggregates in natural environments (see 'Discussion'). The model aggregates were prepared using fucoidan (a sulfated polysaccharide

found in brown seaweed) and chitosan (a partially deacetylated derivative of the amino polysaccharide, chitin) according to a gel preparation protocol originally developed by Nakamura et al. (2008) for pharmaceutical purposes. Fucoidan was extracted from *Kjellmanialla crassifolia* (Gagomekombu) according to Nakamura et al. (2008). Gagome-kombu powder (10 g) (Toyonaka Matumae Konbu Honpo Corp., Osaka, www.kobuya.net) was added to 100 ml 70% by volume ratio (v/v) ethanol containing 0.1 M acetic acid in a 200 ml conical glass flask. After gentle mixing, the suspension was filtered through polycarbonate filters (10 µm pore size, 47 mm diameter; Whatman). The filtrate was air-dried and added to 200 ml 8.8 µM $CaCl_2$ solution. After boiling for 30 min, the extract was centrifuged (2330 × g) at room temperature for 10 min. The supernatant was filtered through polycarbonate filters (10 µm pore size, 47 mm diameter; Whatman). The filtrate was mixed with 2× volume of 99.5% ethanol (total volume, ca. 300 ml). The precipitated materials were collected on polycarbonate filters (10 µm pore size, 47 mm diameter; Whatman) and transferred to a 500 ml conical glass flask. The increasing volumes of NaCl solution (0.9% by weight to volume ratio [wt/vol], containing 10 mM EDTA-2Na) were slowly added to the precipitates until the mixture became clear (the total volume of NaCl solution added was ca. 75 ml). Precipitates that were not completely dissolved were eliminated by successive filtration through 2 types of glass fiber filter (GF/D and GF/C filters, 47 mm diameter; Whatman) and polycarbonate filters (0.8 µm pore size, 47 mm diameter; Whatman). The filtrate was mixed with 2× volumes of 99.5%

ethanol (total volume: ca. 150 ml) and centrifuged (2330 × g) at room temperature for 10 min. Finally, the precipitates (fucoidan extracts) were broken into small pieces with spatulas and air-dried in a flow hood. Fucoidan solution (2.1% wt/vol) was prepared by dissolving 16.6 mg fucoidan extract in 790 µl Milli-Q water (Millipore). Chitosan solution (3.8% w v^{-1}) was prepared by dissolving 1.25 g chitosan (LL-40, Yaizu Suisankagaku Industry, ex tracted from Chionoecetes opilo; nominal deacetylation rate: >80%) in 33.1 ml 190 mM HCl.

Model aggregates were prepared by mixing chitosan and fucoidan solutions according to Nakamura et al. (2008) with the following modifications. Before the preparation of aggregates, chitosan and fucoidan solutions (see above) were centrifuged at 1200 × g for 10 min at 23°C. The supernatant of each solution was successively filtered through 0.8 µm and 0.2 µm syringe filters (25 mm diameter, Acrodisc syringe filter with Supor®membrane; Pall) to remove particles. Then, 210 µl chitosan solution was added to 50 ml filtered (0.2 µm) seawater in a 50 ml polypropylene tube (BD Falcon Conical Centrifuge tube; Fisher Scientific). After gentle mixing, 790 µl clear fucoidan solution was added to the seawater and then mixed. At this stage, the formation of aggregates was observed. After storage of the suspension at 4°C for 3 h, aggregates that settled at the bottom of the tube were collected by removing the supernatant by aspiration (~10 ml solution remaining). Then, 40 ml of the filtered (0.2 µm) seawater was added to the tube. The aggregate suspension was filtered through a nylon mesh (Nitex screen, mesh size 200 µm; Wildlife Supply Company) to remove large aggregates. The aggregate suspension

(hereafter, 50 ml working suspension) was stored at 4°C for 3 h until it was used for the settling velocity experiments.

3.2.2 Collection of seawater samples and incubation of model aggregates

Surface seawater samples were collected using a plastic bucket at the shore of Oarai Beach, Ibaraki, Japan (36°19’3’’N, 140°35’29’E), on January 30 (water temperature: 10.1°C, salinity: 29.2), August 29 (24.0°C, 29.2), and November 15 (17.3°C, 28.8), 2011. Within 12 h of sampling, seawater samples were filtered through 0.8 μm polycarbonate filters (47 mm diameter; Whatman) to eliminate grazers and other eukaryotes. The filtrate was further filtered through 0.2 μm polycarbonate filters (47 mm diameter; Whatman) using negative pressure (<20 mmHg) to reduce the abundance of bacteria and minimize their effects on aggregate properties.

The 50 ml working suspension of aggregates and 500 μl autoclaved 20 mM Na_2HPO_4 solution were added to three 500 ml polycarbonate bottles (Nalgene; Nalge Nunc International) filled with 450 ml seawater (filtered at 0.8 μm or 0.2 μm). After incubation for 48 h at 23°C in the dark using an incubation shaker (TA-20RLS, Takasaki Scientific Instruments; shaking speed: 100 rpm), both aggregate preparations (those obtained from 0.8 μm and 0.2 μm filtration; hereafter, $AGG_{0.8}$ and $AGG_{0.2}$, respectively) were used for the determination of aggregate settling velocities and the characterization of aggregate properties.

3.2.3 Microscopic examination of aggregates and attached bacteria

Aggregate samples were fixed with 0.2 μm filtered 2% v/v (final concentration) glutaraldehyde (20% glutaraldehyde; Wako). In the January experiment, the aggregate size and abundance of attached bacteria were determined after SYBR Gold-Alcian Blue double staining (Sugimoto et al. 2007). Seawater samples were filtered through 0.02 μm aluminosilicate filters (25 mm diameter; Whatman). Filters were stained with 1% wt/vol Alcian Blue (8GX; Sigma-Aldrich) dissolved in 3% v/v acetic acid (Logan et al., 1994) and then stained with SYBR Green I (0.25% v/v, in a ratio of 1:400 of the supplied concentration diluted with Milli-Q filtered at 0.2 μm; Molecular Probes; Noble & Fuhrman 1998) for 10 min. The filters were mounted on slides using immersion oil (nd = 1.516; Olympus) and observed under an epifluorescence microscope (×1000, BX61; Olympus). Alcian Blue-stained aggregate images observed under the transmitted illumination were captured using a charge-coupled device camera (Olympus DP70; Olympus). The area and morphological features of aggregates (the ratio of long axis to short axis and the circularity) were analyzed using ImageJ software (v. 1.45 with Java, 1.6.0_20). The area was converted into the equivalent spherical diameter (ESD), allowing it to be classified into 5 size classes: 62 μm (56−66 μm), 73 μm (67−78 μm), 86 μm (79−92 μm), 101 μm (93−109 μm), and 119 μm (110−129 μm). Bacteria attached to the aggregates were counted using the epifluorescence optics optimized for SYBR Green I (filter set, U-MNIB2; Olympus). After imaging, the volumes of bacteria (μm^3) attached to aggregates were determined for

$AGG_{0.8}$ and $AGG_{0.2}$ from both their area and perimeter using ImageJ software (Massana et al., 1997).

In the August and November experiments, the abundance of attached bacteria was determined by the 4',6-diamidino-2-phenylindole (DAPI) staining method (Porter and Feig, 1980). Samples were filtered through 12 μm polycarbonate filters (25 mm diameter, Whatman) with a vacuum of <20 mm Hg. The filters were stained with DAPI (1 μg ml^{-1}) for 5 min, mounted on slides using immersion oil (Vectashield, from Vector Laboratories, and from Citifluor Limited), and observed under an epifluorescence microscope (×1000, BX61, Olympus) equipped with epifluorescence optics optimized for DAPI (filter set, U-MWU2, Olympus). The sizes of aggregates, detected as pale-yellow objects, were manually determined using a grid ocular micrometer and classified into the 5 size classes described above.

3.2.4 Abundance, size, and settling velocity of aggregates

Particle size distribution and particle volumes were measured by laser in situ scattering and transmissometry (LISST, LISST-100X, Sequoia Scientific; Agrawal and Pottsmith, 2000) (hereafter, aggregate 'size' refers to the ESD of the aggregate). The settling velocities of aggregates were determined using a settling column (300 ml volume, 15 cm travel path) attached to the chamber of the LISST-100X (Small Volume Horizontal Test Chamber; Sequoia Scientific) (Agrawal and Pottsmith, 2000). The aggregate settling velocity was estimated from

the decrease in aggregate abundance over time. The aggregate abundance data were collected every 30 s (up to 3 h) for each size class (the numbers of aggregates counted at time zero were 841 to 21693 for each size class) to determine the time (T_h, in seconds) at which the aggregate abundance became half of the initial aggregate abundance for a given size class. Then, the median settling velocity (W_{50}, cm s^{-1}, Owen 1971) was calculated by dividing the travel path (15 cm, the distance between the surface of sample seawater and the horizontal position of the LISST detector) by T_h (range: 900−8060 s).

3.2.5 Density of attached bacteria

In the August experiment, the density distribution of bacteria attached to aggregates (after 48 h incubation) was measured according to Inoue et al. (2007). To remove attached bacteria from aggregate matrices, aggregate structures were mechanically destroyed by filtration through a 0.8 μm syringe filter (25 mm diameter; Pall). First, 2 ml $AGG_{0.8}$ was filtered through the syringe filter, and the filtrate was discarded (I assumed that bacteria collected on the 0.8 μm filter represented those associated with $AGG_{0.8}$, although some attached bacteria might have passed through the filters). Then, 2 ml filtered sea water (0.2 μm) was passed through the same syringe filter. The filtrate was passed a second time through the same syringe filter. This operation was repeated 10 times to obtain a bacterial suspension. The recovery of attached bacteria was calculated as follows: (bacterial abundance determined for the bacterial

suspension obtained after aggregate mechanical destruction) / (attached bacterial abundance initially determined using the 0.8 μm pore size filters) × 100. Bacteria were enumerated by the DAPI staining method as described in 'Microscopic examination of aggregates and attached bacteria'. The recovery was 102.1 ± 16.8% (mean ± standard error [SE], n = 7).

To determine attached bacterial density, 1 ml attached bacterial suspension and a 0.1 ml solution of density marker beads (Amersham Biosciences) were layered on top of 9 ml Percoll gradient working solution. The working solution consisted of 30% v/v Percoll, 10% v/v of 10× phosphate buffered saline (pH 7.4), 2.34% wt/vol of NaCl and autoclaved Milli-Q (filtered through the 0.2 μm pore size filter) and was contained in a centrifugation tube (No. 7031; Seton Scientific). Then, the tube was ultra-centrifuged (50512 × g) for 20 min at 20°C (Optima XL-90 with SW40Ti rotor; Beckman Coulter). After centrifugation, the tubes were marked at equal distances from the surface layer of the solution to the bottom to divide it into 10 fractions. Then, 1 ml solution was withdrawn at each mark position, in descending order, by pricking the centrifugation tube wall with a 1 ml syringe with a needle (0.45 × 13 mm; Terumo). The bacterial abundance in each fraction was counted by epifluorescence microscopy (×1000, BX61; Olympus) after DAPI staining. Bacteria recovered in the top and bottom fractions contained bacteria with densities either lower (<1.033 g cm^{-3}) or higher (>1.086 g cm^{-3}) than the analytical limits of the present method. For the calculation of the weighted average density of the total attached bacterial assemblage, I assumed that the densities of bacteria collected in

the top and bottom fractions were 1.033 and 1.086 g cm^{-3}, respectively.

3.2.6 Aggregate porosity

The porosities of $AGG_{0.2}$ and $AGG_{0.8}$ obtained in the November experiment were estimated by comparing aggregate size distributions determined by LISST to those determined using a resistive pulse particle counter (Coulter counter; Multisizer II, Beckman Coulter) (Sterling et al., 2004). This method is based on different principles of 2 instruments to measure particle size distributions. LISST measures light scattering of particles (reflecting particle bulk volume), whereas a Coulter counter determines the electric resistance of particles (reflecting particle solid volume). For porous particles, the particle size distribution determined by a Coulter counter deviates to smaller size categories relative to that determined by LISST, reflecting the degree of porosity (Sterling et al., 2004). I used the following equation to derive the index of porosity (ε):

$$\text{Porosity } (\varepsilon) = 1 - \frac{V_C}{V_L} \qquad \text{[Equation 3–1]}$$

where V_C and V_L are the volume of aggregates (ml $aggregate^{-1}$) determined by the Coulter counter and LISST, respectively. V_C and V_L for each size class were estimated from the Coulter-based aggregate diameter (D_C) and LISST-based diameter (D_L), assuming that the aggregates

were spheres. Because the bins differed between D_C and D_L, I derived the abundance-D_L regression (log-log regression) for the LISST data to estimate the aggregate abundance (l^{-1} μm^{-1}) for the size category between 62 µm (N_{62}) and 119 µm (N_{119}). Then, D_C for the abundance range between N_{62} and N_{119} was compared to the D_L (derived from the abundance-D_L regression) belonging to the same abundance category.

3.2.7 Ectoenzymatic activity

In the August experiment, the activity of the bacterial ectoenzyme that potentially hydrolyzes aggregate polymer constituents (chitosan) was determined using a methylumbelliferyl (MUF) substrate, 4-MUF-N-acetyl-β-D-glucosaminide (Sigma-Aldrich) (Hoppe, 1983). Fluorescent substrate dissolved in 2-methoxyethanol was added to either total or syringe-filtered (0.8 µm) sample waters (final conc. 0.05 mM).The samples were incubated at 23°C for 2 min. After adding borate buffer (0.5 M boric acid with NaOH, pH 10), fluorescence (455 nm emission, 365 nm excitation) was determined using a fluorescence spectrophotometer (RF-1500; Shimadzu). The enzyme activity was calibrated using 4-methylumbelliferone (Sigma-Aldrich) as a standard. The enzyme activity associated with each aggregate ($AGG_{0.2}$ and $AGG_{0.8}$) was estimated by subtracting the enzyme activity determined for filtered samples from that determined for the total sample.

3.3 Results

3.3.1 Aggregate size distribution and total volume

After incubation for 48 h, both $AGG_{0.8}$ and $AGG_{0.2}$ displayed a similar unimodal size distribution with a peak at 119 µm in all experiments (Fig. 3–1). Total volume concentration of aggregates initially added was 97.5 ± 4.3 ppm (mean ± SE, n = 22), which was within the range of typical TEP volume concentrations reported in coastal waters (Passow, 2002). Aggregates belonging to the 62 to 119 µm size class were used to assess the effect of bacterial attachment on aggregate settling velocities. This size range was used because for smaller aggregates (<62 µm size class) the settling velocity was too low to be determined within the time frame of my measurement (up to 3 h) and because LISST could not capture sufficient numbers of settling events for larger aggregates (>119 µm size class).

3.3.2 Abundance and density of attached bacteria, and settling velocity

Aggregates were porous (Fig. 3–2a), clearly stained by Alcian Blue (Fig. 3–2b), and associated with bacteria (Fig. 3–2c). For both $AGG_{0.2}$ and $AGG_{0.8}$, bacterial abundance per aggregate generally increased with increasing aggregate size (Fig. 3–3). Empirical equations that relate attached bacterial abundance (ABA) to the diameter of aggregates (D in µm) were obtained using a linear regression model after a double logarithmic transformation. The following regression equations were derived: $\log ABA = -1.32 + (2.31 \times \log D)$ ($r^2 = 0.98$, $p <$

0.001, n = 15) for $AGG_{0.8}$ and log ABA = −1.51 + (2.04 × log D) (r^2 = 0.57, p < 0.01, n = 15) for $AGG_{0.2}$. For each size class, bacterial abundance associated with $AGG_{0.8}$ was much higher (3.2- to 10.1-fold) than the corresponding value for $AGG_{0.2}$. The differences in bacterial abundance between $AGG_{0.8}$ and $AGG_{0.2}$ were significant (p < 0.01, Student's t-test) for all size classes. In the January experiment, the average size of bacteria associated with $AGG_{0.8}$ was 0.47 ± 0.01 μm^3 (mean ± SE, n = 474), which did not differ significantly (p > 0.05, Student's t-test) from the average size of bacteria associated with $AGG_{0.2}$ (0.46 ± 0.02 μm^3; n = 181). The weighted average density of attached bacteria, determined for $AGG_{0.8}$ collected in the August experiment, was 1.064 ± 0.002 g cm^{-3} (n = 4). Note that this estimate has an error due to the inclusion of bacteria in either top or bottom fractions of the density gradient (these bacteria have densities either lower or higher than the analytical limits; see 'Materials and methods'). While the abundance of bacteria contained in the top fraction accounted for only 3.7 ± 1.6% (n = 4) of total attached bacterial abundance, the contribution of bacteria contained in the bottom fraction was relatively large (38.1 ± 7.1% [n = 4] of total attached bacterial abundance), suggesting that my estimate of average bacterial density might be too low.

The ranges of W_{50} values for $AGG_{0.8}$ and $AGG_{0.2}$ were 0.0025−0.0054 cm s^{-1} and 0.0056−0.0136 cm s^{-1}, respectively. For each size class, the W_{50} values for $AGG_{0.8}$ were lower (1.6- to 4.5-fold) than those of $AGG_{0.2}$ (Fig. 3–4). The differences in the W_{50} values between $AGG_{0.8}$ and $AGG_{0.2}$ were significant (p < 0.05, Student's t-test), except for the 62, 73, and 86

μm size classes in the August experiment (Fig. 3–4).

3.3.3 Aggregate ε, enzyme activity, and morphological parameters

The ε of $AGG_{0.8}$ and $AGG_{0.2}$ varied in the ranges of 0.932−0.981 and 0.719−0.929, respectively. The average ε of $AGG_{0.2}$ was significantly smaller than the corresponding ε of $AGG_{0.8}$ for each size class ($p < 0.05$, Student's *t*-test, Fig. 3–5). Empirical equations that relate ε to D were obtained using a quadratic regression model after a double logarithmic transformation. A quadratic rather than linear regression model was used because the r^2 value of the quadratic regression exceeded that of the linear regression for both $AGG_{0.8}$ and $AGG_{0.2}$. The following regression equations were derived: $\log \varepsilon = 1.214 + (0.719 \times \log D) - [0.166 \times (\log D)^2]$ ($r^2 = 0.73$, $p < 0.001$, $n = 20$) for $AGG_{0.8}$, and $\log \varepsilon = -2.704 + (4.409 \times \log D) - [1.040 \times (\log D)^2]$ ($r^2 = 0.76$, $p < 0.001$, $n = 20$) for $AGG_{0.2}$.

In the August experiment, the ectoenzymatic activity (hydrolysis rate of 4-MUF-N-acetyl-β-D-glucosaminide, mean ± SE, $n = 3$) of $AGG_{0.8}$ and $AGG_{0.2}$ was 4.00 ± 0.99 nM min^{-1} ml^{-1} and 0.03 ± 0.01 nM min^{-1} ml^{-1}, respectively, with the former being significantly ($p < 0.05$, Student's *t*-test) higher than the latter.

Results of morphological analyses of aggregates are tabulated in Table 3–1. Neither the long to short axis ratio nor the circularity differed significantly among different size classes for both $AGG_{0.8}$ and $AGG_{0.2}$ ($p > 0.05$, ANOVA). The average long to short axis ratios for

$AGG_{0.8}$ and $AGG_{0.2}$ were 0.596 and 0.584, respectively, which did not differ significantly from each other ($p > 0.05$, Student's *t*-test). The average circularities for $AGG_{0.8}$ and $AGG_{0.2}$ were 0.072 and 0.044, respectively. The former was significantly larger than the latter ($p < 0.001$, Student's *t*-test).

3.4 Discussion

3.4.1 Use of model aggregates to examine aggregate settling velocity

The model aggregates exhibited the key features of natural marine aggregates: they were spontaneously assembled polymeric aggregates that are abundant in marine waters (Chin et al., 1998; Verdugo, 2012); they were stainable by Alcian Blue, a critical feature that characterizes TEP (Alldredge et al., 1993); they contained sulfate and amino polysaccharides, which are the major constituents of TEP (Passow, 2002; Zhou et al., 1998); and their monomeric constituents, fucose and glucosamine, are ubiquitous and can be abundant in marine waters (Borch and Kirchman, 1997; Myklestad et al., 1997). Furthermore, my experiments modeled the fundamental features of microbe−aggregate interactions in marine systems, i.e. colonization, growth, and enzymatic cleavage of polymers (Azam and Malfatti, 2007; Nagata, 2008). Ectoenzymatic activities cleaving fucoidan and chitin have been detected in seawater (Gooday, 1990; Poulicek et al., 1998; Ziervogel and Arnosti, 2008), indicating that the model aggregates serve not only as attachment surfaces but also as carbon and nutrient sources for microbes. In

fact, in my experiments, $AGG_{0.8}$ were densely colonized by bacteria, with an abundance of 0.050 to 0.074 cells μm^{-2}. This is within the higher range of bacterial abundance reported to be associated with marine TEP within a similar size range of aggregates (0.006 to 0.079 cells μm^{-2}; Mari and Kiorboe, 1996; Passow, 2002; Schuser and Herndl, 1995). The average cell volume of bacteria associated with $AGG_{0.2}$ was relatively large (0.46 μm^3) and differed little from that of $AGG_{0.8}$, suggesting that a fraction of small bacteria initially contained in the 0.2 μm filtered seawater became larger during their growth on the substrate-rich aggregates. The bacterial growth on $AGG_{0.8}$ was accompanied by a substantial increase in ectoenzymatic activity, supporting the notion that bacteria cleaved polymer matrices during colonization and growth. Thus, my model aggregates represent a class of carbohydrate-rich aggregates that harbor dense bacterial communities. The following discussion will focus on the specific mechanisms underlying the regulation of model aggregate settling velocity.

3.4.2 Possible mechanisms of the reduction of aggregate settling velocity via bacterial colonization

The W_{50} values for $AGG_{0.8}$ were significantly (1.6- to 4.5-fold) lower than those for $AGG_{0.2}$. Settling velocities of $AGG_{0.8}$ would have been affected by the adsorption of submicron-sized TEP that existed in the 0.8 μm filtrate but not in the 0.2 μm filtrate. Although submicron-sized TEP are known to be abundant in natural seawaters, their contributions to total TEP

volumes are usually low (<1%), with typical volume concentrations being on the order of 0.1 to 1 ppm in coastal waters (Passow, 2002). These typical submicron-sized TEP volumes may account for only a small fraction (<1%) of the total volume concentration of the model aggregates in my experiments (97.5 ppm). Therefore, it is considered that the effects of the adsorption of submicron-sized TEP on the settling velocities of $AGG_{0.8}$, if any, were minimal. Rather, I consider that my results, to the best of my knowledge, are among the first indicating that bacterial colonization of aggregates can result in a significant reduction in the settling velocity of similar-sized aggregates.

To examine the mechanisms underlying this reduction in settling velocity, I used the Stokes model (Oliver et al., 1981) as a theoretical framework to relate the aggregate settling velocity (v, cm s^{-1}; hereafter, W_{50} is referred to as v for the theoretical considerations in this paragraph) to aggregate properties including size (D, the diameter of the particle in cm), mean density (ρ', g cm^{-3}), and morphology (φ, a dimensionless coefficient of form resistance):

$$v = \frac{gD^2(\rho' - \rho_0)}{18\mu\varphi} \qquad \text{[Equation 3–2]}$$

where g is gravitational acceleration (cm s^{-2}), μ is the viscosity of seawater (g cm^{-1} s^{-1}), and ρ_0 is the density of seawater (g cm^{-3}). Although this model does not perfectly describe the sinking of fractal organic aggregates in the sea (Logan and Wilkinson, 1990), it is useful for considering

the different impacts of size, density, and porosity on aggregate sinking velocities (De La Rocha and Passow, 2007). Because my comparison of v was made for aggregates belonging to the same size category (i.e. D is the same), the difference in v is ascribed to the difference in either ρ' (mean density difference) or φ (morphological effects). For the density effect, there are at least 2 potential mechanisms by which attached bacteria can reduce ρ'. First, bacterial growth may result in the replacement of a certain volume of polysaccharide matrices in aggregates by bacterial cells, which may then result in a reduction in ρ' (bacterial density is generally lower than polysaccharide density). Second, bacteria may increase the ε of aggregates due to the cleavage of polymers. This results in the replacement of polysaccharide matrices by seawater, leading to a reduction in ρ' (seawater density is lower than polysaccharide density). These 2 factors can be considered by the following mass balance equations:

$$\rho' = (1 - \varepsilon)\,\rho_S + \varepsilon\,\rho_0 \qquad \text{[Equation 3–3]}$$

$$\rho_S = (1 - \alpha)\,\rho_{pol} + \alpha\,\rho_{bac} \qquad \text{[Equation 3–4]}$$

where ρ_S (g cm^{-3}) is the density of the solid fraction consisting of polysaccharide matrices with a density of ρ_{pol} (g cm^{-3}) and bacterial cells with a density of ρ_{bac} (g cm^{-3}). ε is the fraction of seawater volume relative to the total aggregate volume, and α is the fraction of bacterial cell volume relative to the total solid volume of the aggregate. Eqs. 3–2, 3–3 and 3−4 can be

rewritten as follows:

$$v = \frac{gD^2(1-\varepsilon)\{(1-\alpha)\rho_{pol} + \alpha\rho_{bac} - \rho_0\}}{18\mu\varphi} \qquad \text{[Equation 3–5]}$$

This model assumes that the aggregates are nonpermeable (there is no advective flow through the aggregates), which is consistent with the suggestion that marine aggregates have very low permeability (Kindler et al., 2010; Ploug and Passow, 2007). Clearly, this assumption does not hold for all aggregate types in marine environments. In fact, for fast-settling, large aggregates (with diameters on the order of a few mm) containing ballast particles, apparent diffusivity within the aggregates has been reported to be high (Ploug et al., 2008). However, for the small (diameters 62 to 119 μm), slowly settling aggregates examined here, it is probably safe to assume that permeability barely influenced aggregate settling velocities (Logan and Hunt, 1987).

Using Eq. 3–5 and the parameters obtained in the present study (ε, α, and ρ_{bac}) and from the literature (Table 3–2), I examined the relative contribution of 2 effects of attached bacteria, i.e. α and ε, to the reduction in the settling velocity of aggregates. Because the morphological effect (φ) was unknown, I first estimated the φ value for which the predicted v becomes equal to the observed v for each size category of $AGG_{0.2}$. Then, the average (±1 SE) φ for different size categories (2.80 ± 0.13, n = 5) was used as a parameter of the morphological

effect for $AGG_{0.2}$ (parameter set 1). Next, by assuming that φ is constant (= 2.80), I determined to what extent the v for $AGG_{0.2}$ changes with increases in α and ε to the levels that I determined for $AGG_{0.8}$ (parameter sets 2 and 3). The results revealed that the increase in α (parameter set 2) resulted in only a 4.9% (range: 3.0 to 7.1%) reduction in v (Table 3–3), which explained a small fraction of the observed difference in v between $AGG_{0.8}$ and $AGG_{0.2}$ (71.2%). Note that the extent of the reduction in v with increasing α might be overestimated because my estimate of bacterial density would be too low (see 'Results'). In contrast, increases in both α and ε (parameter set 3) resulted in a large reduction of v, with an average reduction of 75.4% (range: 74.4 to 76.4%) (Table 3–3). These results indicate that the ε effect was mainly responsible for the difference in v between $AGG_{0.2}$ and $AGG_{0.8}$. Note that the predicted v with parameter set 3 was slightly lower (by 0.9 to 6.3% depending on size categories) than the observed v (Table 3–3). This might be due to differences in morphology (hence φ) between $AGG_{0.2}$ and $AGG_{0.8}$. Consistent with this notion, my results indicated that the circularity of $AGG_{0.8}$ was larger than that of $AGG_{0.2}$. The difference between the predicted v and the observed v for $AGG_{0.8}$ was minimized when φ was 2.42 (parameter set 4; Table 3–3), yielding an average reduction value (71.6%) close to the observed value (71.2%).

The derivation of φ and the examination of other parameters using the modified Stokes model (Eq. 3–5) have limitations, especially regarding the simplification of particle geometry. My model lacks explicit representation of aggregate fractal dimension, which is an important

geometric property influencing aggregate settling velocities (Logan and Wilkinson, 1990; Vahedi and Gorczyca, 2012). Keeping these limitations in mind, I stress that the estimated φ would reflect not only the form resistance but also other hydrodynamic forces not examined here (Logan and Wilkinson, 1990). Nonetheless, the above results concerning the sensitivity of predicted v to different parameter settings can be used to infer the principal mechanism by which v was reduced as a consequence of bacterial colonization. I suggest that the increase in ε, due to bacterial enzymatic cleavage of aggregate matrices, was mainly responsible for the lower v for $AGG_{0.8}$ relative to $AGG_{0.2}$. Bacterial cell volume (α) and morphology (φ) also contributed to the change in v, although their contributions were not as large as that of porosity.

3.4.3 Implications for material cycling in marine environments

The aggregate settling velocities that I determined in the present study (0.003 to 0.014 cm s^{-1}) are within the range of settling velocities reported in the literature for marine particles of similar size (approximately 50 to 100 μm) classes (0.002 to 0.149 cm s^{-1}; Fennessy et al. 1994, Christiansen et al. 2002, Xia et al. 2004). These particles, which are within the smaller size range of marine settling particles (McDonnell and Buesseler, 2012; Simon et al., 2002), are abundant in seawater and can account for a large fraction (up to 20%) of total carbon sinking fluxes, as recently estimated for the subtropical Sargasso Sea (McDonnell and Buesseler, 2012). In addition, smaller sinking particles, especially sticky polymeric aggregates, can serve as the

precursors of larger aggregates (Verdugo, 2012), indicating that changes in settling velocities of smaller particles can alter the depth-dependent patterns of larger aggregate formation in water columns. Considering the timescale of bacterial colonization and growth on fresh aggregates in the upper ocean (day) and the length scale of small aggregates settling at this timescale (10 to 100 m), bacterial porosity enhancement can be an effective mechanism of suppressing the export of organic carbon and other bioelements to depth layers below the euphotic zone. I also note that changes in the porosity of aggregates due to attached bacterial action have implications for the regulation of fluid exchange between interstitial spaces and the ambient water in aggregates. Kindler et al. (2010) suggested that more porous aggregates can retain water for longer at density interfaces because of diffusion-limited fluid entrainment in the interstitial spaces of aggregates. Bacterial enhancement of aggregate porosity can be an important mechanism that promotes aggregate accumulation at density interfaces, a prominent phenomenon widely observed in oceanic environments (Alldredge and Gotschalk, 1988; MacIntyre et al., 1995). In addition, bacterial porosity enhancement may result in a higher retention of dissolved organic carbon in the interstitial spaces of aggregates, which may accelerate the downward delivery of dissolved organic carbon mediated by settling aggregates (Alldredge, 2000).

Natural aggregates in marine waters are complex and variable mixtures of organic and inorganic components. They are often composed of a variety of dense source particles, such as

diatom frustules and dust (Iversen and Ploug, 2010; Ploug et al., 2008). Depending on the nature and compositions of the aggregates, the extent of bacterial effects on the aggregate settling velocities might deviate from the present results. For example, bacterial effects on the settling velocities would be less pronounced for the aggregates with a low content of polysaccharides and a high content of mineral particles because bacterial enzymatic cleavage of polymers may hardly modify bulk physical properties of such aggregates. It is important for future studies to examine the relationship between aggregate compositions and the extent and mechanisms of bacterial effects on aggregate settling velocities.

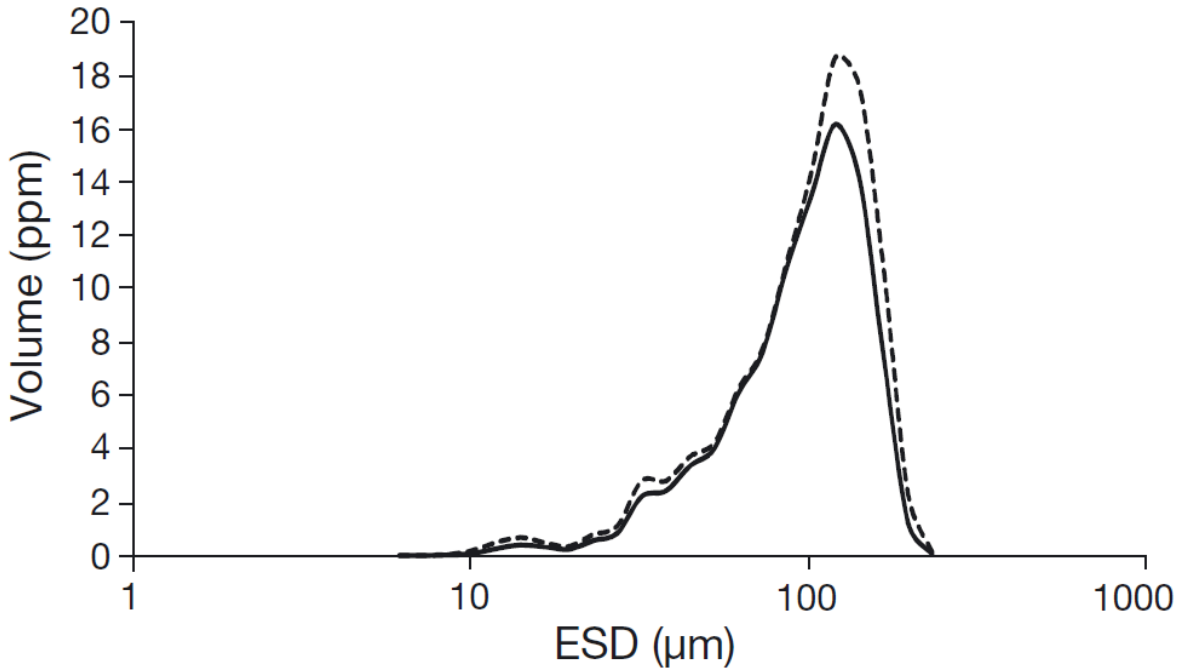

Fig. 3–1. Aggregate size (equivalent spherical diameter [ESD]) distribution for (solid line) $AGG_{0.8}$ and (dashed line) $AGG_{0.2}$. Data are from the August experiment.

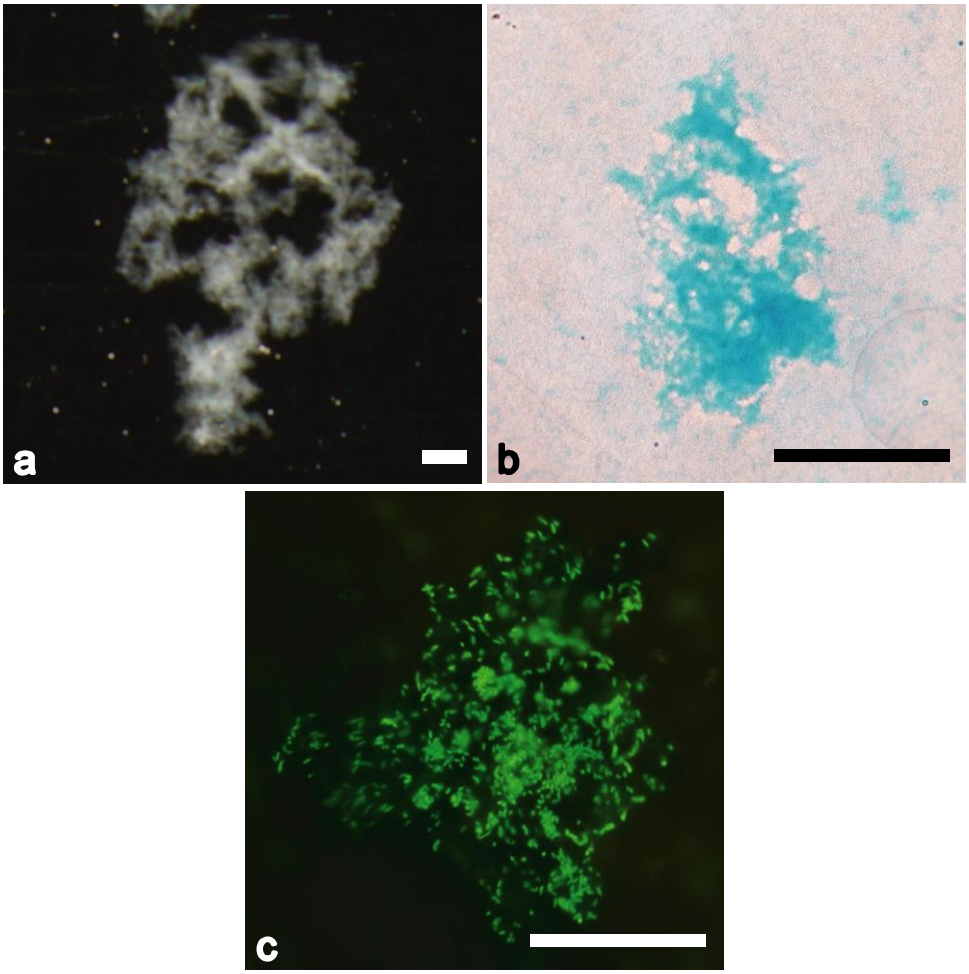

Fig. 3–2. Microscopic images of aggregate $AGG_{0.8}$ (collected during the January experiment). Scale bars = 50 μm. (a) Transmission light microscopic image. (b) Transmission light microscopic image after Alcian Blue-SYBR Green I double staining. (c) Epifluorescence microscopic image after Alcian blue-SYBR Green I double staining. Green particles are bacteria.

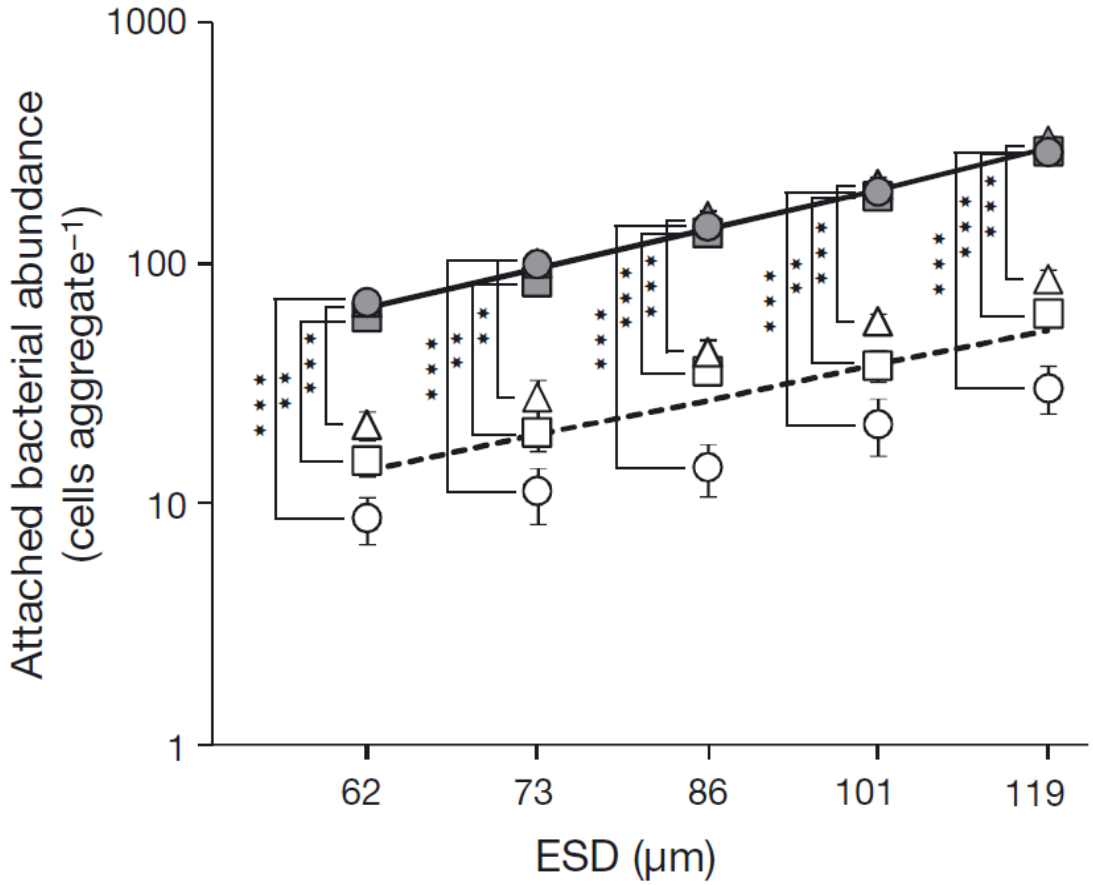

Fig. 3–3. Relationship between attached bacterial abundance and size (equivalent spherical diameter, ESD) of aggregates $AGG_{0.8}$ (■: January; ▲: August; ●: November) and $AGG_{0.2}$ (□: January; △: August; ○: November). Values are means ± SE; error bars are those associated with 3 (January) or 4 (August and November) replicated bottles. For each bottle, 10 to 20 aggregates were analyzed. Asterisks indicate the significance of the difference between $AGG_{0.8}$ and $AGG_{0.2}$ (**$p < 0.01$, ***$p < 0.001$; Student's *t*-test). Solid and dashed lines are linear regressions after double logarithmic transformation for $AGG_{0.8}$ and $AGG_{0.2}$, respectively (see 'Results').

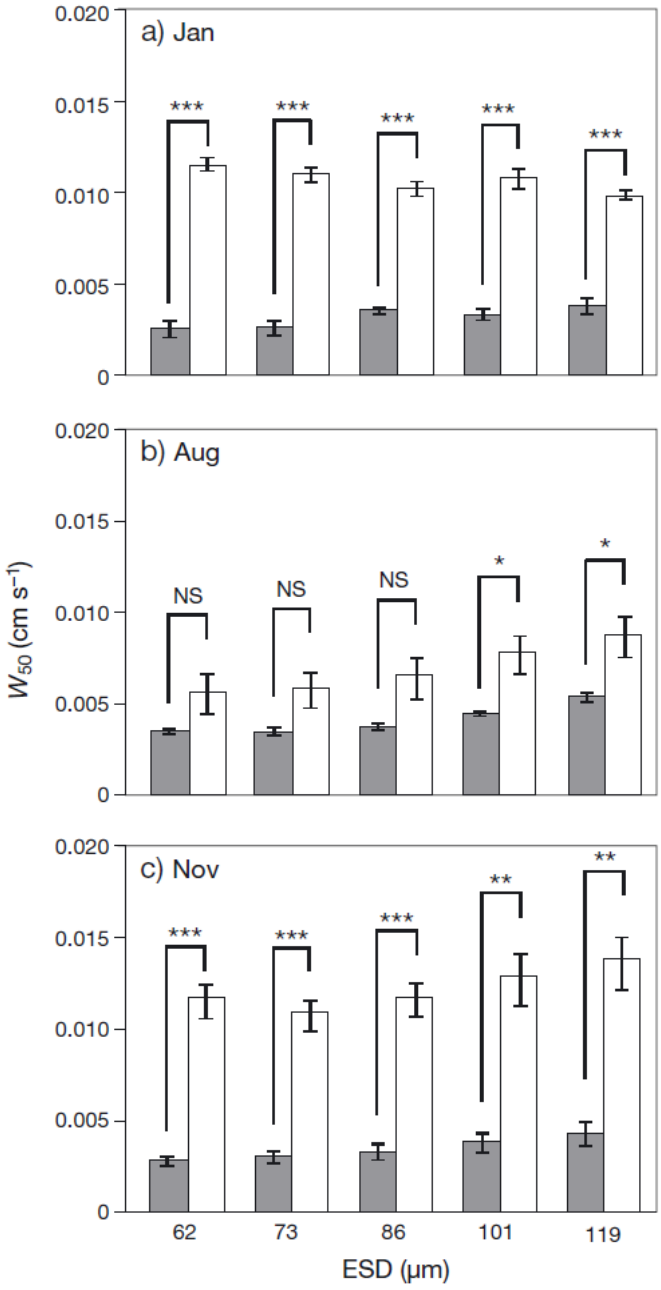

Fig. 3–4. Median settling velocity (W_{50}; cm s^{-1}) of each size class of aggregates $AGG_{0.2}$ (gray bars) and $AGG_{0.8}$ (white bars) in (a) January, (b) August, and (c) November experiments. Values are means ± SE of 3 (January) or 4 (August and November) replicated bottles. Asterisks indicate the significance of the difference between $AGG_{0.8}$ and $AGG_{0.2}$ (*$p < 0.05$, **$p < 0.01$, ***$p < 0.001$, NS: $p > 0.05$; Student's *t*-test).

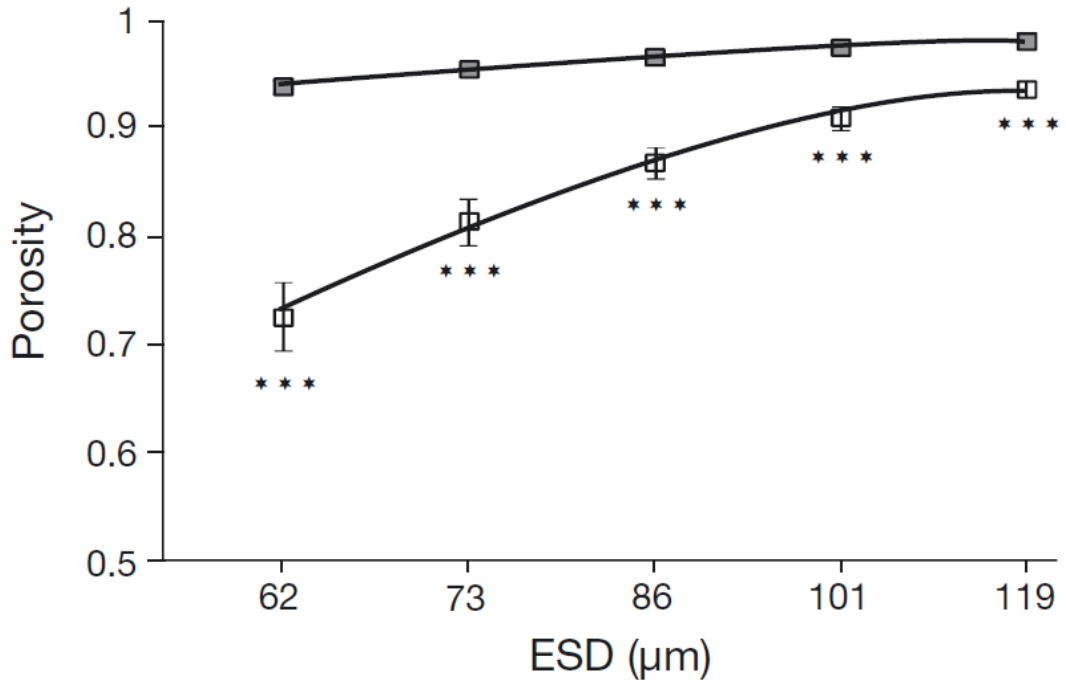

Fig. 3–5. Relationship between porosity and size (equivalent spherical diameter, ESD) of aggregates $AGG_{0.8}$ (■) and $AGG_{0.2}$ (□). Data were collected during the November experiment. Values are means ± SE of 4 replicate bottles. Asterisks indicate the significance of the difference between $AGG_{0.8}$ and $AGG_{0.2}$ (***$p < 0.001$; Student's *t*-test) for each size class. Fitted curves are quadratic regressions after double logarithmic transformation (see 'Results').

Table 3–1. Long to short axis ratio and circularity of aggregates $AGG_{0.8}$ and $AGG_{0.2}$. The data were collected during the January experiment. Values are means ± SE of triplicate bottles (n = 3) for the different size classes. For each bottle, 40 to 71 particles were analyzed. ESD: equivalent spherical diameter.

		ESD (μm)					Mean
		62	73	86	101	119	
Long to short axis ratio	$AGG_{0.8}$	0.586 ± 0.007	0.590 ± 0.003	0.623 ± 0.002	0.630 ± 0.006	0.551 ± 0.011	0.596 ± 0.004
	$AGG_{0.2}$	0.614 ± 0.005	0.581 ± 0.020	0.600 ± 0.006	0.534 ± 0.010	0.593 ± 0.012	0.584 ± 0.005
Circularity	$AGG_{0.8}$	0.072 ± 0.001	0.066 ± 0.001	0.076 ± 0.004	0.076 ± 0.004	0.070 ± 0.003	0.072 ± 0.001
	$AGG_{0.2}$	0.055 ± 0.001	0.043 ± 0.002	0.041 ± 0.001	0.039 ± 0.001	0.040 ± 0.001	0.044 ± 0.001

Table 3–2. Summary of the parameters used for the prediction of aggregate settling velocity (v) according to the model described by Eq. 3–5. *Asterisks indicate the choice of parameters for each parameter set.

Parameters	Units	Parameter set				Values	Remarks
		1	2	3	4		
D	µm	*	*	*	*	62, 73, 86, 101, 119	Diameter of the aggregate
g	m s^{-2}	*	*	*	*	9.8	Gravitational acceleration
μ	kg m^{-1} s^{-1}	*	*	*	*	0.00099	Viscosity of seawater at 23°C and salinity 29 (Fofonoff and Millard, 1983)
ρ_0	g cm^{-3}	*	*	*	*	1.019	Density of seawater at 23°C and salinity 29 (Fofonoff and Millard, 1983)
ρ_{pol}	g cm^{-3}	*	*	*	*	1.6	Density of polysaccharide matrices; Harding (1995); Rickwood (1984)
ρ_{bac}	g cm^{-3}	*	*	*	*	1.064	Density of bacterial cells, determined for bacteria recovered from $AGG_{0.8}$ (see 'Discussion').

ε ($AGG_{0.2}$)	-	*	*	-	-	0.72–0.93	Porosity (ε) for each size class was derived using the empirical relationship between D and ε (see 'Results')
ε ($AGG_{0.8}$)	-	-	-	*	*	0.93–0.98	
α ($AGG_{0.2}$)	-	*	-	-	-	0.002–0.004	α for each size class was calculated by dividing total bacterial volume (= bacterial abundance derived using the empirical relationship between attached bacterial abundance and D × average bacterial cell volume) by total aggregate volume determined by the Coulter counter method (see 'Results')
α ($AGG_{0.8}$)	-	-	*	*	*	0.036–0.080	
φ ($AGG_{0.2}$ or $AGG_{0.8}$)	-	*	*	*	-	2.80	Dimensionless coefficient of form resistance
φ ($AGG_{0.8}$)	-	-	-	-	*	2.42	

Table 3–3. Summary of the observed and predicted aggregate settling velocity (v) for the aggregates $AGG_{0.8}$ and $AGG_{0.2}$. Observed v data were obtained from the November experiment for both $AGG_{0.2}$ and $AGG_{0.8}$. % deviation: deviation between the observed v and predicted v for $AGG_{0.2}$, % reduction: reduction in the predicted v of $AGG_{0.8}$ compared to the predicted v of $AGG_{0.2}$. ESD: equivalent spherical diameter.

ESD (μm)	$AGG_{0.2}$ (cm s^{-1})			$AGG_{0.8}$ (cm s^{-1})							
	Observed	Predicted (parameter set 1)	Deviation (%)	Observed	Reduction (%)	Predicted (parameter set 2)	Reduction (%)	Predicted (parameter set 3)	Reduction (%)	Predicted (parameter set 4)	Reduction (%)
62	0.0115	0.0122	-5.6	0.0028	75.6	0.0118	3.0	0.0029	76.4	0.0033	72.8
73	0.0107	0.0124	-15.0	0.0031	71.5	0.0119	3.8	0.0029	76.2	0.0034	72.5
86	0.0116	0.0119	-3.1	0.0033	71.6	0.0114	4.7	0.0029	75.4	0.0034	71.6
101	0.0127	0.0113	10.6	0.0038	69.8	0.0107	5.8	0.0029	74.4	0.0034	70.4
119	0.0136	0.0118	13.1	0.0043	68.4	0.0110	7.1	0.0030	74.7	0.0035	70.8
Mean	0.0120	0.0119	0.8	0.0035	71.2	0.0113	4.9	0.0029	75.4	0.0034	71.6

Chapter 4 Bacterial control of large organic aggregate formation in seawater

4.1 Introduction

Large organic aggregates (size, 0.1–several cm in linear dimension) play important roles in the regulation of material cycling and food webs in the ocean(Simon et al., 2002). They mediate the vertical delivery of organic carbon and other bioelements in oceanic water columns to affect the sequestration of carbon (biological carbon pump) and nutrients in the deep ocean (Passow and Carlson, 2012). Large organic aggregates also serve as important food sources for detrivores and omnivores (Passow et al., 2001) and provide microhabitats where a diverse range of microbes thrives and mediates biochemical reactions that may not proceed in the surrounding bulk seawater (Azam and Malfatti, 2007). Thus, clarifying the mechanisms and regulation of large organic aggregate formation in seawater is fundamental to a better understanding of ocean biogeochemistry and ecology.

Large organic aggregate formation can be affected by several factors. These may include the abundance and nature of source particles [e.g., alga cells, microgels, and transparent expolymeric particles (TEP)] that stick together (Simon et al., 2002; Verdugo, 2012) and physicochemical factors such as turbulence, temperature, pH, and salinity (Burd and Jackson, 2009). Previous studies have also noted that bacteria can exert a substantial influence on the dynamics of large organic aggregates in the oceans. Some studies have suggested that bacteria release large amounts of extracellular polymers and possess fibrillar appendages, depending on the bacterial type and growth conditions, which facilitate the formation of large organic

aggregates (Biddanda, 1985; Simon et al., 2002). Other studies found that bacteria substantially enhance large aggregate formation in a diatom culture, which was interpreted as a consequence of bacterial stimulation of extracellular polymer excretion by the diatom (Gardes et al., 2011). In contrast, in a mesocosm experiment, Smith et al. (1995) found that bacteria strongly inhibited large aggregate formation during a diatom bloom. This inhibition was ascribed to bacterial ectoenzymatic hydrolysis of extracellular polymers produced by diatoms (Azam and Malfatti, 2007). Thus, bacteria appear to regulate both the formation and disintegration of large organic aggregates. These apparently conflicting roles of bacterial action may be partly explained by the involvement of different types of bacteria in aggregate formation and disintegration (Simon et al., 2002; Teeling et al., 2012). However, there are still many uncertainties in my understanding of the role of bacteria and their specific groups in the regulation of large organic aggregate dynamics in marine systems. This paucity of knowledge represents a major obstacle in my efforts to better describe bacteria–organic matter interactions and the settling fluxes of organic particles in ocean biogeochemical models (Hasumi and Nagata, 2014).

To better understand the role of bacteria in the regulation of large organic aggregate dynamics in seawater, this study investigated the effects of bacteria on the integration of small organic aggregates suspended in seawater. I used self-assembled aggregates (size, ca. 0.01 cm) composed of two polysaccharides, fucoidan and chitosan (Chapter 3), as model particles. Self-assembled polymers are known to be ubiquitous and abundant in marine environments

(Verdugo, 2012; Verdugo et al., 2004) and may potentially serve as important source particles for the formation of large organic aggregates (Burd and Jackson, 2009; Verdugo, 2012). The model aggregates that I used are known to have several key features of the major class of marine aggregates including TEP (Chapter 3). My objectives were as follows: (1) to determine whether marine bacterial assemblages enhance the coagulation of aggregates, (2) to investigate whether specific bacterial groups enhance the coagulation of aggregates, and (3) to determine the settling velocities of the large aggregates derived from aggregates.

4.2 Materials and methods

4.2.1 Collection of seawater samples and incubation of model aggregates

Seawater samples were collected from the shore of Otsuchi Bay (39°21’3”N, 141°55’58”E) and Oarai Beach (36°19’3”N, 140°35’29”E) on the Pacific coast of northeastern Japan using a clean plastic bucket. Sampling dates and seawater properties at the time of sampling (temperature and salinity) are tabulated in the Table 4–1. Within 12 h of sampling, seawater samples were successively filtered through 0.8-μm-pore-size polycarbonate (PC) filters and 0.2-μm-pore-size PC filters (47 mm diameter; Whatman) using negative pressure (<20 mmHg) to prepare 0.8-μm-pore-size-filtered seawater (hereafter, $FSW_{0.8}$) and 0.2-μm-pore-size-filtered seawater ($FSW_{0.2}$). Portions of $FSW_{0.2}$ and $FSW_{0.8}$ were autoclaved for 15 min at 120°C and are hereafter referred to as Aclv-$FSW_{0.2}$ and Aclv-$FSW_{0.8}$, respectively.

Model aggregates composed of fucoidan and chitosan were prepared as previously described (Chapter 2). Aggregates were suspended in Aclv-$FSW_{0.2}$, autoclaved for 15 min at 120°C, and stored for up to 12 h at 20°C until their use in incubation experiments (this suspension is referred to as "aggregate suspension"). The size distribution of aggregates was determined by laser in situ scattering and transmissometry (LISST) (Chapter 2), which indicated little change during autoclaving (data not shown). The total volume concentration of aggregates was adjusted to ca. 100 ppm, which was close to the upper range of the abundance of TEP in coastal seawater (Passow 2002).

I investigated changes in particle abundance and mean volume in rotating tubes (Engel et al., 2009) with and without the presence of live bacterial assemblages. An autoclaved 70-mL glass rotation tube (No. 7L, 4.0-cm diameter; AS ONE Corp., Japan) with a cap sealed by a Teflon-faced nitrile-butadiene-rubber liner (Nichiden-Rika Glass Co., Ltd., Japan) was filled with 56.18 ml of the aggregate suspension and 5.56 ml of either $FSW_{0.8}$ (bacteria-addition treatment) or Aclv-$FSW_{0.8}$ (sterile control). I also prepared another series of bacteria-addition treatments to which inorganic nutrients were added. These treatments received an addition of either phosphorus (P) (Exps. 1, 2, 3, 4, 6, and incubation of *Pseudoalteromonas* isolates: final concentration, 40 μM Na_2HPO_4 solution) or P and nitrogen (N) (Exp. 5: final concentration, 40 μM Na_2HPO_4 solution; 1.6 mM NH_4Cl solution) (Table 4–1). At each sampling time (0, 24, 48, 72, 96 h), three tubes for each bacteria-addition treatment and those for the sterile control were

sacrificed for the determination of particle and bacterial parameters (see below). The rotation speed was adjusted to 16.4 rpm (shear rate, ca. 30 s^{-1}; Kiorboe et al., 1994) using a rotator (ROLAA115S, Low-profile roller: Stovall Life Science, Peosta, IL, USA). The incubation was conducted at 20^{o}C in the dark.

4.2.2 Particle abundance and size

A digital camera (EOS Kiss X6i; Cannon, Tokyo, Japan) equipped with a macro lens (EF5025M; Cannon) and a convertor lens (L.S.CON-EF; Cannon) was used to capture images of particles in the rotating tubes. The images were taken from the bottom of a tube that was laterally illuminated (mean beam depth, 5 mm) using a flashlight (SG-325; Gentos, Tokyo, Japan). The center of each image (1.5 × 1.5 cm square) was used as the sampling area. The depth at which the objects came into focus was determined to be 1.5 cm based on a calibration using images taken for standard beads (Polystyrene Beads, Large 200–300 μm; Polyscience Inc., Warrington, PA, USA). Depending on the treatment and the time of sampling, particle abundance was occasionally too low to be detected in the sampling volume (<75 particles per tube). In this case, the incubation tube was removed from the roller, and particles were allowed to settle completely on the bottom of the tube (1–2 min). An image of particles on the bottom was then taken using a digital camera. The images obtained were analyzed using ImageJ software (v. 1.45 with Java, 1.6.0_20). Image analysis was conducted to estimate the area of

individual particles (detection limit, 2.0×10^{-5} cm^2). The estimated area was converted to an equivalent spherical diameter (ESD) and volume, with an assumption that the particles were spherical.

4.2.3 Bacterial abundance, volume, and carbon mass

In Exps. 1–5, seawater subsamples for bacterial abundance determination were fixed with glutaraldehyde (final concentration, 2%; Wako, Osaka, Japan) for 1–2 h at 4°C. A portion of the fixed sample was first filtered through a 0.8-µm-pore-size syringe filter (Acrodisc syringe filter with Supor®membrane: Pall Corporation, Port Washington, NY, USA), and then the filtrate was further filtered through a 0.2-µm-pore-size PC filter (25 mm diameter; Whatman, UK) to collect unattached bacteria. The other portion of the fixed sample was filtered through a 0.8-µm-pore-size PC filter (25 mm diameter; Whatman, UK) to collect attached bacteria. After staining with DAPI (final concentration, 1 µg ml^{-1}, Porter and Feig 1980) for 5 min, the PC filters were mounted on slides using immersion oil (Vectashield; Vector Laboratories, Burlingame, CA, USA, and Citifluor: Citifluor Ltd., Leicester, UK) and then observed under an epifluorescence microscope (BX-61 equipped with a U-MWU2 cartridge: Olympus, Tokyo, Japan). At least 200 cells, or cells in 20 different fields, were counted for each slide.

In Exp. 5, the area and perimeter of attached bacteria (61–785 cells for each bottle) were determined using ImageJ software to estimate the mean bacterial cell volume. Bacterial

carbon mass was calculated using a conversion factor that relates bacterial cell volume to carbon mass (Fagerbakke et al., 1996).

4.2.4 Respiratory carbon consumption by bacteria

In Exp. 5, bacterial production (BP: attached and unattached bacteria) was estimated by the ^{3}H-leucine incorporation method (Kirchman, 2001; Uchimiya et al., 2013). After gentle mixing by hand (this treatment resulted in the disintegration of loosely connected aggregate structures), a 1-mL sample was contained in a 1.5-mL sterile tube, amended with 100 µL of ^{3}H-leucine (TRK510, Amersham, UK: specific activity 4.29 TBq mmol^{-1}, final concentration 10 nmol L^{-1}), and incubated at 20ºC for 1 h. After the incubation, 52.7 µL of 100% trichloroacetic acid (TCA) was added to the sample. The sample was then filtered through a 0.2-µm PC filter (25 mm diameter: Whatman, Maidstone, UK). After the extraction with 5% ice-cold TCA and 80% ice-cold ethanol, the filter was dried completely. Then, 7 mL of liquid scintillation cocktail (Ultima Gold: PerkinElmer, Waltham, MA, USA) was added to the sample, and the radioactivity was measured using a liquid scintillation counter (TRI-CARB 1500: Packard Bioscience, Meriden, CT, USA). For each sample, two replicates and one TCA-killed control were prepared.

BP was calculated using a leucine-to-carbon conversion factor of 1.55 kg C mol^{-1} (Kirchman, 2001). I estimated the respiratory consumption of organic carbon by bacteria during

the incubation (ΣBR, mg C L^{-1}). For this calculation, BP was integrated over an incubation period of 24, 48, 72, and 96 h (ΣBP, mg C L^{-1}). Then, ΣBR was derived using ΣBP and an assumed growth efficiency of 0.4 (del Giorgio and Cole 1998): $\Sigma BR = (1 - 0.4) \times \Sigma BP / 0.4$.

4.2.5 Analysis of particulate organic carbon

The initial particulate organic carbon (POC) concentration was determined for organic matter collected on pre-combusted (450ºC for 4 h) glass fiber filters (GF/F, Whatman) using an elemental analyzer (Flash 2000, Thermo Fisher Scientific, Waltham, MA, USA).

4.2.6 Determination of bacterial phylogenetic composition by catalyzed reporter deposition fluorescence in situ hybridization (CARD-FISH)

In Exp. 5, the bacterial community composition was determined by the CARD-FISH method (Pernthaler et al., 2002, 2004). Seawater samples were fixed with paraformaldehyde (Wako: final concentration, 2%) for 1 hour at room temperature. The fixed $FSW_{0.8}$ was filtered through a 0.2-μm-pore-size PC filter. Other fixed samples were either filtered through a 0.2-μm-pore-size PC filter after prefiltration using a 0.8-μm-pore-size syringe filter (Acrodisc syringe filter with Supor®membrane: Pall Corporation) (unattached bacteria) or filtered directly through a 0.8-μm-pore-size PC filter (attached bacteria) (see above). The PC filters were dried and stored at -20ºC until later processing. The PC filters were embedded in 0.1%

agarose (Wako), cut into sections, and incubated in lysozyme (10 mg ml^{-1}; Sigma-Aldrich Corp., St. Louis, MO, USA) for 1 hour at 37°C. After inactivation of lysozyme by 0.01 M HCl at room temperature for 20 min, hybridization with horseradish peroxidase-labelled oligonucleotide probes (Table 4–2) and tyramide (Alexa Fluor® 488) signal amplification were performed. The filter sections were dehydrated with 95% ethanol and mounted on microscope slides using anti-fading reagents (Vectashield and Citifluor) containing DAPI (final concentration, 1 mg ml^{-1}). Slides were stored at -20°C until later analysis. Slides were examined using an epifluorescence microscope (BX-61 equipped with a U-MNIBA3 and U-MWU2 cartridges; Olympus).

4.2.7 Particle settling velocity

The settling velocities of the large particles collected in Exp. 6 (incubation period, 24–48 hours) were determined using a sedimentation column (Ploug et al., 2010). A 1-L graduated cylinder (7 cm wide, Iwaki, Japan) was filled with $FSW_{0.2}$. After stabilization in a temperature-constant room (25°C), individual particles were gently introduced into the upper part of the water column using a micropipette (Finnpipette F2: Thermo Fisher Scientific) whose tip end had been cut to broaden its opening. The travel time of individual particles (n = 45) over a distance of 20.5 cm (between 6 cm below the surface and 6 cm above the bottom of the cylinder) was recorded with a manual stopwatch. Particle ESD was estimated as the average of the major and minor axis lengths for particles placed on a petri dish.

4.2.8 Effects of *Pseudoalteromonas* isolates on particle dynamics

Pseudoalteromonas isolates were obtained from the Leibniz Institute DSMZ–German Collection of Microorganisms and Cell Cultures, Germany [*P. agarivorans* (DSM14585), *P. rubra* (DSM6842), *P. tunicate* (DSM14096), *P. citrea* (DSM8771), *P. flavipulchra* (DSM14401)], the Japan Collection of Microorganisms (Riken, BioResource Center, Japan) [*P. atlantica* (JCM8845), *P. luteoviolacea* (JCM21275), *P. haloplanktis* (JCM20767), *P. spongiae* (JCM12884), *P. undina* (JCM20773)], and the Belgian Coordinated Collection of Microorganisms [*P. ruthenica* (LMG19699)]. The design of the incubation experiments was similar to that described for Exps. 1–5, except for the following aspects. (1) The aggregate suspension enriched with P was prepared using artificial seawater (Cavanaugh 1975) rather than coastal seawater. (2) To prepare bacterial inocula, the following pretreatments were conducted. Isolates were grown on marine broth agar plates at 20°C. Bacterial cells were transferred from each plate to 1 mL of the aggregate suspension enriched with P. This bacterial suspension (100 μL) was transferred to a 50-mL aggregate suspension enriched with P and incubated at 20°C in the dark for 1–2 d. This pre-incubated bacterial suspension was used as an inoculum and was added to a rotating tube containing the aggregate suspension enriched with P. The abundance of bacterial cells was adjusted to be in the range of 10^3–10^4 cells mL^{-1}. (3) A sterile control was

prepared using an autoclaved, preincubation culture of *P. citrea*. (4) Seawater subsamples were filtered through 0.2-μm-pore-size PC filter to prepare the slides for counting total bacterial abundance.

4.3 Results

4.3.1 Dynamics of particles and bacteria

Patterns in the time course of particle abundance and mean volume differed between the bacteria-addition treatments and the sterile control (Fig. 4–1 shows the results obtained in Exp. 3 as an example). In the bacteria-addition treatment, particle abundance decreased by ca. 400 fold, and mean volume increased by ca. 10^5 fold during the incubation period (Figs. 1a, 1b, 2). This substantial increase in particle mean volume reflected a large, successive shift in the ESD peak position (Fig. 4–3a). In contrast, in the sterile control, both the particle abundance and mean volume changed only slightly during incubation (<1.5-fold difference) (Fig. 4–1a, 4–1b), displaying a minimal shift in the ESD peak position (Fig. 4–3a). A conspicuous formation of large particles in the bacteria addition treatment, but not in the sterile control, was consistently observed in other experiments. The maximum mean volume of particles (V_{max}) determined for the bacteria-addition treatment (V_{max} was attained between 48 and 96 h) ranged between 10^{-4} and 10^0 cm^3, which was significantly greater (by 10^2–10^5 fold) than the value

obtained for the sterile control in all experiments (Fig. 4–4). Among the bacteria-addition treatments, V_{max} values increased (by 20–110 fold) in response to the addition of P in Exps. 1 and 2. In Exp. 5, the V_{max} in the treatment with the addition of both P and N was slightly (2.2 fold) yet significantly ($p < 0.05$) higher than the V_{max} in the treatment with the addition of only P.

Changes in bacterial abundance were investigated in Exps. 3–5 (Fig. 4–1c shows the result of Exp. 3 as an example). Generally, both the attached and unattached bacterial abundance increased during the initial 24–48 h and then reached a stationary phase.

4.3.2 Bacterial biomass and respiratory consumption

The initial concentration of POC ($[POC]_{ini}$) was 2.72 ± 0.47 mg C L^{-1} [mean ± standard deviation (SD), $n = 9$]. In the P and P+N addition treatments of Exp. 5, I investigated the changes in attached bacterial biomass and respiratory carbon consumption (ΣBR) during incubation. The carbon biomass of attached bacteria accounted for up to 13% of $[POC]_{ini}$, and ΣBR accounted for up to 15% of $[POC]_{ini}$ (Table 4–3).

4.3.3 Bacterial phylogenetic group composition

Attached and unattached bacteria displayed generally similar patterns in terms of the changes in community composition in Exp. 5 (Fig. 4–5). At the level of the major phylogenetic

group, *Bacteroidetes* was the most abundant group in $FSW_{0.8}$, followed by *Gammaproteobacteria* and *Alphaproteobacteria*. During the incubation, the abundance of the *Bacteroidetes* group initially decreased drastically to <2% (at T_{24}), before increasing to reach higher values (12–16%) at T_{96}. During the whole incubation period, *Gammaproteobacteria* and *Alphaproteobacteria* were the predominant major phylogenetic groups. At a finer phylogenetic level (genus), there was a remarkable increase in the abundance of *Psuedoalteromonas* (PSU730 probe-positive cells) during the early period of incubation. The *Psuedoalteromonas* group accounted for only a minor fraction (2%) of the bacteria in the $FSW_{0.8}$, whereas it represented a substantial fraction (up to 28%) of bacteria at T_{24} in both the attached and unattached bacterial fractions. The growth rate of this bacterial group during the initial 24 h was estimated to be 5.9 d^{-1} (attached bacteria) and 5.7 d^{-1} (unattached bacteria). These values were much higher than the corresponding growth rates of the bulk bacteria community (3.3 d^{-1} and 3.1 d^{-1} for attached and unattached bacteria, respectively). After T_{24}, *Psuedoalteromonas* group abundance remained high (9–25% of the total bacterial abundance) (Fig. 4–5).

4.3.4 Effects of *Pseudoalteromonas* isolates on particle dynamics

Based on my CARD-FISH results and other information regarding the general surface-associated life style of *Pseudoalteromonas* species (see Discussion), I hypothesized that one type of bacteria that can enhance the formation of large organic aggregates is affiliated with the

genus *Pseudoalteromonas*. To test this hypothesis, I examined 11 isolates of *Pseudoalteromonas* to determine their ability to promote the formation of large aggregates.

Pseudoalteromonas isolates displayed high growth rates in aggregate suspensions, reaching a level of 10^5–10^6 cells mL^{-1}, although the growth yield of *P. ruthenica* was low (< 10^5 cells mL^{-1}). For four of the 11 isolates examined (*P. citrea*, *P. luteoviolacea*, *P. flavipruchra*, and *P. spongiae*), the addition of the isolate resulted in a significant increase in particle mean volume relative to the sterile control. Increases in particle volume were generally accompanied by decreases in particle abundance (data not shown), indicating that the coagulation of source particles was enhanced by the addition of these isolates. Among these isolates, the V_{max} values of *P .citrea* and *P. luteoviolace* (10^{-2}–10^0 cm^3) were higher than those for *P. flavipulchra* and *P. spongiae* (10^{-5}–10^{-4} cm^3). For this multiple comparison, the data for *P. undina* and *P. ruthenica* were not used because the equal-variance requirement for an analysis of variance (ANOVA) was not fulfilled when these data were included in the analysis. Although these isolates caused a slight increase in mean particle volume (Fig. 4–6), there was no concomitant decrease in particle abundance under these treatments (data not shown). Based on these results, I considered that the effects of these two isolates on the coagulation of aggregates were minimal.

4.3.5 Settling velocity of large particles

The large particles collected in Exp. 6 were used to determine settling velocities (*U*)

(Fig. 4–7a). *U* increased with increasing ESD, with higher values of 100–270 m day^{-1} obtained for the ESD class of 0.4–0.85 cm.

4.4 Discussion

4.4.1 Enhancement of aggregate coagulation by marine bacterial assemblages

In this study, the addition of marine bacterial assemblages to aggregate suspensions resulted in a substantial increase (up to 10^5 fold) in particle mean volume and a reduction in particle abundance during the incubation period of 24–96 hours, with an accompanying increase in bacterial abundance. In contrast, in the sterile control, the aggregates were notably stable, displaying minimal changes in abundance and mean volume. These results suggest that bacteria strongly enhanced the coagulation of aggregates. The proposition that biotic rather than abiotic factors largely governed aggregate coagulation is consistent with the results showing that V_{max} increased in response to the addition of P (Exps. 1 and 2) or N (Exp. 5). These results suggest that, depending on the seawater conditions, bacterial effects on aggregate coagulation are at least partly regulated by nutrient availability. It is unlikely that the large particles produced during the incubation were mainly composed of bacterial biomass produced by the consumption of the gel (polysaccharide) matrices and other constituents in seawater. In support of this notion, bacterial biomass and respiratory carbon consumption were estimated to account for only a

moderate fraction (up to 13% for biomass and 15% for respiratory consumption) of $[POC]_{ini}$. This indicates that a large fraction (>72%) of the bulk mass of the gel matrices that were initially added was conserved even at the end of incubation (T_{96}). Note that my consideration does not explicitly account for the conversion of POC to dissolved organic carbon (DOC). However, by assuming that the released DOC was rapidly consumed by unattached bacteria (this assumption is reasonable given that a tight coupling of a POC-DOC-unattached bacteria pathway is generally found in marine environments; Nagata 2008), my calculation of ΣBR, which is based on the determination of total bacterial production (i.e., attached and unattached bacteria), may account for the loss of gel matrices due to the release of DOC. Based on these results, I consider that source particle (small organic aggregate) coagulation accounted for most of the increase in particle mean volume and the decrease in particle abundance, although this proposition does not preclude the possibility that the physico-chemical properties of aggregates were modified by bacteria (see below). My data confirm and add to previous reports that have suggested a dynamic role of polymeric organic aggregates in marine systems (Verdugo, 2012; Verdugo et al., 2004). Specifically, my results are among the first to demonstrate that the coagulation of self-assembled gels can be strongly enhanced by bacteria that readily colonize aggregates.

4.4.2 Possible involvement of *Psudoalteromonas* in the enhancement of aggregate coagulation

The CARD-FISH results revealed that *Psuedoalteromonas* grew rapidly during the initial phase of incubation when coagulation occurred. Their growth rates were much higher than the growth rate of the bulk bacterial community, which suggests that this group of bacteria was competitively superior to others, at least during the early phase of the incubation. *Pseudoalteromonas* are known to be widely distributed, yet are usually less abundant in natural seawaters (García-Martínez et al., 2002). However, they can be abundant in surface-associated environments such as biofilms, microlayers, and the surfaces of macroalgae and invertebrates (Bowman, 2007; Rao et al., 2006). The CARD-FISH results and surface-associated life style of the genus *Pseudoalteromonas* suggest that this group of bacteria may be involved in the enhancement of aggregate formation.

The results obtained using the isolates of *Pseudoalteromonas* strains supported this notion by showing that some isolates did enhance the coagulation of aggregates. Previous studies have indicated that some *Pseudoalteromonas* species create biofilms by excreting polysaccharides and extracellular polymers (Ortega-Morales et al., 2007), have a strong surface attachment system contributing to the enhancement of biofilm formation (Hall-Stoodley and Stoodley, 2002), and potentially produce Type IV pili, which is believed to be important for

attachment and the initial stage of biofilm formation (Thomas et al., 2008). These general properties of *Pseudoalteromonas* species may help explain the enhancement of aggregate formation that I found for some *Pseudoalteromonas* isolates. However, it should be noted that all of the *Psudoalteromonas* isolates, except for *P. ruthenica,* displayed a similarly high growth yield in aggregate suspensions, but only four isolates enhanced large aggregate formation. Thus, there may be specific types of *Psudoalteromonas* that share common traits that enhance the coagulation of aggregates. This notion is partly supported by the results of comparative genomic analyses conducted by Yang et al. (pers. comm.), who identified a gene that was associated with *Pseudoalteromonas* strains capable of enhancing aggregate coagulation. This gene (designated as the *mag* gene) has a periplasmic sugar-binding domain, and may have functions related to extracellular polysaccharide sensing (Yang et al., pers. comm.). The *mag* gene is potentially a promising target for future studies to investigate the molecular basis of the bacterial enhancement of aggregate coagulation.

4.4.3 Settling velocity of aggregates

The settling velocities of the aggregates determined in this study (up to 270 m day^{-1}) were comparable to or exceeded those previously reported for various marine particles in a similar size range (0.1–1 cm), including marine snow, appedicularian house, and laboratory-

made aggregates containing mineral ballasts (Alldredge and Gotschalk, 1988; Iversen et al., 2010; Iversen and Ploug, 2010). Although higher settling velocities (>500 m day^{-1}) have been reported for some types of aggregates (e.g., Engel et al. 2009), the larger aggregates that I examined clearly belonged to the class of fast-settling particles in the sea. Generally, previous studies have considered that the large degree of variability and generally weak size dependency in large aggregate settling velocities can be ascribed to compositional variability in aggregate constituents (Ploug et al., 2010), suggesting that fast-settling aggregates generally contain high density ballast particles such as diatom frustules, coccolith shells, and mineral dust (Iversen et al., 2010; Iversen and Ploug, 2010). In contrast, my data showing high settling velocities of aggregates that are composed of polysaccharides and bacteria indicate that aggregate coagulation can result in the formation of fast-settling aggregates without the association of mineral ballasts. Do large aggregates derived from aggregates have some physical or geometric features that are distinct from those reported for other marine aggregates reported in the literature? To address this issue, I examined the geometric and hydrodynamic properties of the aggregates, and considered whether the observed settling velocities were consistent with predictions deduced on a hydrodynamic model (Ploug et al., 2008):

$$U = \left(\frac{2g\Delta_\rho \mathrm{V}}{\rho_f C_D A} \right)^{0.5} \qquad \text{[Equation 4–1]}$$

where U is the settling velocity of the aggregate (cm s^{-1}), g is the acceleration caused by gravity (cm s^{-2}), $\Delta\rho$ is the excess density of the aggregate (g cm^{-3}), ρ_f is the density of sea water (g cm^{-3}), V is the volume of the aggregate (cm^3), A is the cross-sectional area of the aggregate (cm^2), and C_D is the drag coefficient (dimensionless), which, when the Reynolds number (Re) is over 0.5, is calculated as:

$$R_e = \frac{Ud}{v} \qquad \text{[Equation 4–2]}$$

$$C_D = \frac{24}{R_e} + \left(\frac{6}{1 + R_e^{0.5}} \right) + 0.4 \qquad \text{[Equation 4–3]}$$

where d is the ESD of the aggregate (cm), and v is the kinematic viscosity of seawater (cm^2 s^{-1}). In my model analysis, $\Delta\rho$ was calculated using the aggregate solid matter density (ρ_s, g cm^{-3}), ρ_f, and aggregate porosity (ε_{AGG}).

$$\Delta_\rho = (1 - \varepsilon_{AGG})(\rho_S - \rho_f) \qquad \text{[Equation 4–4]}$$

ε_{AGG} was derived as follows:

$$\varepsilon_{AGG} = 1 - (1 - \varepsilon_S)(1 - \varepsilon_L) \qquad \text{[Equation 4–5]}$$

where ε_S is the porosity of the source particle themselves (intra-source particle porosity), and ε_L is the porosity arising from the space between the source particles constituting an aggregate

(inter-source particle porosity). ε_L was estimated according to Logan and Wilkinson (1990) as follows:

$$\varepsilon_L = 1 - \frac{NV_0}{V} \qquad \text{[Equation 4–6]}$$

where N is the number of source particles constituting an aggregate (estimated from the decrease in source particle abundance during the incubation), and V_0 is the volume of source particles (cm^3). Because ε_L increased with increasing ESD, I derived the double logarithmic regression that relates $(1 - \varepsilon_L)$ to ESD for use for the derivation of U as a function of ESD. The exponent of this regression (f) was used to obtain the aggregate fractal dimension $(3 + f)$ (Logan and Wilkinson, 1990). For ε_S, I used fucoidan/chitosan aggregate porosity reported previously (Table 4–4). For the estimation of $\Delta\rho$ (Eq. 4–4), I assumed, as a default setting, that ρ_s was identical to the density of polysaccharide (ρ_{pol}, g cm^{-3}) and that the polysaccharide matrices that were added initially were conserved during the incubation. However, this assumption is probably unrealistic because the attached bacterial biomass replaced a part of the polysaccharide matrices, and the polysaccharides that were added initially were partly remineralized by bacterial respiration. These two effects were taken into account by introducing two parameters, α (contribution of the bacterial biomass to the total aggregate mass) and β (the fraction of the total gel matrices remineralized by bacterial respiration), for the derivation of ρ_s and ε_{AGG}, respectively:

$$\rho_S = (1-\alpha)\rho_{pol} + \alpha\rho_{bac} \quad \text{[Equation 4–7]}$$

$$\varepsilon_{AGG} = 1-(1-\beta)(1-\varepsilon_L)(1-\varepsilon_S) \quad \text{[Equation 4–8]}$$

Using Eqs. from 4–1 to 4–8 and the parameters listed in Table 4–4, I derived a theoretically predicted *U* as a function of ESD (Fig. 4–7b).

The aggregates were highly porous (ε_{AGG} = 0.9956–0.9999), with their fractal dimension estimated to be 1.67 (95% confidence interval, 1.39–1.95). This fractal dimension is within the range of values previously reported for marine snow and other types of aggregates (1.26–2.14; Logan and Wilkinson 1990, Kilps et al. 1994). A comparison of the observed and predicted *U* value (Fig. 4–7b) underscores the following two important points. First, the high settling velocities (100–270 m day^{-1}) determined for larger aggregates (> ca. 0.4 cm) agreed reasonably well with the predicted *U*, with the deviation (0.9–1.6 fold) being generally within the range of inherent uncertainties stemming from the errors in *f* and the assumption about the α and β parameters. This agreement provides a theoretical basis to suggest that polysaccharide-rich, large aggregates derived from aggregates can represent, even without the inclusion of mineral ballasts, a class of fast-settling particles in the ocean. Second, the dependency of observed *U* on ESD was stronger than theoretical predictions, resulting in a large deviation (up to four fold) of the observations from the predictions (observed *U* < predicted *U*) for relatively small aggregates (ESD < 0.4 cm). These large, albeit variable, deviations might be partly

explained by the form resistance of the aggregates (i.e., the reduction in settling velocity due to their non-spherical form), a potentially important geometric parameter that was not incorporated in my model.

My results were obtained under a simple experimental setting using model aggregates. Obviously, these results do not fully capture the complexities of the bacterial control of aggregate formation and settling velocities in natural marine environments. Future studies should investigate the general applicability of the results reported here to natural aggregates, composed of different kinds of polysaccharides with different charges and polymer lengths (Verdugo, 2012; Verdugo et al., 2004). Given that aggregates serve as a hot spot of microbial consortia, it would be beneficial for future studies to examine the effects of biotic interactions (protist grazing, viral lysis, and symbiotic/antagonistic relationships) on the regulation of aggregate coagulation and aggregate settling velocity.

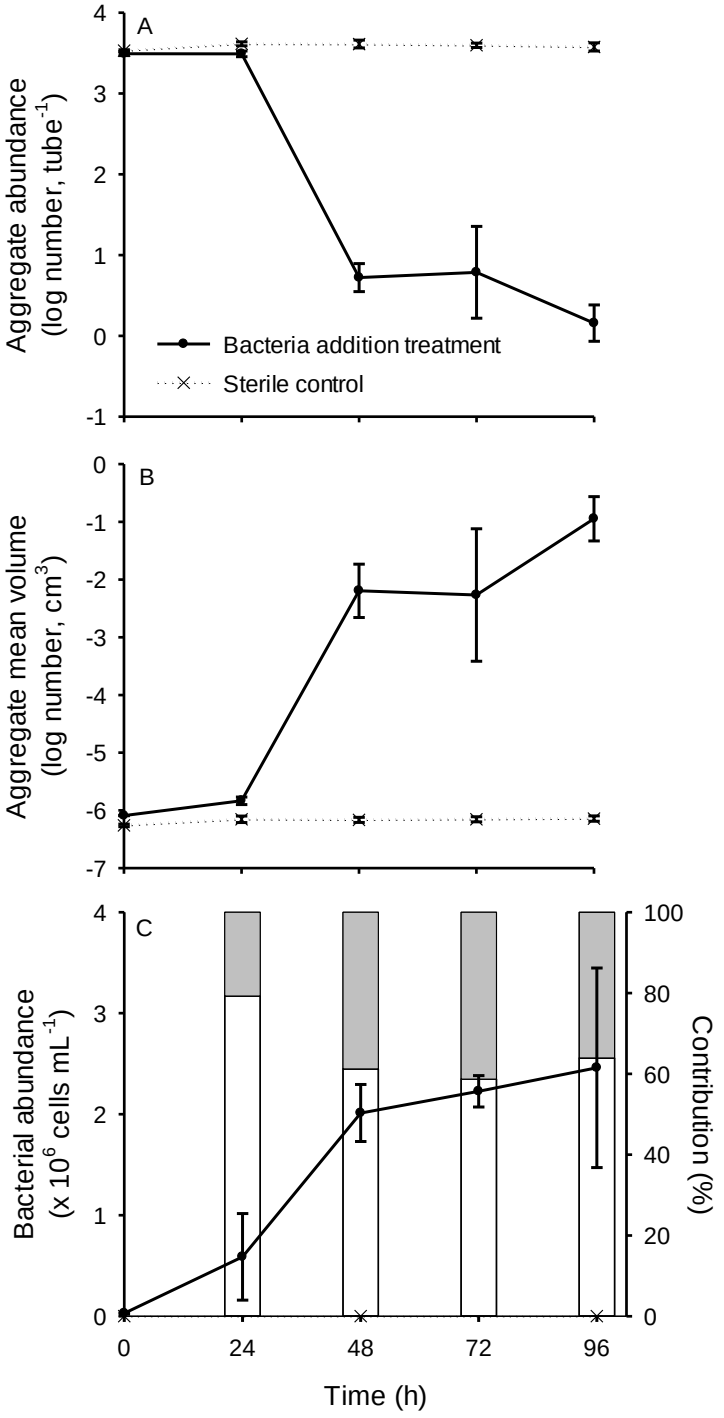

Fig. 4–1 Time course changes in (A) aggregate abundance, (B) aggregate mean volume and (C) bacterial abundance [relative contribution of attached (open bar) and unattached bacteria (closed bar) to total bacterial abundance in the bacteria addition treatment are also shown] for

the data collected in the sterile control and the bacteria addition treatment in Exp. 3 (errors are SD, $n = 3$).

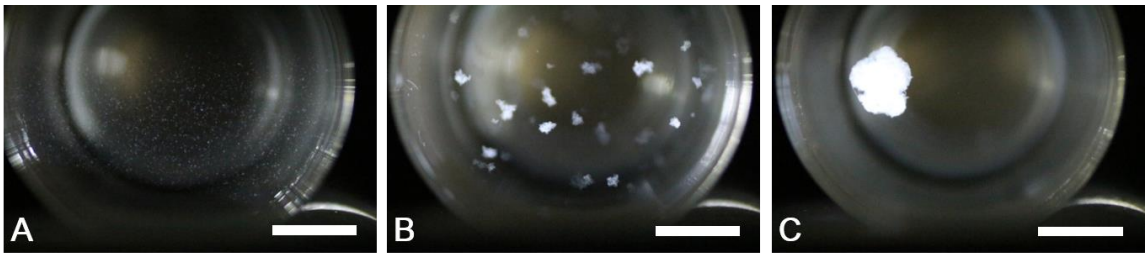

Fig. 4–2. Images of the aggregates in the bacteria addition treatment in Exp. 3 [(A) T_0, (B) T_{48} and (C) T_{96}]. Scale: 1 cm.

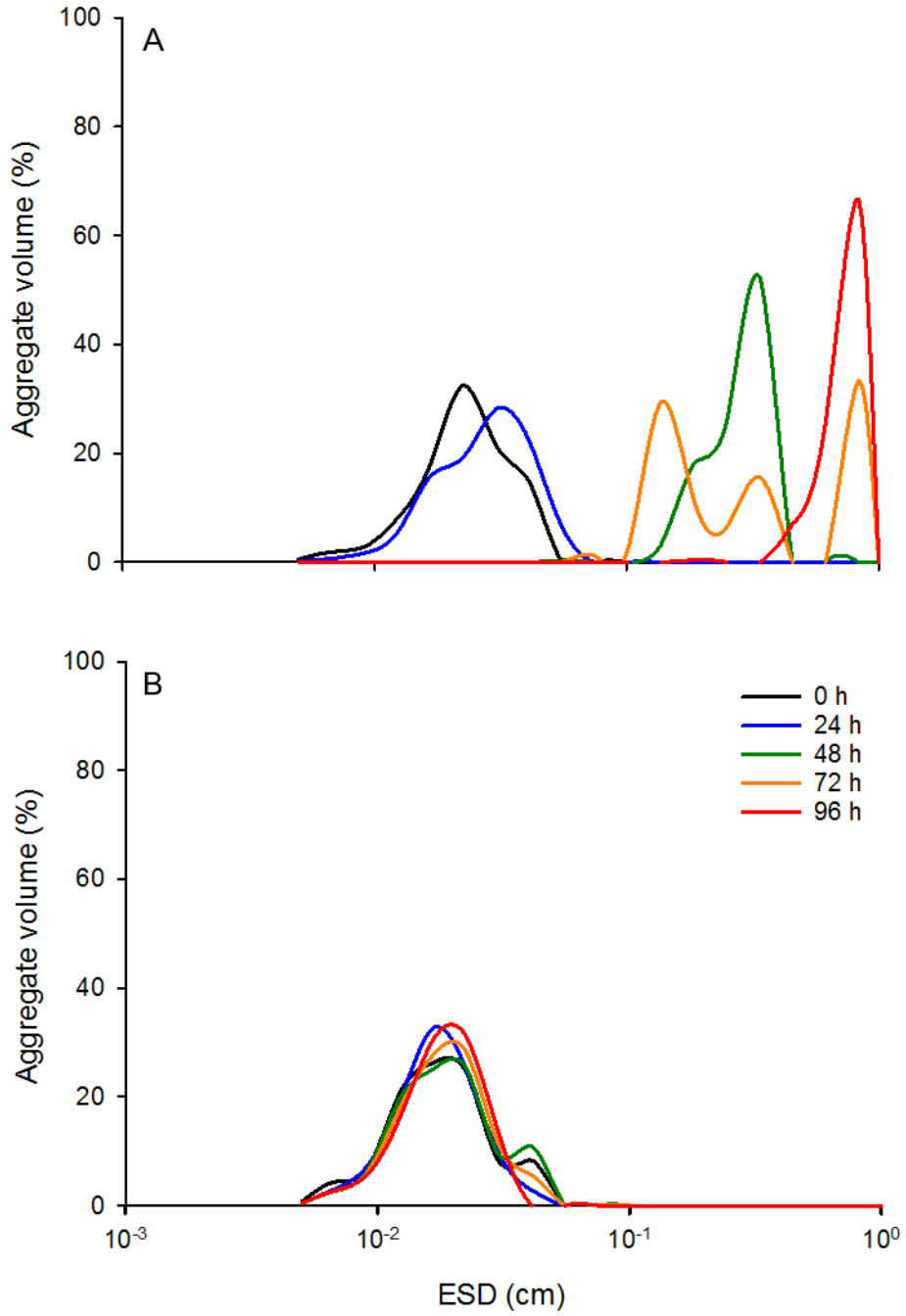

Fig. 4–3. Time course changes in aggregate size (ESD) distribution (18 logarithmic bins are placed on the x-axis) in Exp. 3 for (A) the bacteria addition treatment and (B) the sterile control. The number of particles determined (*n*) was 9128–12390 for the sterile control and for the initial sampling times (T_0 and T_{24}) of the bacteria addition treatment. *n* was 17, 33 and 5 for T_{48}, T_{72} and T_{96}, respectively, for the bacteria addition treatment.

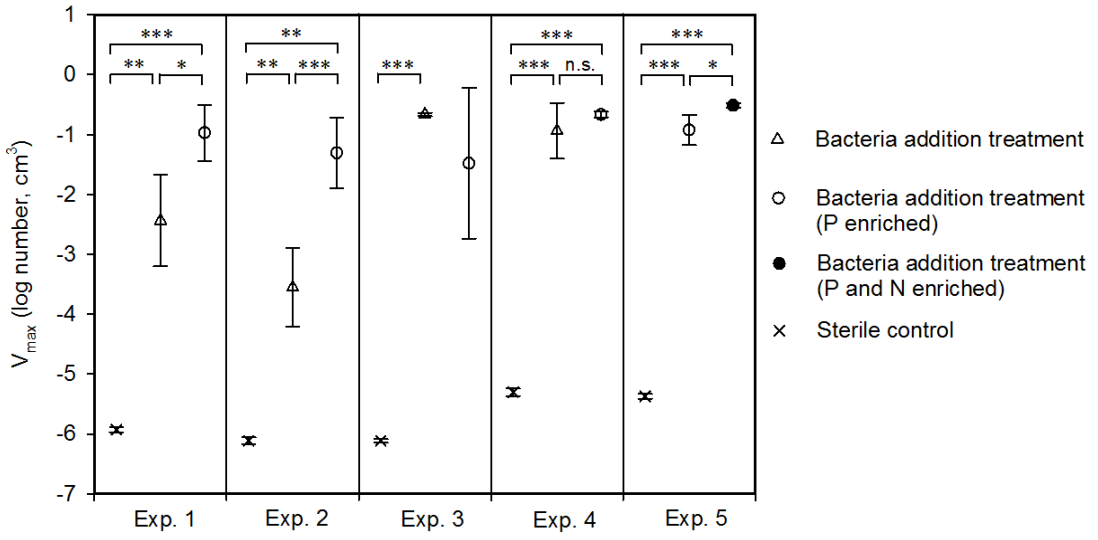

Fig. 4–4. Mean V_{max} (± SD, n = 3) in different treatments. Differences in mean V_{max} (log transformed) among the treatments for each experiment were tested by an ANOVA with a Holm-Sidak multiple comparison (*** $p < 0.001$, ** $p < 0.01$, * $p < 0.05$, n.s.; not significant). The data from the bacteria addition treatment (P enriched) in Exp. 3 were not included in this statistical comparison because the equal variance requirement was not met.

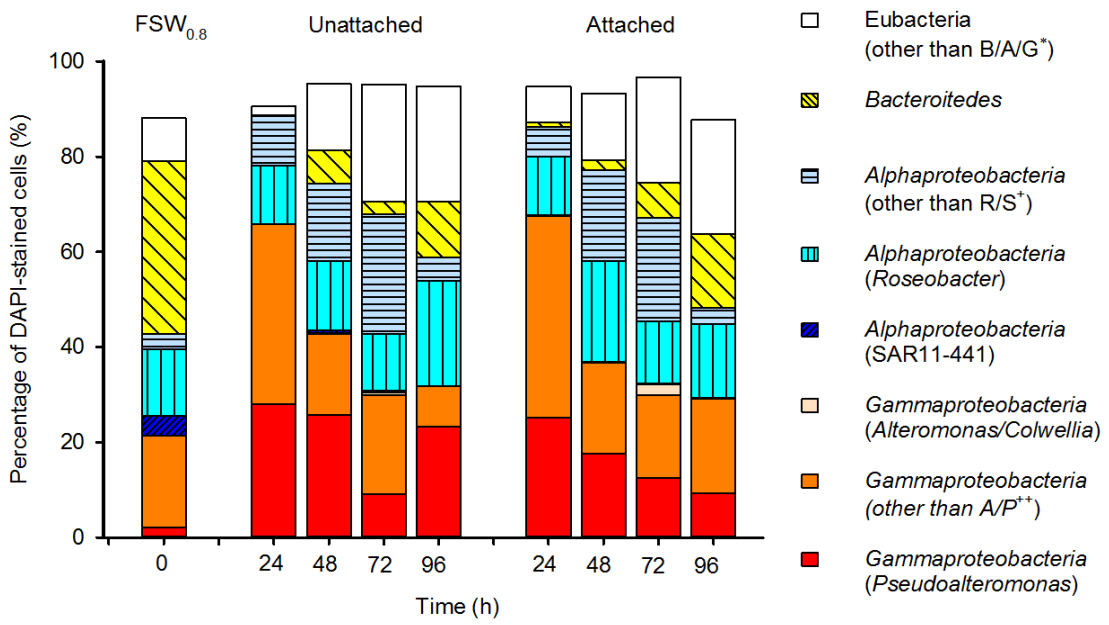

Fig. 4–5. Time course changes in the composition of phylogenetic groups for attached and unattached bacteria in Exp. 5 [bacteria addition treatment (P enriched)]. Values are the means of three bottles (coefficient of variation = 34.2 ± 36.6%, mean ± SD, n = 64) except for $FSW_{0.8}$ (n = 2). The probes used for this analysis are tabulated in Table 4–2. * Eubacteria other than *Bacteroidetes*, *Alphaproteobacteria* and *Gammaproteobacteria*; + *Alphaproteobacteria* other than *Roseobactor* and SAR11-441; ++ *Gammaproteobacteria* other than *Alteromonas/Colwellia* and *Pseudoalteromonas*.

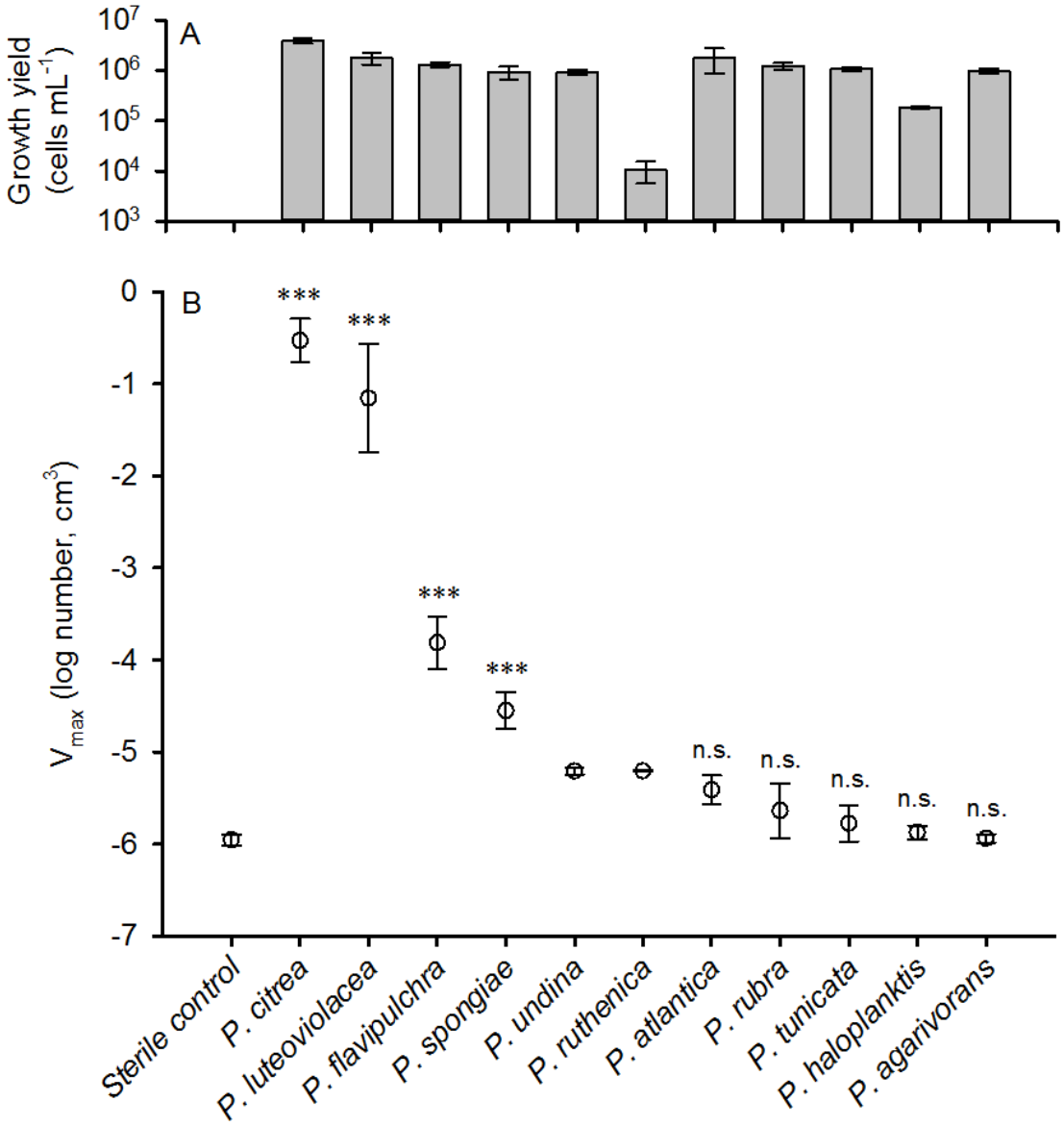

Fig. 4–6. (A) Growth yield and (B) V_{max} for different isolates affiliated with the genus *Pseudoalteromonas*. Growth yield was defined as the maximum total bacterial abundance determined during the incubation. Differences in mean V_{max} (log transformed) between the treatments relative to the sterile control (autoclaved *P. citrea*) were tested by an ANOVA with a Holm-Sidak multiple comparison (*** $p < 0.001$, ** $p < 0.01$, * $p < 0.05$, n.s.; not significant).

P. undina and *P. ruthenica* were not included for this statistical comparison because the equal variance requirement was not met.

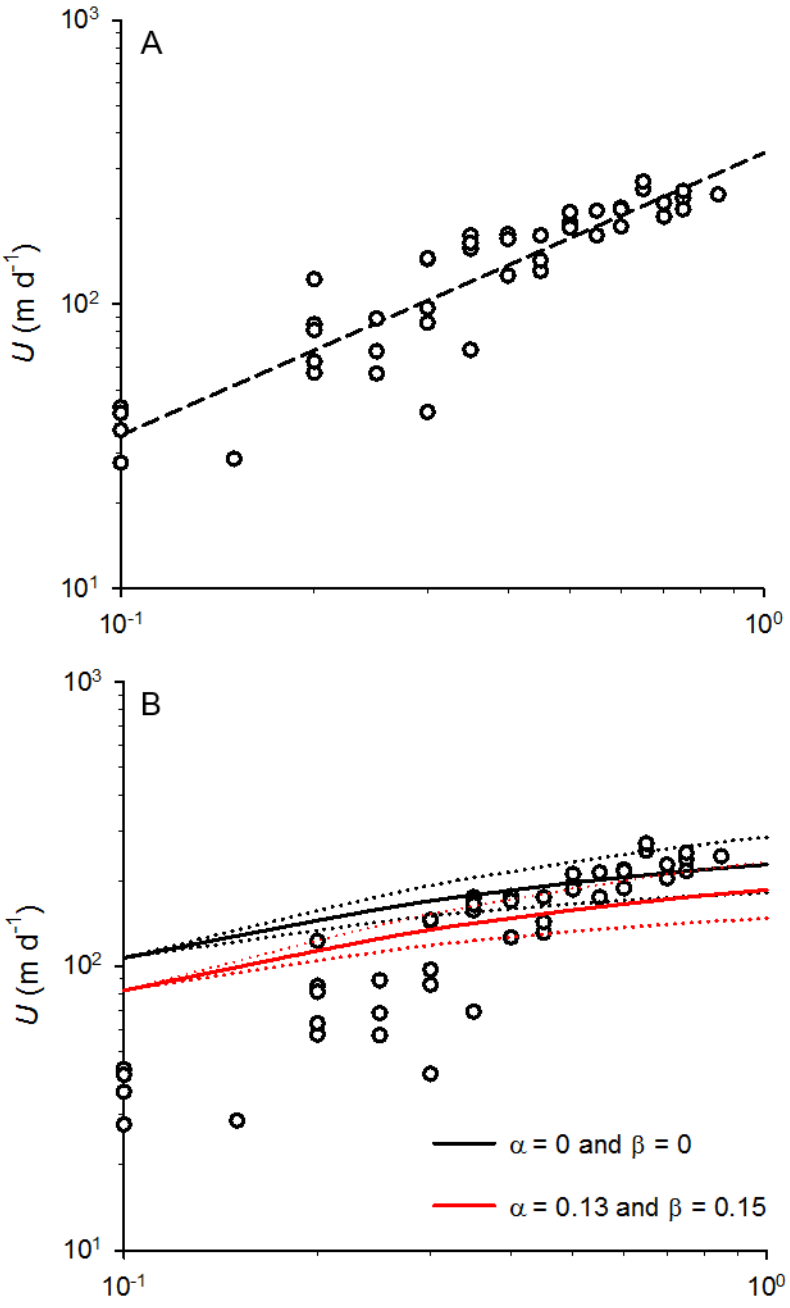

Fig. 4–7. (A) Relationship between U and ESD for the large particles collected from Exp.6. The regression line is also given: log U = 1.54 (± 0.04) + 0.99 (± 0.07) × log ESD (r^2 = 0.82, p < 0.001, n = 45, errors are standard errors). (B) Comparison of predicted and observed U. Predicted U was numerically derived using the model described in the text with a constraint on U (10^0–10^3 m d^{-1}). The divergence of two prediction curves reflects the sensitivity of the model

outcome to α and β parameterization. The error range accompanying each of the curves reflects the error (95% confidence interval) associated with the geometric parameter f (= fractal dimension – 3).

Table 4–1. Sampling location and sampling date for each experiment, with seawater temperature and salinity at the time of sampling. A summary of the experimental setup (the plus sign indicates that the corresponding treatment was prepared) is also given.

Exp #	Location	Sampling date dd/mm/yy	Water temperature (°C)	Salinity	Experimental setup			
					Bacteria addition treatment	Bacteria addition treatment (P enriched)	Bacteria addition treatment (P and N enriched)	Sterile control
Exp. 1	Otsuchi Bay	20/07/12	17.3	32.1	+	+	–	+
Exp. 2	Otsuchi Bay	26/07/12	21.1	30.8	+	+	–	+
Exp. 3	Oarai Beach	07/02/13	18.2	28.2	+	+	–	+
Exp. 4	Oarai Beach	13/05/13	20.1	29.0	+	+	–	+
Exp. 5	Oarai Beach	12/08/13	24.1	24.3	–	+	+	+
Exp. 6	Oarai Beach	18/11/13	17.1	28.8	–	+	–	–

Table 4–2. Oligonucleotide sequences used as CARD-FISH probes (Loy et al., 2007).

Probe	Target	Probe sequence (5'–3')	FA* (%)
Eub338-I	Bacteria	GCTGCCTCCCGTAGGAGT	35
Eub338-II	Supplement to Eub338	GCAGCCACCCGTAGGTGT	35
Eub338-III	Supplement to Eub338	GCTGCCACCCGTAGGTGT	35
Non338	Negative control	ACTCCTACGGGAGGCAGC	20
Alf968	*Alphaproteobacteria*	GGTAAGGTTCTGCGCGTT	20
SAR11-441	SAR11 clade	GGACCTTCTTATTCGGGT	25
ROS537	*Roseobacter* clade	CAACGCTAACCCCCTCC	35
Gam42a†	*Gammaproteobacteria*	GCCTTCCCACATCGTTT	35
Alt1413	*Alteromonas/Colwellia*	TTTGCATCCCACTCCCAT	40
PSU730	*Pseudoalteromonas*	TTGACCCAGGTGGCTGCC	40
CF319a	*Bacteroidetes*	TGGTCCGTGTCTCAGTAC	35

*Formamide (FA) concentration in CARD-FISH hybridization buffer.

† Including an unlabelled competitor probe Bet42a (5'-GCCTTCCCACTTCGTTT-3') (Manz et al., 1992).

Table 4–3. Percentages (mean ± SD, n = 3) of ΣBR (integrated from T_0 to a given time) and bacterial biomass relative to $[POC]_{ini}$ in the bacteria addition treatment (P enriched and P and N enriched) of Exp. 5.

Treatments	Variables	Time (h)			
		24	48	72	96
P enriched	ΣBR	2.2 ± 0.1	5.7 ± 0.4	9.7 ± 0.7	14.0 ± 0.6
	Biomass	2.7 ± 0.2	6.9 ± 1.4	8.9 ± 1.3	6.4 ± 1.6
P and N enriched	ΣBR	3.4 ± 0.2	7.4 ± 0.3	11.3 ± 0.3	15.3 ± 0.6
	Biomass	7.7 ± 0.5	10.1 ± 1.2	12.8 ± 1.9	9.4 ± 3.5

Table. 4–4. Parameters used for the prediction of U according to the model described by Equations from 4–1 to 4–8.

Parameters	Unit	Values	Source and/or remarks
d	cm	0.1–1	Particle diameter (ESD is used for the model analysis)
g	cm s^{-2}	980	Acceleration caused by gravity
v	cm^2 s^{-1}	0.0094	Kinematic viscosity of sea water at 25ºC and 29 in salinity (Fofonoff and Millard, 1983)
ρ_f	g cm^{-3}	1.019	Density of seawater at 25ºC and 29 in salinity (Fofonoff and Millard, 1983)
ρ_{pol}	g cm^{-3}	1.6	Density of polysaccharide matrices; Harding (1995); Rickwood (1984)
ρ_{bac}	g cm^{-3}	1.064	Density of attached bacterial; Chapter 3
α	Dimensionless	0 or 0.13	Contribution of bacterial biomass to total particle solid mass
β	Dimensionless	0 or 0.15	Contribution of bacterial respiratory loss to particle solid matter
ε_L	Dimensionless	$\log(1-\varepsilon_L) = -0.96\ (\pm 0.09) - 1.33\ (\pm 0.14) \times \log ESD$	Aggregate porosity (inter source particle porosity), which depended on ESD. Errors are standard errors.
ε_S	Dimensionless	0.960	Aggregate porosity (intra source particle porosity). The data are from Chapter 3*.

* The porosity reported for the aggregates with ESD = 0.0082 cm (Fig. 5 of Chapter 3) was used. Although the mean ESD of the source aggregates in the present study was determined to be 0.0106 cm using the images captured by camera, this ESD likely corresponded to the ESD of 0.0082 cm in Chapter 3, because my comparison indicated that the aggregate mean ESD determined by using camera images tended to be higher (by ca. 20%) than that determined by LISST (the method used in Chapter 3).

Chapter 5 General discussion

My results obtained in this study have added several important aspects to the previous knowledge regarding organic aggregate distributions in the Arctic Ocean and the regulation of organic aggregate settling velocity in marine environments. Here, I summarize these findings and highlight some important areas for future research.

5.1 Spatial distribution of suspended particles in the western Arctic: new evidence and implications for material cycling

My data collected in the western Arctic Ocean (Chapter 2) showed, for the first time, that the % TEP-C in shelf and slope-basin regions were relatively high (>100%) compared to other marine environments, which indicated that the western Arctic Ocean is a TEP dominant ocean. A hotspot (extremely high concentration) of suspended particles, accompanied by high prokaryote abundance and production, was found at the bottom of the shelf. High concentrations of Chl.a (4.8 μg L^{-1} and 2.5 μg L^{-1}) in the surface layer overlying the particle hotspot suggested that phytoplankton produced in the euphotic zone settled to the bottom and were decomposed by prokaryotes to result in the production of abundant TEP and small particles. I also found that particle volumes were high in the thin layer (a few to several meters) near the pycnocline, a phenomenon which was considered to be related to the accumulation of less dense aggregates which were likely produced with an involvement of TEP-induced aggregation. This finding corroborates the previous suggestion that TEP plays a crucial role in

the formation of less dense, porous aggregates (Azetsu-Scott and Passow, 2004), which can accumulate near the density interfaces due to slow solute exchange between inside and outside of the aggregates (Kindler et al., 2010). These aggregates can become even more porous and less easily settlable due to the action of attached bacteria that cleave aggregate polymers (Chapter 3). The increasing aggregate concentration could further accelerate the aggregation of particles entrained at the shear interfaces (Alldredge and Crocker, 1995; Burd and Jackson, 2009; Gallager et al., 2004). Given that concentration gradient was observed from the shelf to basin in the upper 50 m of the water column, these results suggest that aggregates, including TEP, are produced in the shelf region and are transferred to the slope-basin region along the pycnocline. The lateral transport of these aggregates could support productivity and material cycles in the nutrient-depleted basin region of the western Arctic Ocean. Taken together, these results suggest a need of incorporating the role of TEP and less-dense aggregates in lateral transport of organic carbon and other elements in the western Arctic Ocean (Fig. 5, see below).

5.2 Bacterial control of organic aggregate settling velocity: novel mechanisms involving the enhancement of porosity and coagulation efficiency

My results obtained using model aggregates (Chapter 3 and 4) revealed novel mechanism by which bacteria control organic aggregate settling velocity. First, I found that aggregates densely-colonized by bacteria were more slowly settled than those less-densely

colonized by bacteria. Model analysis results indicated that the increase in aggregate porosity due to bacterial cleavage of polymers resulted in the reduction in aggregate settling velocity. These results provide the first experimental evidence in support of the notion that the modification of aggregate structure by attached bacteria (porosity enhancement) can be an important factor controlling the settling velocity of marine particles. Second, I found that marine bacterial assemblages strongly enhanced the coagulation of small aggregates into large aggregates (ESD, 0.1–1 cm) over a period of 24–96 hours. I also found that the genus *Pseudoalteromonas* grew rapidly on the aggregates and are likely involved in the aggregate coagulation enhancement. High settling velocities (up to 270 m d^{-1}) were determined for larger aggregates (ESD, >0.4 cm), which agreed with theoretical predictions derived from a hydrodynamic model. These results demonstrate that specific types of bacteria readily colonize aggregates to impose a strong biotic force that enhances small organic aggregate coagulation and the formation of fast-settling large aggregates in seawater. Taken together, these results indicated that bacteria can affect the settling velocity of organic aggregation by two mechanisms (Fig. 5): 1) bacteria can reduce settling velocity of small organic aggregates via the enhancement of aggregate porosity, 2) bacteria can increase the settling velocity of organic aggregate via the promotion of coagulation of small organic aggregates to larger ones. I propose that these processes must be incorporated into the model of organic aggregate dynamics in marine environments (Fig. 5). The net outcome of these processes may depend on aggregate properties

(e.g. concentration, composition), environmental conditions (e.g. temperature, pH, salinity) and bacterial community composition, which should be clarified in future studies.

5.3 Important areas for future research

In this section, I discuss some important areas for future research.

1) In the present study, I found a hotspot of TEP and other particles near the bottom of the shelf region in Chukchi Sea. I interpreted that this is partly a reflection of high particle settling flux at that locality, although it is also possible that particles accumulated there because of lateral advection. This hypothesis should be tested in future studies. Previous sediment trap studies have failed to fully revolve heterogeneous particle settling field in the Chukchi Sea (Bates et al., 2005; Moran et al., 2005; Walsh et al., 2005). It would be useful for future studies to combine conventional sediment trap experiments with high-resolution particle distribution measurements using LISST.

2) There are also other important questions regarding the formation mechanism of TEP hot spot in the bottom of the shelf. I suggested that TEP were not just transported from the upper layer, but also produced in the bottom layer due to bacterial transformation of organic matter. Indeed, some previous studies have shown that TEP are produced during bacterial decomposition of organic matter (Cowen, 1992; Stoderegger and Herndl, 1998; Sugimoto et al., 2007). However,

we clearly need more data on bacterially-mediated TEP production, especially in perenially cold Arctic waters where bacterial acitivity is generally regarded to be suppressed by low temperature (Pomeroy and Deibel, 1986).

3) On the basis of in-situ particle volume investigation by an optical measurement, I found that particles were abundant in a thin layer near the pycnocline. Although a similar particle distribution pattern has been reported in other oceanic regions (Alldredge and Crocker, 1995; Burd and Jackson, 2009; Gallager et al., 2004), mechanisms by which aggregates accumulate near the pycnocline are still not entirely clear. Mechanistic understanding of this phenomenon has been hampered by the paucity of data on aggregate porosity and its variability in natural marine environments (Alldredge and Gotschalk, 1988). My results showing that attached bacteria can enhance aggregate porosity and reduce aggregate settling velocity (Chapter 3) suggest that future studies should examine organic aggregate porosity and density in natural environments with consideration of the extent of bacterially mediated aggregate transformation.

4) In addition to the localized distribution of TEP and other particles, I also found that there was a strong shelf-to-basin gradient in concentrations of suspended particles. This raises a possibility that lateral transport of these particles play an important role in the delivery of organic carbon and other elements from the productive shelf to the oligotrophic basin. This notion is consistent

with previous findings that particles are lateral transported from shelf to basin in the Arctic Ocean (Moore and Smith, 1986; Smith and Ellis, 1995). However, our knowledge concerning quantitative contributions of the lateral transport of materials to material cycling in Arctic basins is still limited. In the future study, it is necessary to take into account the contribution of TEP and TEP-induced aggregation to the regulation of lateral transport of materials from the shelf to basin.

5) There are some oceanic regions where TEP abundance has been under study. Oligotrophic subtropical oceans are one of these regions, which account for >60% of total sea surface area and are important in the regulation of global carbon cycles (Longhurst et al., 1995). Another oceanic realm where TEP abundance data are limited is the deep (>200 m) layers, where the organic carbon is actively transformed and mineralized. In these oceanic waters, our knowledge is limited regarding TEP abundance distribution and TEP-induced aggregation processes. This paucity of data limits our understanding of the regulation of settling particle fluxes in oceanic regions where ballast particles are scarce (Brown and Yoder, 1994; Francois et al., 2002; Honjo et al., 2008). Future studies are required to examine TEP distributions in these regions and layers.

6) My results regarding bacterial regulation of aggregate settling velocity in seawater (Chapter 3 and 4) were obtained under simple experimental settings using a model aggregate composed

of fucoidan and chitosan. Obviously, these results do not fully capture complexities in the control of aggregate formation and settling velocities in natural marine environments. To examine the general applicability of my findings to natural environments, two types of questions must be answered: 1) Whether or not bacterial effects on aggregate porosity and size enhancement that I found in this study can be generally applicable to other types of aggregates with different compositions and structures. 2) Whether or not the processes that I analyzed using a bacteria-aggregate system can proceed similarly in natural environments where a range of biotic interactions (grazing, viral lysis, symbiotic and antagonistic interactions) can potentially affect bacterial dynamics and metabolic activities. Future studies should address these questions by experiments in order to examine the general applicability of my results to natural environments.

7) Regarding aggregate porosity enhancement that I found in the present study (Chapter 3), the enhancement was assumed to be ascribed to bacterial enzymatic activities. Previous studies indicated that bacteria excrete two types of enzymes including those cleave the polymer chains from their edges (exoenzyme) and those cleave the polymer chains from their inner regions (endoenzyme) (Obayashi and Suzuki, 2005). The measurement of bacterial enzymes, especially endoenzymes, by using fluorescence or radio labeled substrates (Arnosti, 2000; Kirchman and White, 1999) and the observation of aggregate decomposition need to be

examined in greater detail in order to fully clarify the mechanism of aggregate porosity enhancement. If bacterial endoenzymes enhance aggregate porosity, the porosity enhancement of aggregates might be largely influenced by surrounding seawater conditions (pH, seawater temperature and pressure) (Hoppe et al., 2002; Hoppe, 1983; Teeling et al., 2012). It is also important to investigate the effects of bacterial community composition on bacterial porosity enhancement.

8) Regarding aggregate size enhancement, I proposed that increasing aggregate stickiness could be one plausible mechanism (Chapter 4). Previous microscopic observations suggested that particle coagulation could be mediated by a lectin-like protein (Waite et al., 1995) and fibrillar materials excreted by bacteria (Chin et al., 1998; Passow, 2002; Verdugo, 2012). These substances and structures could contribute to the enhancement of aggregate stickiness, but this hypothesis has yet to be tested. Clearly, clarification of the molecular basis of the bacterial enhancement of aggregate coagulation is an important theme for the future study.

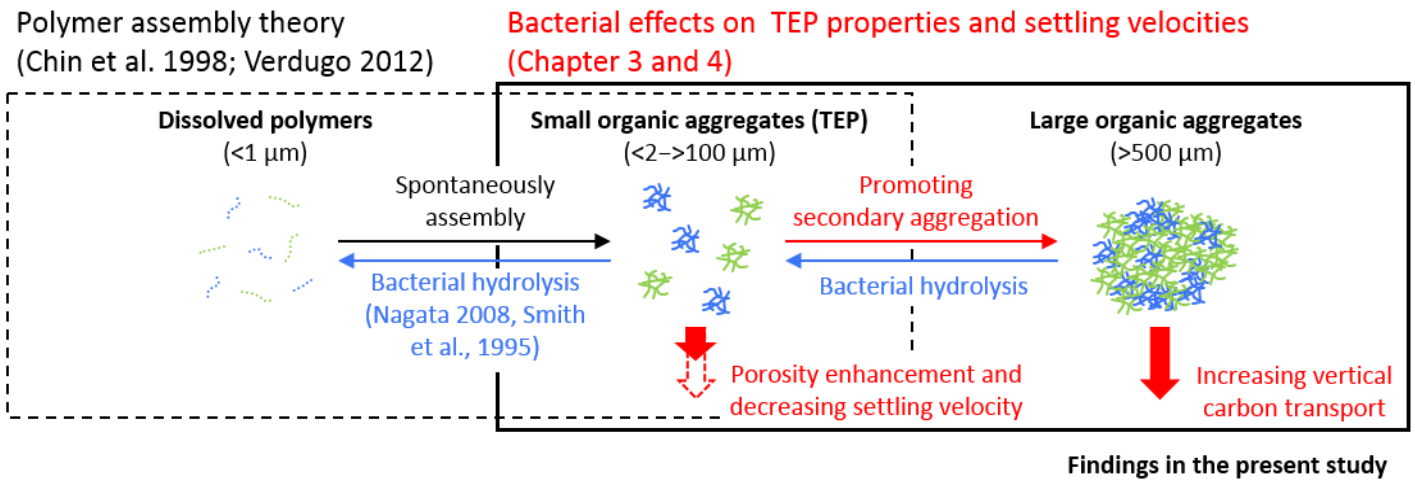

Fig. 5. A new model of organic aggregate formation, 'polymeric organic aggregation', with a previous concept of spontaneously polymer assembly. Dissolved polymers spontaneously assembled into small organic aggregates (TEP) (Chin et al., 1998; Verdugo, 2012). The settling velocity and secondary aggregation of small organic aggregates are enhanced bacterial attachment and activities (This study).

Acknowledgements

I would like to appreciate my supervisor Professor Toshi Nagata, Atmosphere and Ocean Research Institute, University of Tokyo, giving me full suggestions, supports and guidance during the course of my study.

I am thankful to Assistant Professor Hideki Fukuda, Atmosphere and Ocean Research Institute, University of Tokyo. He gave me many advices to improve my study and supports the experimental setups.

I also wish to thank the members of my Ph.D. committee: Professor Ichiro Terashima, Professor Jin Murata, Associate Professor Ko Noguchi, Graduate School of Science, University of Tokyo, and Professor Kazuhiro Kogure, Atmosphere and Ocean Research Institute, University of Tokyo, for warm encouragement to improve my study.

I would like to thank the officers and crew of the R.V. Mirai, Japan Agency for Marine-Earth Science and Technology (JAMSTEC), for their assistance support for sample collection.

I also would like to appreciate Marine biogeochemistry members in Atmosphere and Ocean Research institute for helping in many different ways in laboratory.

Lastly I thank my family for their great supports during the course of my study.

References

Aagaard, K., Weingartner, T.J., Danielson, S.L., Woodgate, R.A., Johnson, G.C., Whitledge, T.E., 2006. Some controls on flow and salinity in Bering Strait. Geophysical Research Letters 33, L19602.

Agrawal, Y.C., Pottsmith, H.C., 2000. Instruments for particle size and settling velocity observations in sediment transport. Marine Geology 168, 89–114.

Alldredge, A.L., 1979. The chemical composition of macroscopic aggregates in two neritic seas. . Limnology and Oceanography 24, 855–866.

Alldredge, A.L., 2000. Interstitial dissolved organic carbon (DOC) concentrations within sinking marine aggregates and their potential contribution to carbon flux. Limnology and Oceanography 45, 1245–1253.

Alldredge, A.L., Crocker, K.M., 1995. Why do sinking mucilage aggregates accumulate in the water column? The Science of the total environment 165, 15–22.

Alldredge, A.L., Gotschalk, C.C., 1988. In situ settling behavior of marine snow. Limnology and Oceanography 33, 339–351.

Alldredge, A.L., Gotschalk, C.C., 1989. Direct observations of the mass flocculation of diatom blooms: characteristics, settling velocities and formation of diatom aggregates. Deep-Sea Research 36, 159–171.

Alldredge, A.L., Passow, U., Logan, B.E., 1993. The abundance and significance of a class of large, transparent organic particles in the ocean. Deep-Sea Research I 40, 1131–1140.

Alldredge, A.L., Silver, M.V., 1988. Characteristics, Dynamics and Significance of Marine Snow. Progress Oceanography 20, 41–82.

Andrews, S.W., Nover, D.M., Reardon, K.E., Reuter, J.E., Schladow, S.G., 2011. The influence of ambient light intensity on in situ laser diffractometers. Water Resources Research 47, W06509.

Arnosti, C., 2000. Substrate specificity in polysaccharide hydrolysis: Contrasts between bottom water and sediments. Limnology and Oceanography 45, 1112–1119.

Antoine, D., André, J.-M., Morel, A., 1996. Oceanic primary production: 2. Estimation at global

scale from satellite (Coastal Zone Color Scanner) chlorophyll. Global Biogeochemical Cycles 10, 57–69.

Armstrong, R.A., Lee, C., John I. Hedges, Susumu Honjo, Wakeham, S.G., 2002. A new, mechanistic modelfor organic carbon fluxes in the ocean based on the quantitative association of POC with ballast minerals. Deep-Sea Research II 49, 219–236.

Arrigo, K.R., van Dijken, G.L., 2011. Secular trends in Arctic Ocean net primary production. Journal of Geophysical Research 116, C09011.

Ashjian, C.J., Gallager, S.M., Plourde, S., 2005. Transport of plankton and particles between the Chukchi and Beaufort Seas during summer 2002, described using a Video Plankton Recorder. Deep-Sea Research II 52, 3259–3280.

Azam, F., Malfatti, F., 2007. Microbial structuring of marine ecosystems. Nature reviews. Microbiology 5, 782–791.

Azetsu-Scott, K., Passow, U., 2004. Ascending marine particles: Significance of transparent exopolymer particles (TEP) in the upper ocean. Limnology and Oceanography 49, 741–748.

Balkanski, Y., Monfray, P., Battle, M., Heimann, M., 1999. Ocean primary production derived from satellite data: An evaluation with atmospheric oxygen measurements. Global Biogeochemical Cycles 13, 257–271.

Banse, K., 1977. Determining the carbon-to-chlorophyll ratio of natural phytoplankton. Marine biology 41, 199–212.

Bar-Zeev, E., Berman-Frank, I., Girshevitz, O., Berman, T., 2012. Revised paradigm of aquatic biofilm formation facilitated by microgel transparent exopolymer particles. Proceedings of the National Academy of Sciences of the United States of America 109, 9119–9124.

Bar-Zeev, E., Berman, T., Rahav, E., Dishon, G., Herut, B., Berman-Frank, I., 2011. Transparent exopolymer particle (TEP) dynamics in the eastern Mediterranean Sea. Marine Ecology Progress Series 431, 107–118.

Bates, N.R., Hansell, D.A., Bradley Moran, S., Codispoti, L.A., 2005. Seasonal and spatial distribution of particulate organic matter (POM) in the Chukchi and Beaufort Seas. Deep-Sea Research II 52, 3324–3343.

Bhaskar, P.V., Bhosle, N., 2006. Modelling the aggregation and break-up of fractal aggregates in a shear flow. Journal of Earth System Science 115, 403–413.

Biddanda, B.A., 1985. Microbial synthesis of macroparticulate matter. Marine Ecology Progress Series 20, 241–251.

Borch, N.H., Kirchman, D.L., 1997. Concentration and composition of dissolved combined neutral sugars (polysaccharides) in seawater determined by HPLC-PAD. Marine Chemistry 57, 85–95.

Bowman, J.P., 2007. Bioactive compound synthetic capacity and ecological significance of marine bacterial genus *Pseudoalteromonas*. Marine drugs 5, 220–241.

Brown, C.W., Yoder, J.A., 1994. Coccolithophorid blooms in the global ocean. Journal of Geophysical Research 99, 7467–7482.

Buesseler, K.O., 1998. The decoupling of production and particulate export in the surface ocean. Global Biogeochemical Cycles 12, 297–310.

Burd, A.B., Jackson, G.A., 2009. Particle aggregation. Annual review of marine science 1, 65–90.

Chester, R., 2000. Marine Geochemistry, second ed. Blackwell Science.

Chin, W.C., Orellana, M.V., Verdugo, P., 1998. Spontaneous assemblyof marine dissolved organic matter into polymer gels. Nature 391, 568–572.

Christiansen, C., 2002. Material transport from the nearshore to the basinal environment in the southern Baltic Sea I. Processes and mass estimates. Journal of Marine Systems 35, 133–150.

Corzo, A., Rodriguez-Galvez, S., Lubian, L., Sangra, P., Martinez, A., Morillo, J.A., 2005. Spatial distribution of transparent exopolymer particles in the Bransfield Strait, Antarctica. Journal of Plankton Research 27, 635–646.

Cowen, J.P., 1992. Morphological study of marine bacterial capsules implications for marine aggregate. Marine biology 114, 85–95.

De La Rocha, C.L., Passow, U., 2007. Factors influencing the sinking of POC and the efficiency of the biological carbon pump. Deep-Sea Research II 54, 639–658.

Decho, A.W., Moriaty, D.J.W., 1990. Bacterial exopolymer utilization by a harpacticoid copepod: A methodology and results. Limnology and Oceanography 35, 1039–1049.

Ducklow, H.W., Steinberg, D.K., Buesseler, K.O., 2001. Upper ocean carbon export and the biological pump. Oceanography 14, 50–58.

Dunton, K.H., Goodall, J.L., Schonberg, S.V., Grebmeier, J.M., Maidment, D.R., 2005. Multi-decadal synthesis of benthic–pelagic coupling in the western arctic: Role of cross-shelf advective processes. Deep-Sea Research II 52, 3462–3477.

Eglinton, T.I., Repeta, D.J., 2004. Marine organic geochemistry, in: Elderfield, H. (Ed.), Treatise on geochemistry. Elsevier, pp. 145–180.

Engel, A., 2000. The role of transparent exopolymer particles (TEP) in the increase in apparent particle stickiness (α) during the decline of a diatom bloom. Journal of Plankton Research 22, 485–497.

Engel, A., 2004. Distribution of transparent exopolymer particles (TEP) in the northeast Atlantic Ocean and their potential significance for aggregation processes. Deep-Sea Research I 51, 83–92.

Engel, A., Passow, U., 2001. Carbon and nitrogen content of transparent exopolymer particles (TEP) in relation to their Alcian Blue adsorption. Marine Ecological Progress Series 219, 1–10.

Engel, A., Szlosek, J., Abramson, L., Liu, Z., Lee, C., 2009. Investigating the effect of ballasting by $CaCO_3$ in Emiliania huxleyi: I. Formation, settling velocities and physical properties of aggregates. Deep-Sea Research II 56, 1396–1407.

Eppley, R.W., 1989. New production: History, methods, problems, in: Berger, W.H., Smetacek, V.S., Wefer, G. (Eds.), Productivity of the ocean: present and past. Wiley, pp. 85–97.

Fagerbakke, K.M., Heldal, M., Norland, S., 1996. Content of carbon, nitrogen, oxygen, sulfur and phosphorus in native aquatic and cultured bacteria. Aquatic Microbial Ecology 10, 15–27.

Falkowski, P.G., 1998. Biogeochemical controls and feedbacks on ocean primary production. Science 281, 200–206.

Falkowski, P.G., Davis, C.S., 2004. Redfield ratios: the uniformity of elemental ratios in the oceans and the life they contain underpins our understanding of marine biogeochemistry. Natue 431, 131.

Fennessy, M.J., Dyer, K.R., Huntley, D.A., 1994. An instrument to measure the size and settling velocity of flocs in situ. Marine Geology 117, 107–117.

Field, C.B., 1998. Primary production of the biosphere: Integrating terrestrial and oceanic components. Science 281, 237–240.

Fischer, G., Karakas, G., 2009. Sinking rates and ballast composition of particles in the Atlantic Ocean: implications for the organic carbon fluxes to the deep ocean. Biogeosciences 6, 85–102.

Fischer, G., Wefer, G., Romero, O., Dittert, N., Ratmeyer, V., Donner, B., 2003. Transfer of particles into the deep Atlantic, in: Wefer, G., Mulitza, S., Ratmeyer, V. (Eds.), The south Atlantic in the late quaternary: reconstruction of material budgets and current systems. . Springer-Verlag, pp. 12–46.

Fisher, N.S., Nolan, C.V., Fowler, S.W., 1991. Scavenging and retention of metals by zooplankton fecal pellets and marine snow. . Deep-Sea Research 38, 1261–1275.

Fofonoff, N.P., Millard, R.C.J., 1983. Algorithms for computation of fundamental properties of seawater. UNESCO Technical Paper in Marine Science 44.

Forest, A., Sampei, M., Hattori, H., Makabe, R., Sasaki, H., Fukuchi, M., Wassmann, P., Fortier, L., 2007. Particulate organic carbon fluxes on the slope of the Mackenzie Shelf (Beaufort Sea): Physical and biological forcing of shelf-basin exchanges. Journal of Marine Systems 68, 39–54.

Francois, R., Honjo, S., Krishfield, R., Manganini, S., 2002. Factors controlling the flux of organic carbon to the bathypelagic zone of the ocean. Global Biogeochemical Cycles 16, 34.

Fujiwara, A., Hirawake, T., Suzuki, K., Imai, I., Saitoh, S.I., 2014. Timing of sea ice retreat can alter phytoplankton community structure in the western Arctic Ocean. Biogeosciences 11, 1705–1716.

Fukuda, R., Ogawa, H., Nagata, T., Koike, I., 1998. Direct determination of carbon and nitrogen contents of natural bacterial assemblages in marine environments. Applied and Environmental Microbiology 64, 3352–3358.

Fung, I.Y., Tucker, C.J., Prentice, K.C., 1987. Application of advanced very high resolution radiometer vegetation index to study atmosphere-biosphere exchange of CO_2. Journal of Geophysical Research 92, 2999–3015.

Gallager, S.M., Yamazaki, H., Davis, C.S., 2004. Contribution of fine-scale vertical structure and swimming behavior to formation of plankton layers on Georges Bank. Marine Ecological Progress Series 267, 27–43.

García-Martínez, J., Acinas, G.S., Massana, R., Rodríguez-Valera, R., 2002. Prevalence and microdiversity of Alteromonas macleodii-like microorganisms in different oceanic regions. Environmental microbiology 4, 42–50.

Garcia, C.M., Prieto, L., Vargas, M., Echevarria, F., Garcia-Lafuente, J., Ruiz, J., Rubin, J.P., 2002. Hydrodynamics and the spatial distribution of plankton and TEP in the Gulf of Cádiz (SW Iberian Peninsula). Journal of Plankton Research 24, 817–833.

Gardes, A., Iversen, M.H., Grossart, H.P., Passow, U., Ullrich, M.S., 2011. Diatom-associated bacteria are required for aggregation of *Thalassiosira weissflogii*. The ISME journal 5, 436–445.

Gonzalez, E.A., Hill, P.S., 1998. A method for estimating the flocculation time of monodispersed sediment suspensions. Deep-Sea Research I 45, 1931–1954.

Gooday, G.W., 1990. Physiology of microbial degradation of chitin and chitosan. Biodegradation 1, 177–190.

Grebmeier, J.M., Cooper, L.W., Feder, H.M., Sirenko, B.I., 2006. Ecosystem dynamics of the pacific-influenced northern Bering and Chukchi Seas in the amerasian Arctic. Progress in Oceanography 71, 331–361.

Grossart, H.P., Berman, T., Simon, M., Pohlmann, K., 1998. Occurrence and microbial dynamics of macroscopic organic aggregates (lake snow) in Lake Kinneret, Israel, in fall. Aquatic Microbial Ecology 14, 59–67.

Grossart, H.P., Czub, G., Simon, M., 2006. Algae-bacteria interactions and their effects on aggregation and organic matter flux in the sea. Environmental microbiology 8, 1074–1084.

Hall-Stoodley, L., Stoodley, P., 2002. Developmental regulation of microbial biofilms. Current Opinion in Biotechnology 13, 228–233.

Hansell, D.A., 2002. DOC in the global ocean carbon cycle, in: Hansell, D.A., Carlson, C.A. (Eds.), Biogeochemistry of marine dissolved organic matter. Academic Press, pp. 685–715.

Hansell, D.A., Carlson, C.A., 1998. Deep-oceangradients in theconcentration of dissolvedorganiccarbon. Nature 395, 263–266.

Harding, S.E., 1995. Some recent developments in the size and shape analysis of industrial polysaccharides in solution using sedimentation analysis in the analytical ultracentrifuge. Carbohydrate Polymers 28, 227–237.

Hasumi, H., Nagata, T., 2014. Modeling the global cycle of marine dissolved organic matter and its influence on marine productivity. Ecological Modelling 288, 9–24.

Henson, S.A., Sanders, R., Madsen, E., Morris, P.J., Le Moigne, F., Quartly, G.D., 2011. A reduced estimate of the strength of the ocean's biological carbon pump. Geophysical Research Letters 38, L04606.

Herndl, G.J., Reinthaler, T., 2013. Microbial control of the dark end of the biological pump. Nature Geoscience 6, 718–724.

Hioki, N., Kuma, K., Morita, Y., Sasayama, R., Ooki, A., Kondo, Y., Obata, H., Nishioka, J., Yamashita, Y., Nishino, S., Kikuchi, T., Aoyama, M., 2014. Laterally spreading iron, humic-like dissolved organic matter and nutrients in cold, dense subsurface water of the Arctic Ocean. Scientific reports 4, 6775.

Hong, Y., Smith, W.O., White, A.-M., 1997. Studies on transparent expolymer particles (TEP) produced in the Ross sea (Antarctica) and by *Phaeocystis antarctica* (Prymnesiophyceae). Journal of Phycology 33, 368–376.

Honjo, S., Eglinton, T., Taylor, C., Ulmer, K., Sievert, S., Bracher, A., German, C., Edgcomb, V., Francois, R., Iglesias-Rodriguez, M.D., Van Mooy, B., Rapeta, D., 2014. Understanding the role of the biological pump in the global carbon cycle: An imperative for ocean science. Oceanography 27, 10–16.

Honjo, S., Manganini, S.J., Krishfield, R.A., Francois, R., 2008. Particulate organic carbon fluxes to the ocean interior and factors controlling the biological pump: A synthesis of global sediment trap programs since 1983. Progress in Oceanography 76, 217–285.

Hopcroft, R., Bluhm, B., Gradinger, R., 2008. Arctic ocean synthesis: Analysis of climate change impacts in the chukchi and beaufort seas with strategies for future research. University of Alaska, Fairbanks, Institute of Marine Science.

Hoppe, H.G., 1983. Significance of exoenzymatic activities in the ecology of brackish water: measurements by means of methylumbelliferyl-substrates. Marine Ecological Progress Series 11, 299–308.

Hoppe, H. G., Arnosti, C., Herndl, G., 2002. Ecological Significance of Bacterial Enzymes in the Marine Environment, in: Burns, R.G., Dick, R.P. (Eds.), Enzymes in the environment: Activity, ecology, and applications. CRC Press, pp. 73–108.

Horobin, R.W., 1988. Understanding histochemistry: selection, evaluation, and design of biological stains. Wiley.

Inoue, K., Nishimura, M., Nayak, B.B., Kogure, K., 2007. Separation of marine bacteria

according to buoyant density by use of the density-dependent cell sorting method. Appl Environ Microbiol 73, 1049–1053.

Iversen, M.H., Ploug, H., 2010. Ballast minerals and the sinking carbon flux in the ocean: carbon-specific respiration rates and sinking velocity of marine snow aggregates. Biogeosciences 7, 2613–2624.

Johnson, B.D., Kranck, t.l.K., Muschebheim, D.K., 1994. Physico-chemical factors in particle aggregation, in: Wotton, R.S. (Ed.), The biology of particles in aquatic systems, second ed. CRC Press, pp. 75–96.

Jonasz, M., Fournier, G.R., 2007. Light scattering by particles in water -Theoretical and experimental foundations. Elsevier.

Jouon, A., Ouillon, S., Douillet, P., Lefebvre, J.P., Fernandez, J.M., Mari, X., Froidefond, J.-M., 2008. Spatio-temporal variability in suspended particulate matter concentration and the role of aggregation on size distribution in a coral reef lagoon. Marine Geology 256, 36–48.

Juhl, A.R., Krembs, C., Meiners, K.M., 2011. Seasonal development and differential retention of ice algae and other organic fractions in first-year Arctic sea ice. Marine Ecology Progress Series 436, 1–16.

Karl, D.M., Christian, J.R., Dore, J.E., Hebel, D.V., Letelier, R.M., Tupas, L.M., Winn, C.D., 1996. Seasonal and interannual variability in primary production and particle flux at Station ALOHA. Deep-Sea Research II 43, 539–568.

Kepkay, P.E., 2000. Colloids and the ocean carbon cycle, in: Wangersky, P.J. (Ed.), The handbook of environmental chemistry, Springer, pp. 35–56.

Kilps, J.R., Logan, B.E., Alldredge, A.L., 1994. Fractal dimensions of marine snow determined from image analysis of in situ photographs. Deep-Sea Research I 41, 1159–1169.

Kindler, K., Khalili, A., Stocker, R., 2010. Diffusion-limited retention of porous particles at density interfaces. Proceedings of the National Academy of Sciences of the United States of America 107, 22163–22168.

Kiorboe, T., Lundsgaard, C., Olesen, M., Hansen, J.L.S., 1994. Aggregation and sedimentation on processes during a spring phytoplankton bloom: A field experiment to test coagulation theory. Journal of Marine Research 52, 297–323.

Kirchman, D.L., 2001. Measuring bacterial biomass production and growth rates from leucine

incorporation in natural aquatic environments, in: paul, J.H. (Ed.), Methods in Microbiology. Academic Press.

Kirchman, D.L., Moran, X.A., Ducklow, H., 2009. Microbial growth in the polar oceans -role of temperature and potential impact of climate change. Nature reviews. Microbiology 7, 451–459.

Kirchman, D.L., White, J., 1999. Hydrolysis and mineralization of chitin in the Delaware Estuary. Aquatic Microbial Ecology 18, 187–196.

Klaas, C., Archer, D.E., 2002. Association of sinking organic matter with various types of mineral ballast in the deep sea: Implications for the rain ratio. Global Biogeochemical Cycles 16, 63-61–63-14.

Koike, I., Fukuda, H., 2007. Mini-review: Assessment of size distribution of suspended particles in coastal and estuarine environments using in situ instruments. Coastal Marine Science 31, 1–8.

Koike, I., Hara, S., Terauchi, K., Kogure, K., 1990. Role of sub-micronmeter particles in the ocean. Nature 345, 242–244.

Krembs, C., Eicken, H., Junge, K., Deming, J.W., 2002. High concentrations of exopolymeric substances in Arctic winter sea ice: implications for the polar ocean carbon cycle and cryoprotection of diatoms. Deep-Sea Research I 49, 2163–2181.

Kwok, R., Rothrock, D.A., 2009. Decline in Arctic sea ice thickness from submarine and ICESat records: 1958–2008. Geophysical Research Letters 36, L15501.

Lam, P.J., Doney, S.C., Bishop, J.K.B., 2011. The dynamic ocean biological pump: Insights from a global compilation of particulate organic carbon, $CaCO_3$, and opal concentration profiles from the mesopelagic. Global Biogeochemical Cycles 25, GB3009.

Lee, S.H., Joo, H.M., Liu, Z., Chen, J., He, J., 2012. Phytoplankton productivity in newly opened waters of the western Arctic Ocean. Deep-Sea Research II 81–84, 18–27.

Logan, B.E., Grossart, H.P., Simon, M., 1994. Direct observation of phytoplankton, TEP and aggregates on polycarbonate filters using brightfield microscopy. Journal of Plankton Research 16, 1811–1815.

Logan, B.E., Hunt, J.R., 1987. Advantages to microbes of growth in permeable aggregates in marine systems. Limnology and Oceanography 32, 1034–1048.

Logan, B.E., Wilkinson, D.B., 1990. Fractal geometry of marine snow and other biological aggregates. Limnology and Oceanography 35, 130–136.

Longhurst, A., Sathyendranath, S., Platt, T., Caverhill, C., 1995. An estimate of global primary production in the ocean from satellite radiometer data. Journal of Plankton Research 17, 1245–1271.

Loy, A., Maixner, F., Wagner, M., Horn, M., 2007. probeBase-an online resource for rRNA-targeted oligonucleotide probes: new features 2007. Nucleic acids research 35, D800–D804.

MacIntyre, S., Alldredge, A.L., Gotschalk, C.C., 1995. Accumulation of marine snow at density discontinuities in the water column. Limnology and Oceanography 40, 449–468.

Malpezzi, M.A., Sanford, L.P., Crump, B.C., 2013. Abundance and distribution of transparent exopolymer particles in the estuarine turbidity maximum of Chesapeake Bay. Marine Ecology Progress Series 486, 23–35.

Manz, W., Amann, R., Ludwig, W., Wagner, M., Schleifer, K.-H., 1992. Phylogenetic oligodeoxynucleotide probes for the major subclasses of proteobacteria: Problems and solutions. Systematic and Applied Microbiology 15, 593–600.

Mari, X., Kiorboe, T., 1996. Abundance, size distribution and bacterial colonization of transparent exopolymeric particles (TEP) during spring in the Kattegat. Journal of Plankton Research 18, 969–986.

Mari, X., Torréton, J.-P., Bich-Thuy Trinh, C., Bouvier, T., Van Thuoc, C., Lefebvre, J.-P., Ouillon, S., 2012. Aggregation dynamics along a salinity gradient in the Bach Dang estuary, North Vietnam. Estuarine, Coastal and Shelf Science 96, 151–158.

Martín, J., Miquel, J.-C., 2010. High downward flux of mucilaginous aggregates in the Ligurian Sea during summer 2002: similarities with the mucilage phenomenon in the Adriatic Sea. Marine Ecology 31, 393–406.

Massana, R., Gasol, J.M., Bjørnsen, P.K., Blackburn, N., Hagström, A., Hietanen, S., Hygum, B.H., Kuparinen, J., Pedrós-Alió, C., 1997. Measurement of bacterial size via image analysis of epifluorescence preparations: description of an inexpensive system and solutions to some of the most common problems. Scientia Marina 61, 397–407.

McDonnell, A.M.P., Buesseler, K.O., 2012. A new method for the estimation of sinking particle fluxes from measurements of the particle size distribution, average sinking velocity, and carbon content. Limnology and Oceanography: Methods 10, 329–346.

Meiners, K., Krembs, C., Gradinger, R., 2008. Exopolymer particles: microbial hotspots of enhanced bacterial activity in Arctic fast ice (Chukchi Sea). Aquatic Microbial Ecology 52, 195–207.

Melillo, J.M., McGuire, A.D., Kicklighter, D.W., Moore, B., Vorosmarty, C.J., Schloss, A.L., 1993. Global climate change and terrestrial net primary production. Nature 363, 234–240.

Moore, R.M., Smith, J.N., 1986. Disequilibria between^{226}Ra, ^{210}Pb and ^{210}Po in the Arctic Ocean and the implications for chemical modification of the Pacific water inflow. Earth and Planetary Science Letters 77, 285–292.

Mopper, K., Zhou, J., Ramana, K.S., Passow, U., Dam, H.G., Drapeau, D.T., 1995. The role of surface-active carbohydrates in the floculation of a diatom bloom in a mesocosm. Deep-Sea Research 42, 47–73.

Moran, S.B., Kelly, R.P., Hagstrom, K., Smith, J.N., Grebmeier, J.M., Cooper, L.W., Cota, G.F., Walsh, J.J., Bates, N.R., Hansell, D.A., Maslowski, W., Nelson, R.P., Mulsow, S., 2005. Seasonal changes in POC export flux in the Chukchi Sea and implications for water column-benthic coupling in Arctic shelves. Deep Sea Research Part II: Topical Studies in Oceanography 52, 3427–3451.

Moran, S.B., Smith, J.N., 2000. ^{234}Th as a tracer of scavenging and particle export in the Beaufort Sea. Continental Shelf Research 20, 153–167.

Morison, J., Kwok, R., Peralta-Ferriz, C., Alkire, M., Rigor, I., Andersen, R., Steele, M., 2012. Changing arctic ocean freshwater pathways. Nature 481, 66–70.

Myklestad, A.M., Skanoy, E., Hestmann, S., 1997. A sensitive and rapid method for analysis of dissolved mono- and polysaccharides in seawater. Marine Chemistry 56, 279–286.

Nagata, T., 2008. Organic matter-bacteria interactions in sea water, in: Kirchman, D.L. (Ed.), Microbial ecology of the oceans, second ed. Wiley.

Nagata, T., Meon, B., Kirchman, D.L., 2003. Microbial degradation of peptidoglycan in seawater. Limnology and Oceanography 48, 745–754.

Nakamura, S., Nambu, M., Ishizuka, T., Hattori, H., Kanatani, Y., Takase, B., Kishimoto, S., Amano, Y., Aoki, H., Kiyosawa, T., Ishihara, M., Maehara, T., 2008. Effect of controlled release of fibroblast growth factor-2 from chitosan/fucoidan micro complex-hydrogel on in vitro and in vivo vascularization. Journal of biomedical materials research A 85, 619–627.

Nishino, S., Kikuchi, T., Yamamoto-Kawai, M., Kawaguchi, Y., Hirawake, T., Itoh, M., 2011. Enhancement/reduction of biological pump depends on ocean circulation in the sea-ice reduction regions of the Arctic Ocean. Journal of Oceanography 67, 305–314.

Noble, R.T., Fuhrman, J.A., 1998. Use of SYBR Green I for rapid epifluorescence counts of marine viruses and bacteria. Aquatic Microbial Ecology 14, 113–118.

Obayashi, Y., Suzuki, S., 2005. Proteolytic enzymes in coastal surface seawater: Significant activity of endopeptidases and exopeptidases. Limnology and Oceanography 50, 722–726.

Oliver, R.L., Kinnear, A.J., Ganf, G.G., 1981. Mearument of cell density of three freshwater phytoplankton. Limnology and Oceanography 26, 285–294.

Ortega-Morales, B.O., Santiago-Garcia, J.L., Chan-Bacab, M.J., Moppert, X., Miranda-Tello, E., Fardeau, M.L., Carrero, J.C., Bartolo-Perez, P., Valadez-Gonzalez, A., Guezennec, J., 2007. Characterization of extracellular polymers synthesized by tropical intertidal biofilm bacteria. Journal of Applied Microbiology 102, 254–264.

Ortega-Retuerta, E., Reche, I., Pulido-Villena, E., Agustí, S., Duarte, C.M., 2009. Uncoupled distributions of transparent exopolymer particles (TEP) and dissolved carbohydrates in the Southern Ocean. Marine Chemistry 115, 59–65.

Parkinson, C.L., Comiso, J.C., 2013. On the 2012 record low Arctic sea ice cover: Combined impact of preconditioning and an August storm. Geophysical Research Letters 40, 1356–1361.

Passow, U., 2002. Transparent exopolymer particles (TEP) in aquatic environments. Progress in Oceanography 55, 287–333.

Passow, U., Alldredge, A.L., 1994. Distribution, size and bacterial colonization of transparent exopolymer particle (TEP) in the ocean. Marine Ecology Progress Series 113, 185–198.

Passow, U., Alldredge, A.L., 1995. A dye-binding assay for the spectrophotometric measurement of transparent exopolymer particles (TEP). Limnology and Oceanography 40, 1326–1335.

Passow, U., Carlson, C., 2012. The biological pump in a high CO_2 world. Marine Ecological Progress Series 470, 249–271.

Passow, U., De La Rocha, C.L., 2006. Accumulation of mineral ballast on organic aggregates. Global Biogeochemical Cycles 20, GB1013.

Passow, U., Shipe, R.F., Murray, A., Pak, D.K., Brzezinski, M.A., Alldredge, A.L., 2001. The origin of transparent exopolymer particles (TEP) and their role in the sedimentation of particulate matter. Continental Shelf Research 21, 327–346.

Pernthaler, A., Pernthaler, J., Amann, R., 2002. Fluorescence In situ hybridization and catalyzed reporter deposition for the Identification of marine bacteria. Applied and Environmental Microbiology 68, 3094–3101.

Pernthaler, A., Pernthaler, J., Amann, R., 2004. Sensitive multicolor fluorescence in situ hybridization for the identification of environmental microorganisms, in: Kowalchuk, G., de Bruijn, F.J., Head, I.M., Akkermans, A.D.L., van Elsas, J.D. (Eds.), Molecular Microbial Ecology Manual, 2 ed. Kluwer Academic Publishers, pp. 711–726.

Perovich, D., Meier, W., Maslanik, J., Richter-Menge, J., 2010. Sea cover. Arctic Report Card, 16–20.

Ploug, H., Iversen, M.H., Fischer, G., 2008. Ballast, sinking velocity, and apparent diffusivity within marine snow and zooplankton fecal pellets: Implications for substrate turnover by attached bacteria. Limnology and Oceanography 53, 1878–1886.

Ploug, H., Passow, U., 2007. Direct measurement of diffusivity within diatom aggregates containing transparent exopolymer particles. Limnology and Oceanography 52, 1–6.

Ploug, H., Terbruggen, A., Wolf-Gladrow, D., Passow, U., 2010. A novel method to measure particle sinking velocity in vitro, and its comparison to three other in vitro methods. Limnology and Oceanography: Methods 8, 386–393.

Pomeroy, L.R., 1974. The ocean's food web, a changing paradigm. BioScience 24, 499–504.

Pomeroy, L.R., Deibel, D., 1986. Temperature regulation of bacterial activity during the spring bloom in Newfoundland coastal waters. Science 233, 359–361.

Porter, K.G., Feig, Y.S., 1980. The use of DAPI for identifying and counting aquatic microflora. Limnology and Oceanography 25, 943–948.

Poulicek, M., Gaill, F., Goffinet, G., 1998. Chitin biodegradation in marine environments, in: Stankiewicz, B.A., van Bergen, P.F. (Eds.), Nitrogen-containing macromolecules in the bio- and geosphere. American Chemical Society, pp. 163-210.

Ramaiah, N., Furuya, K., 2002. Seasonal variations in phytoplankton composition and transparent exopolymer particles in a eutrophicated coastal environment. Aquatic Microbial

Ecology 30, 69–82.

Ramaiah, N., Yoshikawa, T., Furuya, K., 2001. Temporal variations in transparent exopolymer particles (TEP) associated with a diatom spring bloom in a subarctic ria in Japan. Marine Ecological Progress Series 212, 79–88.

Rao, D., Webb, J.S., Kjelleberg, S., 2006. Microbial colonization and competition on the marine alga *Ulva australis*. Applied and Environmental Microbiology 72, 5547–5555.

Reynolds, R.A., Stramski, D., Wright, V.M., 2008. Particle size distributions of coastal waters measured with an in situ laser diffractometer. Ocean Optics 19.

Rickwood, D., 1984. Preparative centrifugation; a practical approach, second ed. IRL/Oxford University Press.

Riebesell, U., Reigstad, M., Wassmann, P., Noji, T., Passow, U., 1995. On the trophic fate of *Phaeocystis pouchetii* (hariot): VI. Significance of Phaeocystis-derived mucus for vertical flux. Netherlands Journal of Sea Research 33, 193–203.

Riebesell, U., Schulz, K.G., Bellerby, R.G., Botros, M., Fritsche, P., Meyerhofer, M., Neill, C., Nondal, G., Oschlies, A., Wohlers, J., Zollner, E., 2007. Enhanced biological carbon consumption in a high CO_2 ocean. Nature 450, 545–548.

Riemann, L., Steward, G.F., Azam, F., 2000. Dynamics of bacterial community composition and activity during a mesocosm diatom bloom. Applied and Environmental Microbiology 66, 578–587.

Ruimy, A., Saugier, B., Dedieu, G., 1994. Methodology for the estimation of terrestrial net primary production from remote sensed data. Journal of Geophysical Research 99, 5263–5283.

Sabine, C.L., Feely, R.A., Gruber, N., Key, R.M., Lee, K., Bullister, J.L., Wanninkhof, R., Wong, C.S., Wallace, D.W.R., Tilbrook, B., Millero, F.J., Peng, T.-H., Kozyr, A., Ono, T., Rios, A.F., 2004. The oceanic sink for anthropogenic CO_2. Science 305, 367–371.

Samo, T.J., Malfatti, F., Azam, F., 2008. A new class of transparent organic particles in seawater visualized by a novel fluorescence approach. Aquatic Microbial Ecology 53, 307–321.

Sanders, R., Henson, S.A., Koski, M., De La Rocha, C.L., Painter, S.C., Poulton, A.J., Riley, J., Salihoglu, B., Visser, A., Yool, A., Bellerby, R., Martin, A.P., 2014. The biological carbon pump in the north Atlantic. Progress in Oceanography 129, 200–218.

Schuser, S., Herndl, G.J., 1995. Formation and significance of transparent exopolymeric particles in the northern Adriatic Sea. Marine Ecological Progress Series 124, 227–236.

Sheldon, R.W., 1972. Size separation of marine seston by membrane and grass-fiber filter. Limnology and Oceanography 17, 494–498.

Simon, M., Azam, F., 1989. Protein content and protein synthesis rates of planktonic marine bacteria. Marine Ecological Progress Series 51, 201–213.

Simon, M., Grossart, H.P., Schweitzer, B., Ploug, H., 2002. Microbial ecology of organic aggregates in aquatic ecosystems. Aquatic Microbial Ecology 28, 175–211.

Smith, D.C., Simon, M., Alldredge, A.L., Azam, F., 1992. Intense hydrolytic enzyme activity on marine aggregates and implications for rapid particle dissolution. Nature 359, 139–142.

Smith, D.C., Steward, G.F., Long, R.A., Azam, F., 1995. Bacterial mediation of carbon fluxes during a diatom bloom in a mesocosm. Deep-Sea Research II 42, 75–97.

Smith, J.N., Ellis, K.M., 1995. Radionuclide tracer profiles at the CESAR Ice Station and Canadian Ice Island in the western Arctic Ocean. Deep-Sea Research II 42, 1449–1470.

Springer, A.M., McRoy, C.P., 1993. The paradox of pelagic food webs in the northern Bering Sea. III. Patterns of primary production. Continental Shelf Research 13, 575–599.

Stemmann, L., Boss, E., 2012. Plankton and particle size and packaging: from determining optical properties to driving the biological pump. Annual review of marine science 4, 263–290.

Sterling, M.C., Jr., Bonner, J.S., Ernest, A.N., Page, C.A., Autenrieth, R.L., 2004. Characterizing aquatic sediment-oil aggregates using in situ instruments. Marine pollution bulletin 48, 533–542.

Stoderegger, K., Herndl, G.J., 1998. Production and release of bacterial capsular material and its subsequent utilization by marine bacterioplankton. Limnology and Oceanography 43, 877–884.

Styles, R., 2006. Laboratory evaluation of the LISST in a stratified fluid. Marine Geology 227, 151–162.

Sugimoto, K., Fukuda, H., Baki, M.A., Koike, I., 2007. Bacterial contributions to formation of transparent exopolymer particles (TEP) and seasonal trends in coastal waters of Sagami Bay, Japan. Aquatic Microbial Ecology 46, 31–41.

Sun, C.-C., Wang, Y.-S., Li, Q.P., Yue, W.-Z., Wang, Y.-T., Sun, F.-L., Peng, Y.-L., 2012. Distribution characteristics of transparent exopolymer particles in the Pearl river estuary, China. Journal of Geophysical Research 117, G00N17.

Teeling, H., Fuchs, B.M., Becher, D., Klockow, C., Gardebrecht, A., Bennke, C.M., Kassabgy, M., Huang, S., Mann, A.J., Waldmann, J., Weber, M., Klindworth, A., Otto, A., Lange, J., Bernhardt, J., Reinsch, C., Hecker, M., Peplies, J., Bockelmann, F.D., Callies, U., Gerdts, G., Wichels, A., Wiltshire, K.H., Glockner, F.O., Schweder, T., Amann, R., 2012. Substrate-controlled succession of marine bacterioplankton populations induced by a phytoplankton bloom. Science 336, 608–611.

Thill, A., Moustier, S., Garnier, J.-M., Estournel, C., Naudin, J.-J., Bottero, J.-Y., 2001. Evolution of particle size and concentration in the Rhone river mixing zone: influence of salt flocculation. Continental Shelf Research 21, 2127–2140.

Thomas, T., Evans, F.F., Schleheck, D., Mai-Prochnow, A., Burke, C., Penesyan, A., Dalisay, D.S., Stelzer-Braid, S., Saunders, N., Johnson, J., Ferriera, S., Kjelleberg, S., Egan, S., 2008. Analysis of the *Pseudoalteromonas tunicata* genome reveals properties of a surface-associated life style in the marine environment. PloS one 3, e3252.

Tréguer, P., Legendre, L., Rivkin, R.T., Ragueneau, O., Dittert, N., 2003. Water column biogeochemistry below the euphotic zone, in: Fasham, M.J.R. (Ed.), Ocean biogeochemistry: A synthesis of the Joint Global Ocean Flux Study (JGOFS), pp. 145–156.

Uchimiya, M., Fukuda, H., Nishino, S., Kikuchi, T., Ogawa, H., Nagata, T., 2013. Vertical distribution of prokaryote production and abundance in the mesopelagic and bathypelagic layers of the Canada Basin, western Arctic: Implications for the mode and extent of organic carbon delivery. Deep-Sea Research I 71, 103–112.

Vahedi, A., Gorczyca, B., 2012. Predicting the settling velocity of flocs formed in water treatment using multiple fractal dimensions. Water research 46, 4188–4194.

Vanderploeg, H.A., 1994. Zooplankton particle selection and feeding mechanisms, in: Wotton, R.S. (Ed.), The biology of particles in aquatic systems, second ed. CRC press, pp. 205–234.

Verdugo, P., 2012. Marine microgels. Annual review of marine science 4, 375–400.

Verdugo, P., Alldredge, A.L., Azam, F., Kirchman, D.L., Passow, U., Santschi, P.H., 2004. The oceanic gel phase: a bridge in the DOM-POM continuum. Marine Chemistry 92, 67–85.

Verzhbitsky, V., Savostina, T., Frantzen, E., Little, A., Sokolov, S.D., Tuchkova, M.I., 2008.

Russian Chukchi Sea. GEO ExPro 5.

Wangersky, P.J., 1994. Sampling and analysis of particulate and dissolved matter., in: Wotton, R.S. (Ed.), Biology of particles in aquatic systems. CRC press, pp. 7–43.

Wegner, C., Hölemann, J.A., Dmitrenko, I., Kirillov, S., Tuschling, K., Abramova, E., Kassens, H., 2003. Suspended particulate matter on the Laptev Sea shelf (Siberian Arctic) during ice-free conditions. Estuarine, Coastal and Shelf Science 57, 55–64.

Waite, A.M., Olson, R.J., Dam, H.G., Passow, U., 1995. Sugar-containing compounds on the cell surfaces of marine diatoms measured using Concanavalin A and flow cytometry. Journal of Phycology 31, 925–933.

Walsh, J.J., Dieterle, D.A., Maslowski, W., Grebmeier, J.M., Whitledge, T.E., Flint, M., Sukhanova, I.N., Bates, N., Cota, G.F., Stockwell, D., Moran, S.B., Hansell, D.A., McRoy, C.P., 2005. A numerical model of seasonal primary production within the Chukchi/Beaufort Seas. Deep-Sea Research II 52, 3541–3576.

Wells, M.L., Goldberg, E.D., 1992. Marine submicron particles. Marine Chemistry 40, 5–18.

Welschmeyer, N.A., 1994. Fluorometric analysis of chlorophyll a in the presence of chlorophyll b and pheopigments. Limnology and Oceanography 39, 1985–1992.

White, M., 1974. Viscous fluid flow, second ed. McGraw-Hill.

Wotton, R.S., 1994. Particulate and dissolved organic matter as food, in: Wotton, R.S. (Ed.), The biology of particles in aquatic systems, second ed. CRC press, pp. 235–288.

Wurl, O., Holmes, M., 2008. The gelatinous nature of the sea-surface microlayer. Marine Chemistry 110, 89–97.

Wurl, O., Miller, L., Vagle, S., 2011. Production and fate of transparent exopolymer particles in the ocean. Journal of Geophysical Research 116, C00H13.

Xia, X.M., Li, Y., Yang, H., Wu, C.Y., Sing, T.H., Pong, H.K., 2004. Observations on the size and settling velocity distributions of suspended sediment in the Pearl River Estuary, China. Continental Shelf Research 24, 1809–1826.

Yamamoto-Kawai, M., McLaughlin, F.A., Carmack, E.C., Nishino, S., Shimada, K., Kurita, N., 2009. Surface freshening of the Canada Basin, 2003–2007: River runoff versus sea ice meltwater. Journal of Geophysical Research 114, C00A05.

Yamasaki, A., Fukuda, H., Fukuda, R., Miyajima, T., Nagata, T., Ogawa, H., Koike, I., 1998. Submicrometer particles in northwest Pacific coastal environments: Abundance, size distribution, and biological origins. Limnology and Oceanography 43, 536–542.

Yang, Y., Motegi, C., Yokokawa, T., Nagata, T., 2010. Large-scale distribution patterns of virioplankton in the upper ocean. Aquatic Microbial Ecology 60, 233–246.

Zhou, J., Mopper, K., Passow, U., 1998. The role of surface-active carbohydrates in the formation of transparent exopolymer particles by bubble adsorption of seawater. limnology and Oceanography 43, 1860–1871.

Ziervogel, K., Arnosti, C., 2008. Polysaccharide hydrolysis in aggregates and free enzyme activity in aggregate-free seawater from the north-eastern Gulf of Mexico. Environmental microbiology 10, 289–299.